1967

Mode analysis of the unsymmetrically fed ground-plane aperture

John G. Hemmann

Department:

MODE ANALYSIS OF THE UNSYMMETRICALLY FED GROUND-PLANE APERTURE

BY

JOHN G. HEMMANN —1942—

A

THESIS

submitted to the faculty of

THE UNIVERSITY OF MISSOURI AT ROLLA

in partial fulfillment of the requirements for the

Degree of

MASTER OF SCIENCE IN ELECTRICAL ENGINEERING

Rolla, Missouri

1967

Approved by

H H Skilling (advisor) Ralph L Carson

Charles E. Antle J Mikes

ABSTRACT

The problem of radiation from a waveguide-fed ground-plane aperture perturbed with a wedge-shaped dielectric insert was examined more carefully. The work initiated by Blumberg[3] was continued, using a greater range of dielectric constants and smaller increments of angle.

Aperture field measurements were made over a range of dielectric constants for each wedge angle, in order to determine the change in amplitude distribution as a function of permittivity. Aperture phase measurements were also taken for selected angles. These were used with the amplitude data to predict, using numerical integration, the far-field radiation patterns of the perturbed aperture. Far-field patterns were then measured in an anechoic chamber and compared with the calculated patterns.

Results of the measurements were evaluated with respect to the application of this type of aperture loading to a beam scanning antenna. The relationship of modes appearing in the aperture amplitude distribution to the changes in far-field patterns were especially considered. A partially-filled-waveguide approximation model was developed, for which it was shown that modes similar to those found in the wedge perturbed aperture could be produced.

TABLE OF CONTENTS

		Page
LIST OF ILLUSTRATIONS		iv
I.	INTRODUCTION	1
II.	REVIEW OF LITERATURE	5
III.	EXPERIMENTAL PROCEDURE	7
	A. Sample Preparation	7
	B. Aperture Electric Field Magnitude Measurements	7
	C. Aperture Phase Measurements	8
	D. Far-field Measurements	10
IV.	QUALITATIVE ANALYSIS OF APERTURE DISTRIBUTION	12
V.	PARTIALLY FILLED WAVEGUIDE APERTURE DISTRIBUTION APPROXIMATION	36
VI.	CORRELATION OF APERTURE DISTRIBUTIONS AND FAR-FIELD PATTERNS	44
	A. 50^{o} Wedge Inserts	44
	B. 60^{o} Wedge Inserts	46
	C. 70^{o} Wedge Inserts	47
VII.	CONCLUSIONS	68
	Vita	69
	Bibliography	70
APPENDIX A		71
APPENDIX B		73

LIST OF ILLUSTRATIONS

Figures		Page
1a.	Geometry of Aperture with Dielectric Wedge Insert	2
1b.	Dimensions of Dielectric Wedge Inserts	2
2.	Phase Measuring Technique	9
3.	Aperture Magnitude Distribution 50^{o} K = 1.7, K = 3	16
4.	Aperture Magnitude Distribution 50^{o} K = 4, K = 5	17
5.	Aperture Magnitude Distribution 50^{o} K = 6, K = 7	18
6.	Aperture Magnitude Distribution 50^{o} K = 8, K = 10	19
7.	Aperture Magnitude Distribution 55^{o} K = 1.7, K = 3	20
8.	Aperture Magnitude Distribution 55^{o} K = 4, K = 5	21
9.	Aperture Magnitude Distribution 55^{o} K = 6, K = 7	22
10.	Aperture Magnitude Distribution 55^{o} K = 8, K = 10	23
11.	Aperture Magnitude Distribution 60^{o} K = 1.7, K = 3	24
12.	Aperture Magnitude Distribution 60^{o} K = 4, K = 5	25
13.	Aperture Magnitude Distribution 60^{o} K = 6, K = 7	26
14.	Aperture Magnitude Distribution 60^{o} K = 8, K = 10	27
15.	Aperture Magnitude Distribution 65^{o} K = 1.7, K = 3	28
16.	Aperture Magnitude Distribution 65^{o} K = 4, K = 5	29
17.	Aperture Magnitude Distribution 65^{o} K = 6, K = 7	30
18.	Aperture Magnitude Distribution 65^{o} K = 8, K = 10	31
19.	Aperture Magnitude Distribution 70^{o} K = 1.7, K = 3	32
20.	Aperture Magnitude Distribution 70^{o} K = 4, K = 5	33

Figures

		Page
21.	Aperture Magnitude Distribution 70^{o} K = 6, K = 7	34
22.	Aperture Magnitude Distribution 70^{o} K = 8, K = 10	35
23.	Possible Solutions in Free-Space Region	39
24.	Approximation Solution 50^{o} Wedge, K = 1.7	41
25.	Approximation Solution 50^{o} Wedge, K = 5	42
26.	Approximation Solution 50^{o} Wedge, K = 10	43
27.	Measured Radiation Pattern 50^{o} K = 1.7, K = 3	48
28.	Measured Radiation Pattern 50^{o} K = 4, K = 5	49
29.	Aperture Phase Distribution 50^{o} K = 4, K = 5	50
30.	Calculated vs. Measured Radiation Pattern 50^{o} K = 5	51
31.	Measured Pattern 50^{o} K = 6, K = 7	52
32.	Aperture Phase Distribution 50^{o} K = 6, K = 7	53
33.	Calculated vs. Measured Radiation Pattern 50^{o} K = 7	54
34.	Measured Radiation Pattern 50^{o} K = 8, K = 10	55
35.	Aperture Phase Distribution 50^{o} K = 8, K = 10	56
36.	Measured Radiation Pattern 60^{o} K = 1.7, K = 3	57
37.	Measured Radiation Pattern 60^{o} K = 4, K = 5	58
38.	Measured Radiation Pattern 60^{o} K = 6, K = 7	59
39.	Aperture Phase Distribution 60^{o} K = 6, K = 7	60
40.	Calculated vs. Measured Radiation Pattern 60^{o}, K = 7	61
41.	Measured Radiation Pattern 60^{o} K = 8, K = 10	62
42.	Aperture Phase Distribution 60^{o} K = 8, K = 10	63

Figures Page

43. Measured Radiation Pattern 70^{o} K = 1.7, K = 3 64

44. Measured Radiation Pattern 70^{o} K = 4, K = 5 65

45. Measured Radiation Pattern 70^{o} K = 6, K = 7 66

46. Measured Radiation Pattern 70^{o} K = 8, K = 10 67

I. INTRODUCTION

The problem of an unloaded waveguide radiating through a ground-plane (waveguide-fed aperture) is treated in detail in microwave literature. The mathematical solution predicts a simple single-lobe pattern with maximum amplitude along the axis of the waveguide.

It is desired that the waveguide aperture be somehow perturbed, producing a lobe (or multiple lobes) whose maximum is shifted from the center line of the waveguide. If this perturbation can be controlled in somewhat linear fashion, a scanning pattern would result. Further refinements and addition of similar elements could then produce a scanning antenna.

G. G. Skitek* has suggested that triangular slabs of dielectric material be placed in the aperture, as shown in Figure 1[a]. A varying phase and amplitude front might be expected across the aperture, due to the nature of the boundary conditions at the interface of the slab within the guide, and also due to the higher propagation constant of the dielectric. The combination of these two variations would produce a change in the lobe of the radiation pattern. Unfortunately, the boundary value problem associated with this geometrical configuration becomes mathematically complex. A general method of solution for this type of problem is given by Schelkenoff[1], the application of which is rather difficult.

---

*UMR Electrical Engineering Department.

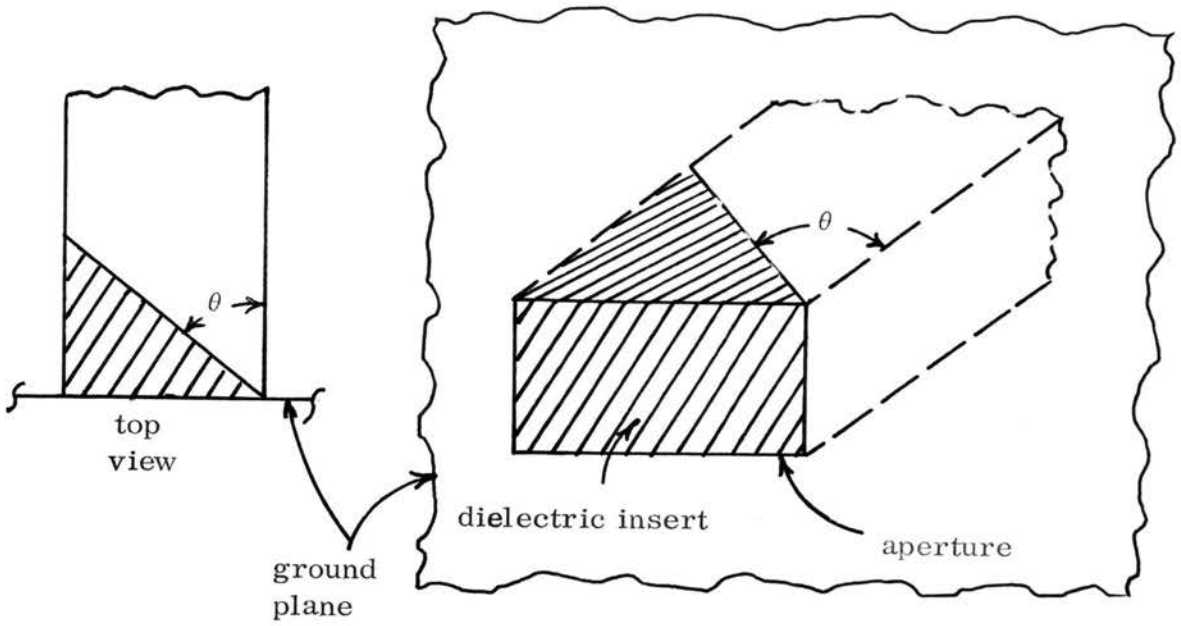

Figure 1[a]. GEOMETRY OF APERTURE WITH DIELECTRIC WEDGE INSERT

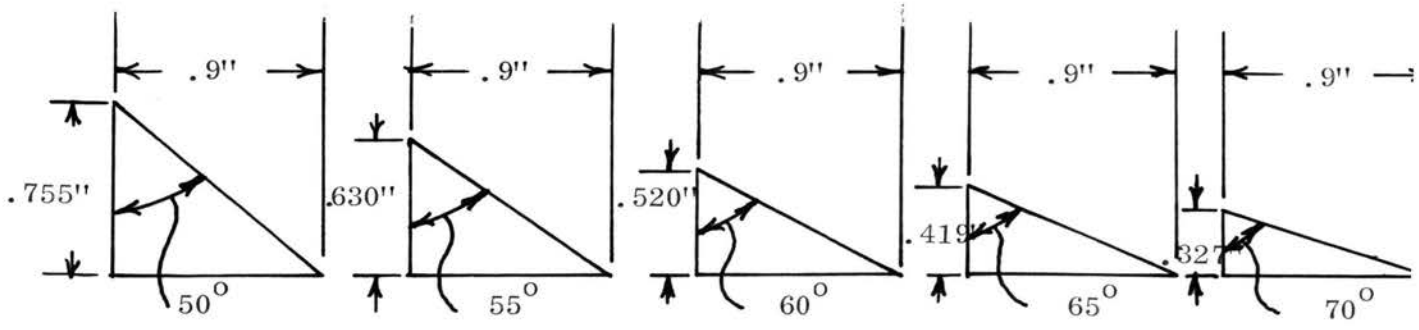

Figure 1[b]. DIMENSIONS OF DIELECTRIC WEDGE INSERTS

Blumberg's[3] preliminary investigation of this problem has shown that the greatest shifts in far-field radiation pattern are to be expected with a wedge angle of approximately 60^{o}. His investigation, however, was limited to 15^{o} increments of angle and only a few values of dielectric constant. The purpose of the present investigation was to examine the problem in greater detail, with a range of angles on either side of 60^{o}, and with a more complete range of dielectric constants, in order to determine the change in aperture distribution and consequently in far-field pattern with change in permittivity. The pertinent measurements which were made are as follows:

1) Measurements of aperture electric-field amplitude distributions for wedge angles of 50^{o}, 55^{o}, 60^{o}, 65^{o}, and 70^{o}, with dielectric constants of 1.7, 3, 4, 5, 6, 7, 8, and 10 for each wedge angle. (A total of 40 different wedge inserts.)

2) Measurement of far-field radiation patterns for the complete range of permittivity change with fixed wedge angle. This was conducted for three wedge angles, 50^{o}, 60^{o}, and 70^{o}.

3) Measurement of aperture phase distributions for selected wedge angles and permittivities. This phase data was used with the amplitude data to predict the far-field patterns by numerical integration.

The sliding probe devised by Blumberg was used for the aperture measurements, and an anechoic radiation chamber for the far-field pattern measurements. All measurements were taken at a frequency of 10.0 GHz. The aperture dimensions are those of standard X-band waveguide, i.e., 0.9

by 0.4 inches.

The essential consideration in evaluating these aperture measurements was the relative change in the amplitude and phase distributions, and correspondingly in the far-field patterns, with gradually changing dielectric constant. It was assumed that varying permittivity would be the means of producing scanning in a practical antenna.

The analysis will attempt to correlate the appearance of higher order modes in the amplitude distributions with the appearance of variations in the far-field patterns.

Mathematically, the wedge-loaded aperture can be approximated by an aperture fed with a partially filled waveguide. Although this approximation is far from ideal, and contains arbitrary parameters, it does show that the same type of amplitude distributions can be produced.

II. REVIEW OF THE LITERATURE

The problem of radiation of a perturbed waveguide in a ground plane may be divided into two general areas: 1) determination of the electric field magnitude and phase components in the waveguide aperture, and 2) determination of the far-field radiation pattern.

In determining the aperture field, the usual technique of solving Maxwell' s equations and applying separation of variables fails because of the unusual nature of the boundary of the dielectric insert. Schelkunoff[1] described a general technique for the solution of complex boundary problems in a waveguide. This method consists of finding functions which match the required boundary conditions and then constructing a series solution of these functions which satisfies Maxwell' s equations. Hord[2] applied this technique to evaluate the fields at various types of dielectric boundaries within waveguides.

From an experimental viewpoint, Blumberg[3] measured aperture fields for several dielectric inserts. His sliding-probe apparatus was used without alteration in making measurements for this thesis. Angelakos and Korman[4] experimentally studied radiation from a ground-plane aperture with a rectangular ferrite insert which totally fills the guide transversely. Varying the permeability of the ferrite with an applied magnetic field, they found considerable variations in the aperture field magnitude and phase. In agreement with theory, they reported that the energy tends to propagate into the region of highest $\mu\epsilon$ product. Lewin[5] solved the problem of dielectrically loaded waveguide with a step discontinuity. His technique might be extended to obtain an approximate solution to the angular boundary problem

Once the aperture field is known, there are several accepted techniques for evaluating the radiation far field. Harrington[6] utilized the concepts of equivalence and image theory to evaluate the far field of a ground-plane aperture. This technique, detailed in Appendix A, was used to predict the far-field patterns for several of the dielectric wedge inserts used in this thesis.

Silver[8] approached the problem of determining the far-field radiation pattern from an optical viewpoint, utilizing Huygens principle. Kraus[9], Harvey[10], and Bolljahn[11] discussed the general area of radiation from a rectangular waveguide.

In approximating the wedge-loaded waveguide, a partially-filled-waveguide model is used. Pincherle's[12] technique, discussed in Appendix B, was used to solve Helmhotz's wave equation in each region which matched boundary conditions. The resulting characteristic equation has multiple roots which correspond to the various modes in the totally filled guide.

III. EXPERIMENTAL PROCEDURE

A. SAMPLE PREPARATION

The dielectric wedges were cut from Stycast "Hi K" or "Lo K" low-loss dielectric material.* This material has the advantage of controlled permittivity, but is rather brittle and difficult to machine. Cutting was done on a circular saw with a diamond-dust cutting blade. Demineralized water was used as coolant to insure non-contamination of the dielectric surface. Because of the large number of samples (40) and the relatively small dimensions of each, there were minor discrepancies in dimensions. The wedges were brought as near to correct size as possible on a sanding table. Figure 1[b] shows the ideal dimensions of the dielectric wedges.

B. APERTURE ELECTRIC FIELD MAGNITUDE MEASUREMENTS

A measure of the aperture field strength was obtained by means of a sliding probe which traversed the lower edge of the radiating waveguide. (See Blumberg[3] for construction details.) No attempt was made to probe the field in the vertical direction since the modes (TE_{mo}) created by the dielectric load were assumed to be constant in the vertical direction. The symmetry of the load with respect to the horizontal axis seems to justify this assumption. A minimum amount of probe penetration into the aperture was desired, in order to minimize the effect of the probe upon the field; however, sufficient

---

*Emerson & Cuming, Inc., Canton, Massachusetts.

penetration must be used to obtain a measurable signal of sufficient amplitude. A compromise probe penetration of approximately 1/16" above the bottom of the aperture was used. The probe was spaced about 1/64" in an outward direction from the aperture face, and was thus not measuring exactly the aperture distribution, but rather the near radiated field at a short distance. This is shown in the aperture field measurements, which do not become zero at the ground-plane boundary, as they should if the true aperture distribution were being measured. This probe displacement was necessary, however, to smooth out slight irregularities in the electric field due to small imperfections in the dielectric load surfaces, and also to compensate for the non-parallel motion of the probe as it traversed horizontally. The effect of the probe on the electric field is difficult to ascertain, but the negligible change in VSWR when the probe was removed indicated that it has little effect.

C. APERTURE PHASE MEASUREMENTS

Figure 2 illustrates the technique employed in the phase measurements. The basic idea was to introduce a reference signal from the klystron source and a test signal from the aperture probe into a slotted line and adjust the reference signal phase and magnitude to obtain a null. Any change in test signal phase would then require a movement of the reference signal to re-establish the null, the amount of movement being proportional to the shift in phase of the test signal. In order to obtain an exact null, signals must be of the same amplitude. The reference signal was tapped from the waveguide feeding the

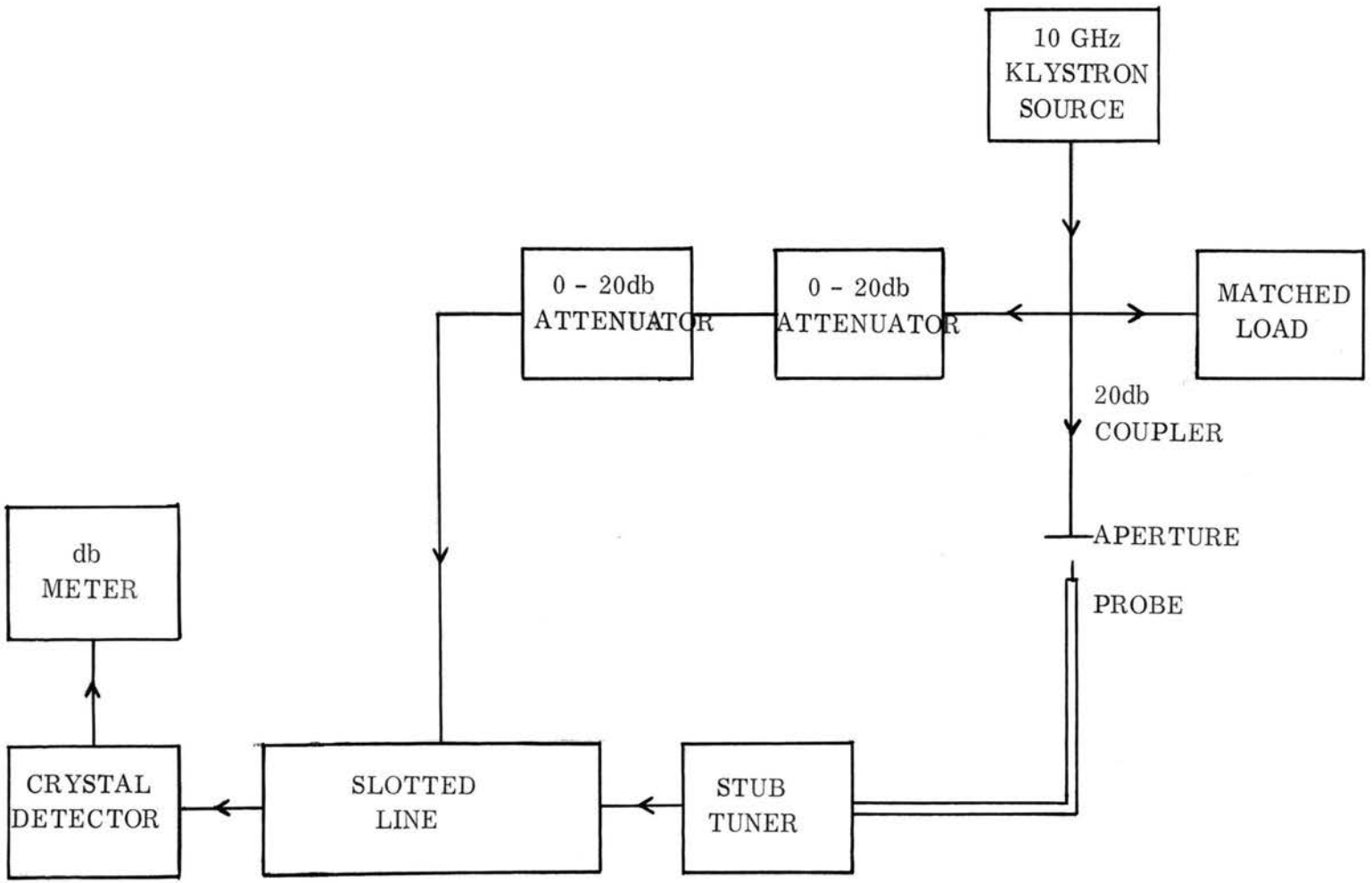

FIGURE 2. PHASE MEASURING TECHNIQUE

the aperture, and was adjusted in amplitude by the variable attenuator. It was fed into the slotted line via the movable probe, the aperture signal being fed into one end and the crystal detector being placed in the other. A stub tuner placed between the probe signal input and the slotted line was adjusted so that the reference signal "viewed" a matched line in that direction. In order to function properly, the variable attenuator must not create phase shift as its attenuation value is changed. Measurements on the open guide showed this to be approximately true.

The null point at low values of signal from the aperture was somewhat broad, and the true null was difficult to locate. This tended to create errors in the phase readings near these points, but because the amplitude was small, these phase errors should have little effect on predicting the far-field pattern by numerical integration.

D. FAR-FIELD MEASUREMENTS

The far-field measurements were made in a microwave anechoic chamber recently constructed by Blumberg.[3] One wall of the chamber consists of a large ground plane with an opening for insertion of test antennae. The other walls are lined with Eccosorb* energy absorbant material. A pickup antenna moves in a horizontal arc at a distance of 1.22 meters from the test device opening. At a frequency of 10 GHz this is approximately 40 wavelengths and thus well into the radiation far field.

---

*Emerson & Cuming Inc., Canton, Massachusetts

The test antenna mounting texture in this case was a one-foot square brass plate with a 0.5 inch by 1 inch centered opening into which a section of X-band waveguide had been soldered. The plate was screwed tightly against the ground plane of the chamber. Dielectric samples were inserted into the aperture from within the chamber.

There were two possible sources of error which could cause discrepencies between the calculated and the measured far-field patterns. The first was errors in the aperture field magnitude and phase measurements, which are used in calculating the patterns. The second was actual errors in pattern measurement due to deficiencies in the anechoic chamber. These deficiencies, such as reflections and discontinuities in the ground plane, are discussed more thoroughly by Blumberg. [3]

The measured radiation lobe for the open (unperturbed) aperture was somewhat wider than that predicted analytically. It might be then expected that the measured lobes for the various perturbed configurations might be somewhat wider than would be measured in a free-space test.

IV. QUALITATIVE ANALYSIS OF APERTURE DISTRIBUTIONS

Figures 3 through 22 show the amplitude distributions obtained in the experimental measurements. The zero 0B level represents the measured field at the center of the unloaded aperture. The maximum electric field produced by each wedge insert, when compared to this reference level, gave an indication of the energy reflected from the wedge, and consequently of the mismatch produced.

For the lowest dielectric constant (K = 1.7), the amplitude plots approximate those of the open aperture for all five of the measured angles. The maximum is shifted to the right slightly for the smallest angles, and gradually approaches the half sinusoidal distribution as the angle increases. Viewing each curve as a superposition of fundamental and higher order modes, the shifting of the maximum could be attributed to the addition of a small second order mode, in phase to the right and out of phase to the left.

For the K = 3 curves, higher order modes are definitely present. The amplitude distribution has a definite concentration to the left of the aperture with a large maximum near 0.3 (inches across aperture from left). A minimum-like dip occurs around 0.6" and a secondary maximum around 0.75". This same basic distribution appears for all angles, with the minimum becoming sharpest and the secondary maximum highest for a wedge angle of 60^{o}. The secondary maximum has decreased for 65^{o} and almost vanished at 70^{o}, leaving an approximately flat distribution from 0.6" to 0.9" for this last angle. The exact modes present and their relative amplitudes and phases

is difficult to ascertain, but the lack of a sharp minimum, corresponding to a zero point in the field distribution, indicates that the fundamental mode is still dominant, while the bunching of the field to the left indicates the presence of the second order mode. The general shape of the secondary peak indicates a third order mode (which would have a maximum at 0.75") at present. However, this is somewhat arbitrary, since no other peaks occur to the left, as would be expected in the presence of this mode.

For a dielectric constant K = 4, the same basic curves appear as those for K = 3, but with a reduced secondary peak. It is assumed that the amplitude of the higher order mode causing it has decreased. This secondary lobe is now definitely seen only for angles of 55^{o} and 60^{o} and was not nearly as pronounced. The 50^{o} curve shows a slight dip near 0.55", indicating a very small component of this higher order mode. The 65^{o} curve shows no dip at all, but now has the flattened portion between 0.7" and 0.9", as originally seen on the 70^{o}, K = 3 curve. The 70^{o} curve represents an almost pure sinusoidal distribution but with the maximum shifted to the left.

For K = 5, a new trend appears at the lower angles, i.e., the appearance of a distinct second order mode distribution. For the 50^{o} wedge, two almost equal maxima occur at 0.3" and 0.75", with a very deep minimum at 0.5". This distribution is certainly not a perfect second order mode, as the left maximum (lobe) is wider, indicating more energy concentrated therein, and the minimum between the two lobes does not occur halfway across the guide. It is emphasized that the formation of pure modes is not to be expected

due to the nature of the boundary conditions within the waveguide, and due to the closeness of the aperture to this boundary. The mode description is merely a convenience which approximately describes the resulting distributions.

The same second order mode occurs at an angle of 55^{o}, with the distribution of the two lobes becoming more nearly equal, but with the minimum not quite as deep and still to the right of center. For 60^{o}, the minimum is far less pronounced and the left lobe has a greater width and magnitude than the right lobe. This curve appears to have fundamental, second, and third order mode components. The 65^{o}, K = 5 curve resembles the 65^{o}, K = 3 curve, with a peak near 0.75". The 70^{o} curve is almost identical with the 70^{o}, K = 4 curve, a displaced sinusoidal distribution.

At the higher dielectric constants, unusual patterns begin to develop. In fact, the K = 6 patterns are the last set of patterns in which the distributions at different angles resemble each other. The 50^{o}, 55^{o}, and 60^{o} curves have a deep minimum between 0.3" and 0.5", with two energy lobes on either side. This double-lobe distribution, originally appearing in the 50^{o} and 55^{o}, K = 5 wedges has now extended to the 60^{o} wedge distribution. The lobes to the left of this minimum are almost sinusoidal, having a shape similar to the third order mode. The lobes to the right are wider and smaller in magnitude, having distorted distributions containing undetermined higher order modes. This double-lobed distribution disappears at the 65^{o} wedge angle, leaving only a single lobe to the left of the aperture. A small dip still occurs between 0.4" and 0.5", indicating the slight presence of higher order

modes. The 70^{o} curve has settled down into the displaced sinusoidal pattern.

Beginning with a dielectric constant of 7, the patterns begin varying erratically with angle change. The 50^{o} angle has the appearance of an almost pure third order mode, but with not quite equal width and amplitude lobes, the central lobe being predominant. The 55^{o} angle distribution has collapsed into a single lobe with a maximum at 0.3" and a very minor secondary lobe at 0.8. The 60^{o} curve has also almost formed a single lobe, but with a slight dip near 0.6", showing the remnants of the two-lobe distribution. The 65^{o} wedge distribution now contains the almost pure second order lobe, its first appearance at this wedge angle. The 70^{o} curve now varies slightly from its sinusoidal distribution, with a slight flattening to the right of the aperture.

The K = 8 and K = 10 curves are very unusual, indicating many higher order modes. The 50^{o}, K = 10 curve approaches the pure third order mode. but again with irregularities and a predominant central lobe. The 55^{o} curves for K = 8 and K = 10 curves both have minimum inflections at 0.35, indicating the possible presence of a third order modes. The 60^{o}, K = 10 curve has a pronounced minimum at 0.5", indicating the second order mode.

Although the preceding discussion is somewhat arbitrary with regard to the description of the various modes, the unusual experimental results preclude any exact mathematical analysis. The partially filled waveguide approximation model will attempt to show that some of the simpler distributions can be duplicated.

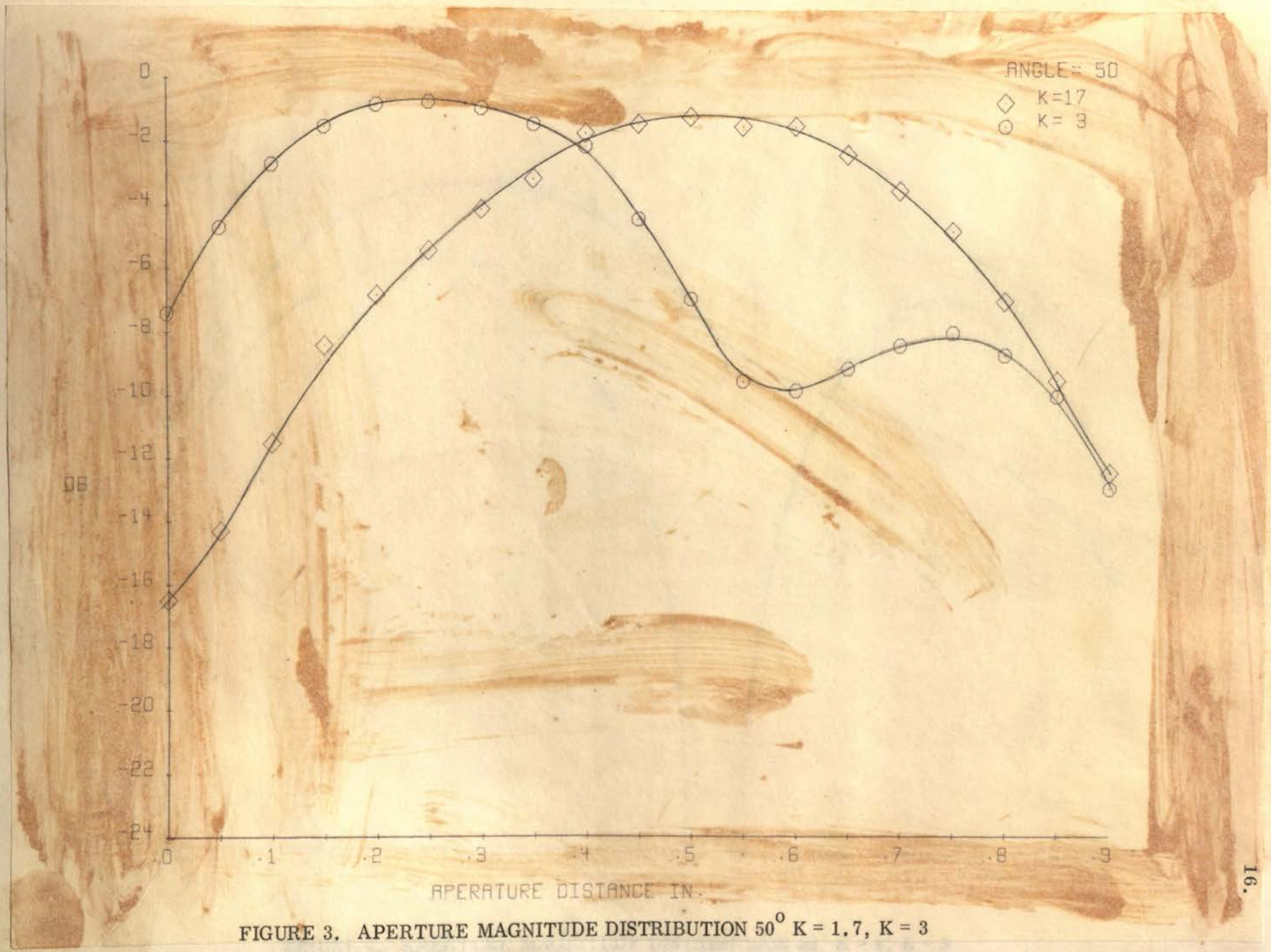

FIGURE 3. APERTURE MAGNITUDE DISTRIBUTION 50^{O} K = 1.7, K = 3

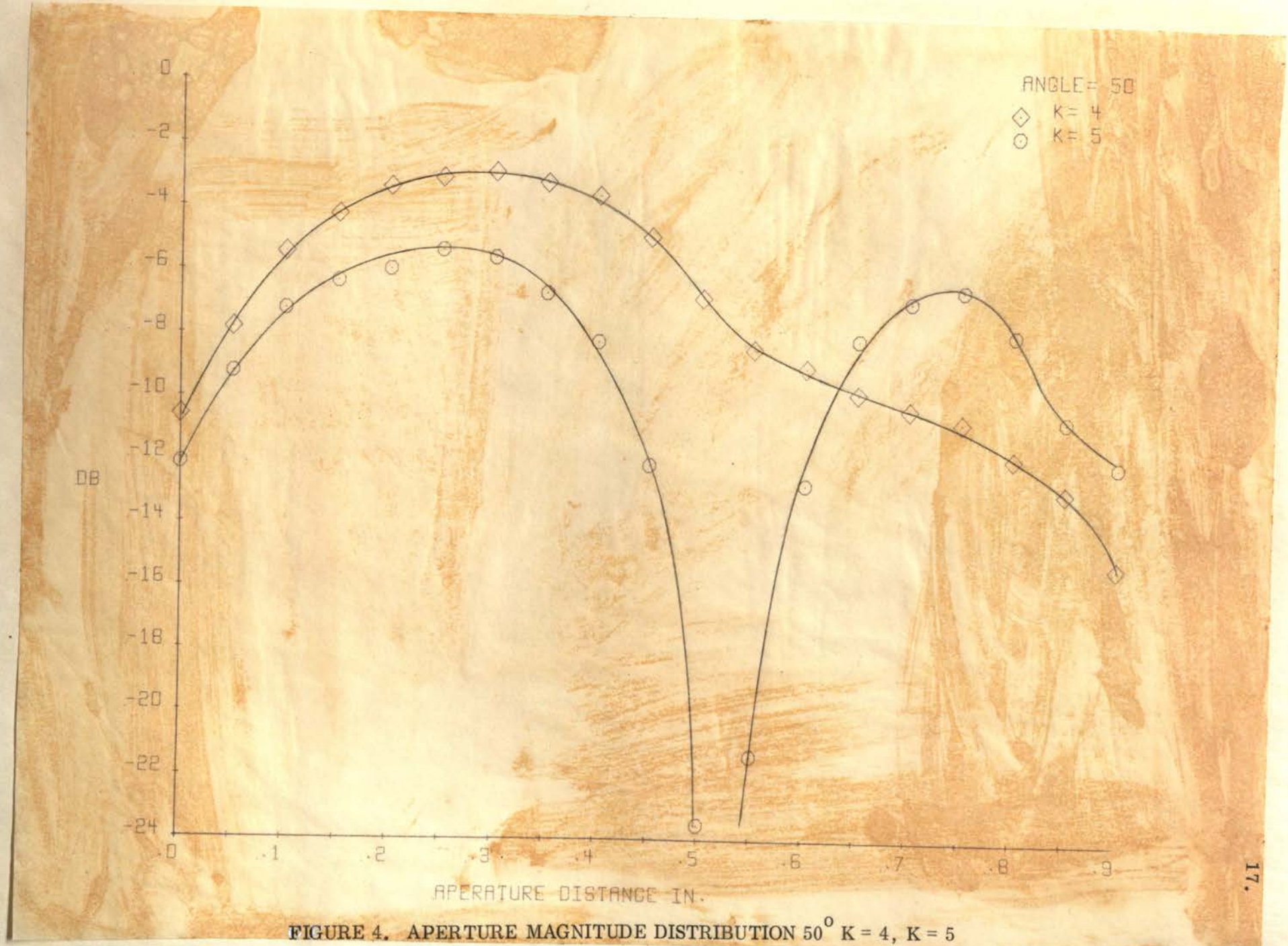

FIGURE 4. APERTURE MAGNITUDE DISTRIBUTION 50^{o} K = 4, K = 5

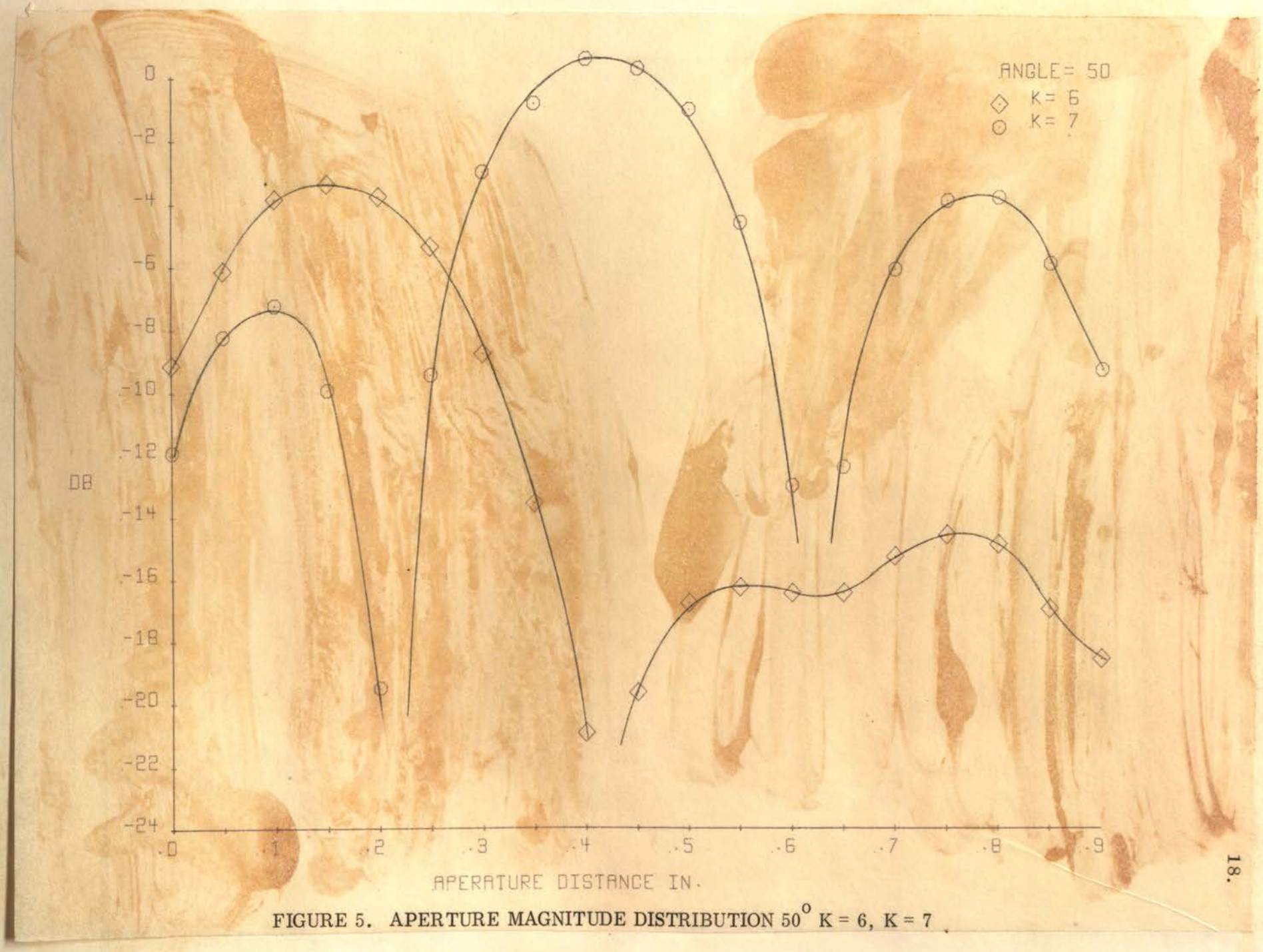

FIGURE 5. APERTURE MAGNITUDE DISTRIBUTION 50^{o} K = 6, K = 7

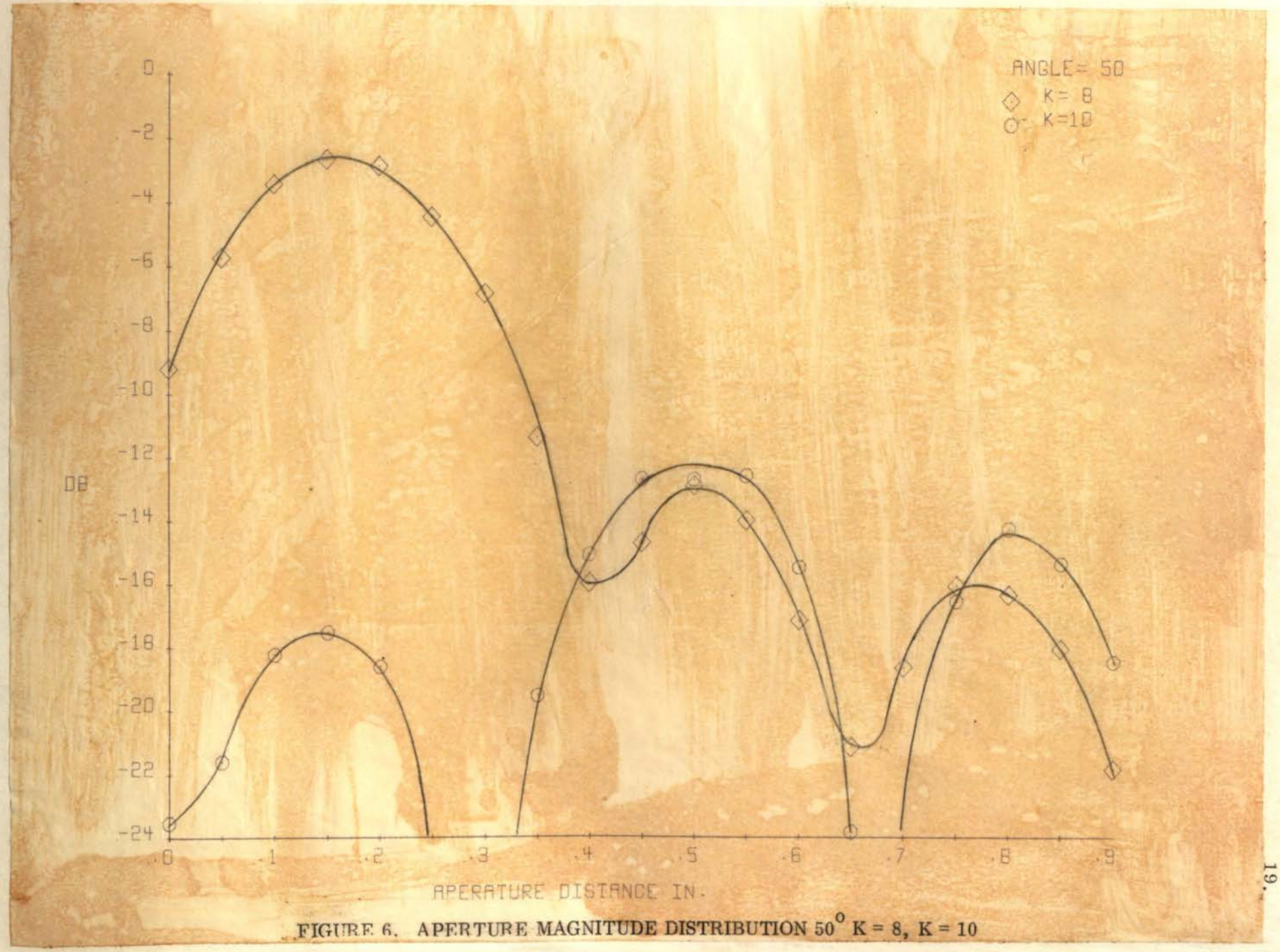

FIGURE 6. APERTURE MAGNITUDE DISTRIBUTION 50° K = 8, K = 10

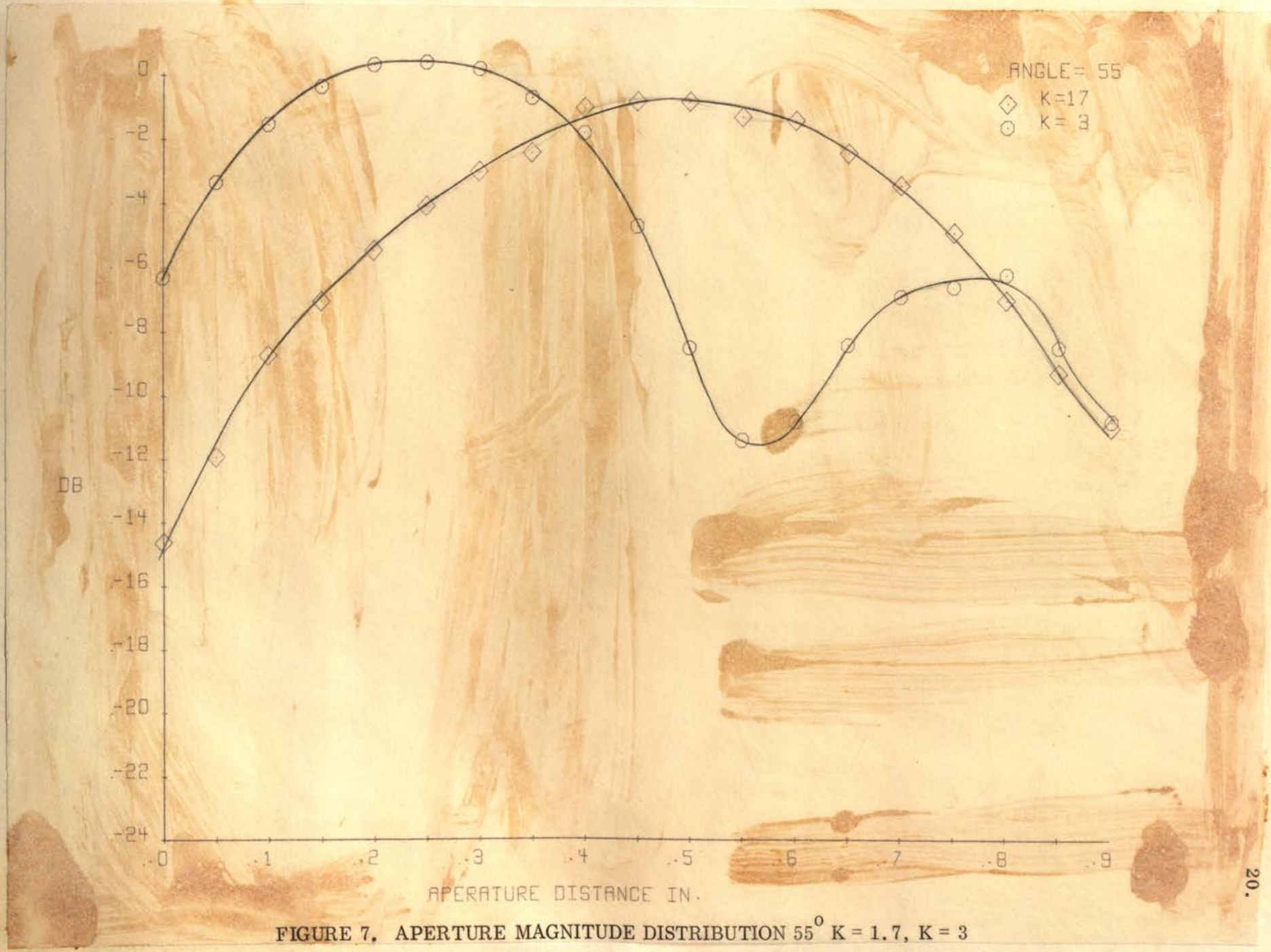

FIGURE 7. APERTURE MAGNITUDE DISTRIBUTION 55^{o} K = 1.7, K = 3

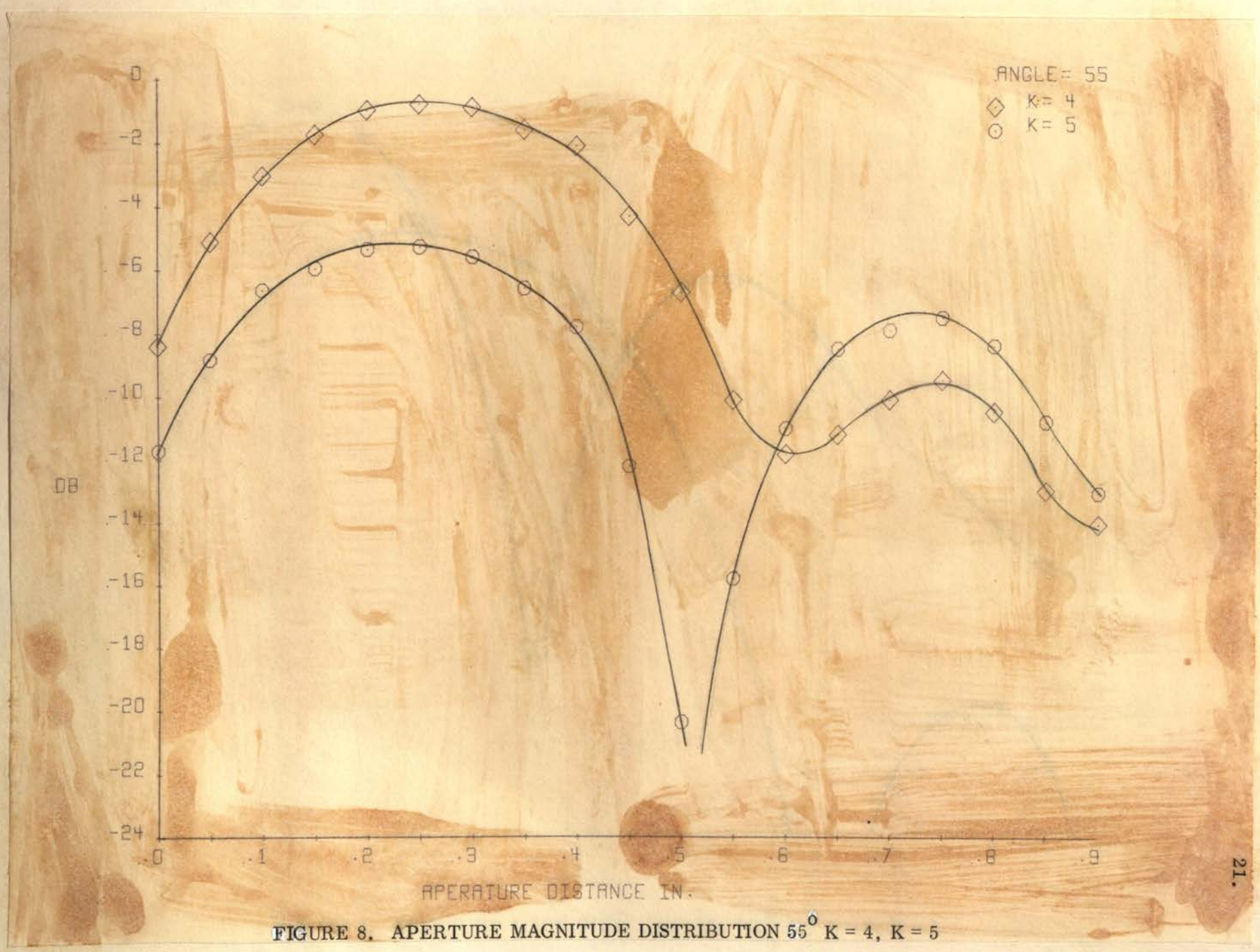

FIGURE 8. APERTURE MAGNITUDE DISTRIBUTION 55^{o} K = 4, K = 5

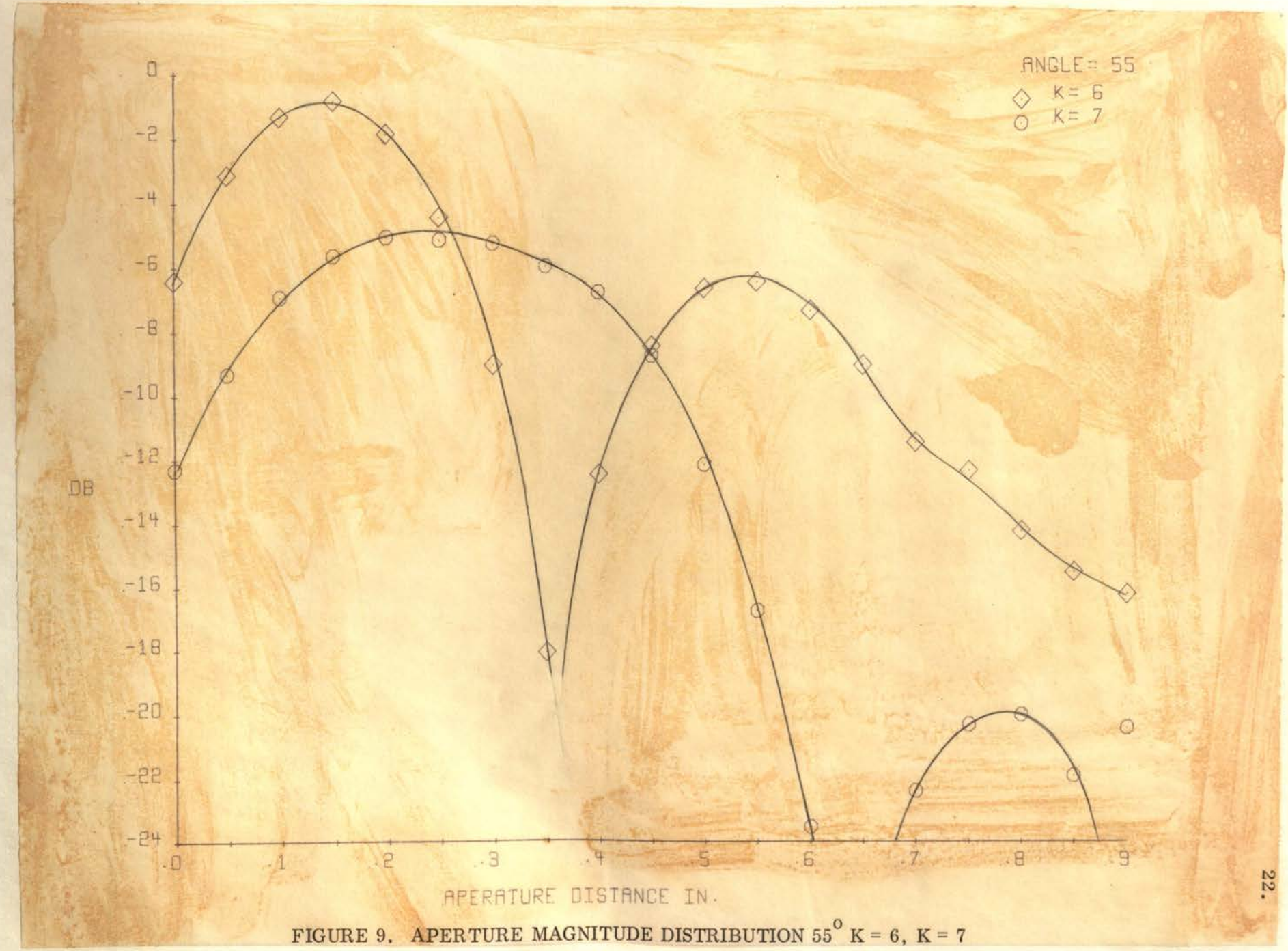

FIGURE 9. APERTURE MAGNITUDE DISTRIBUTION 55^{O} K = 6, K = 7

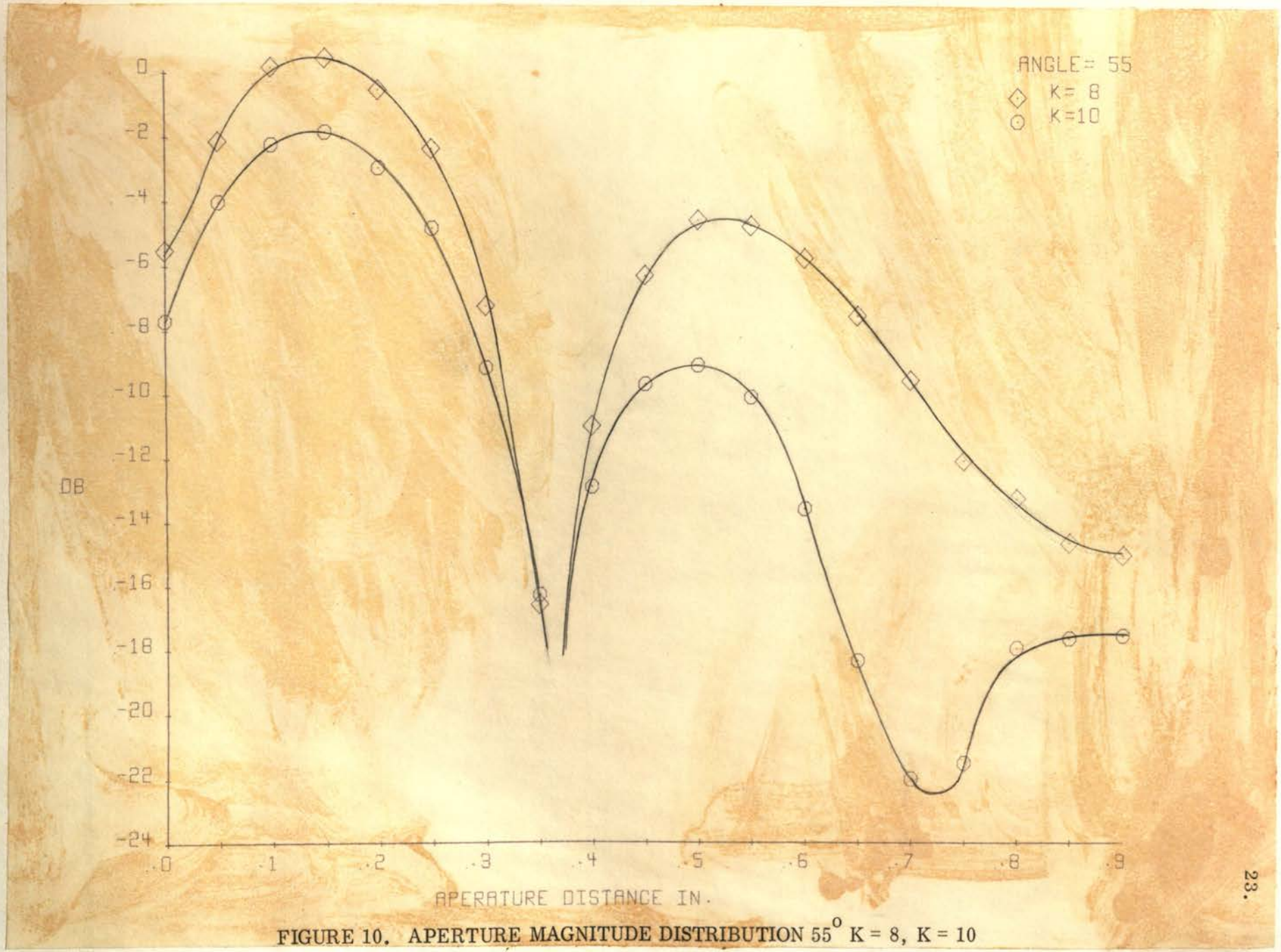

FIGURE 10. APERTURE MAGNITUDE DISTRIBUTION 55^{o} K = 8, K = 10

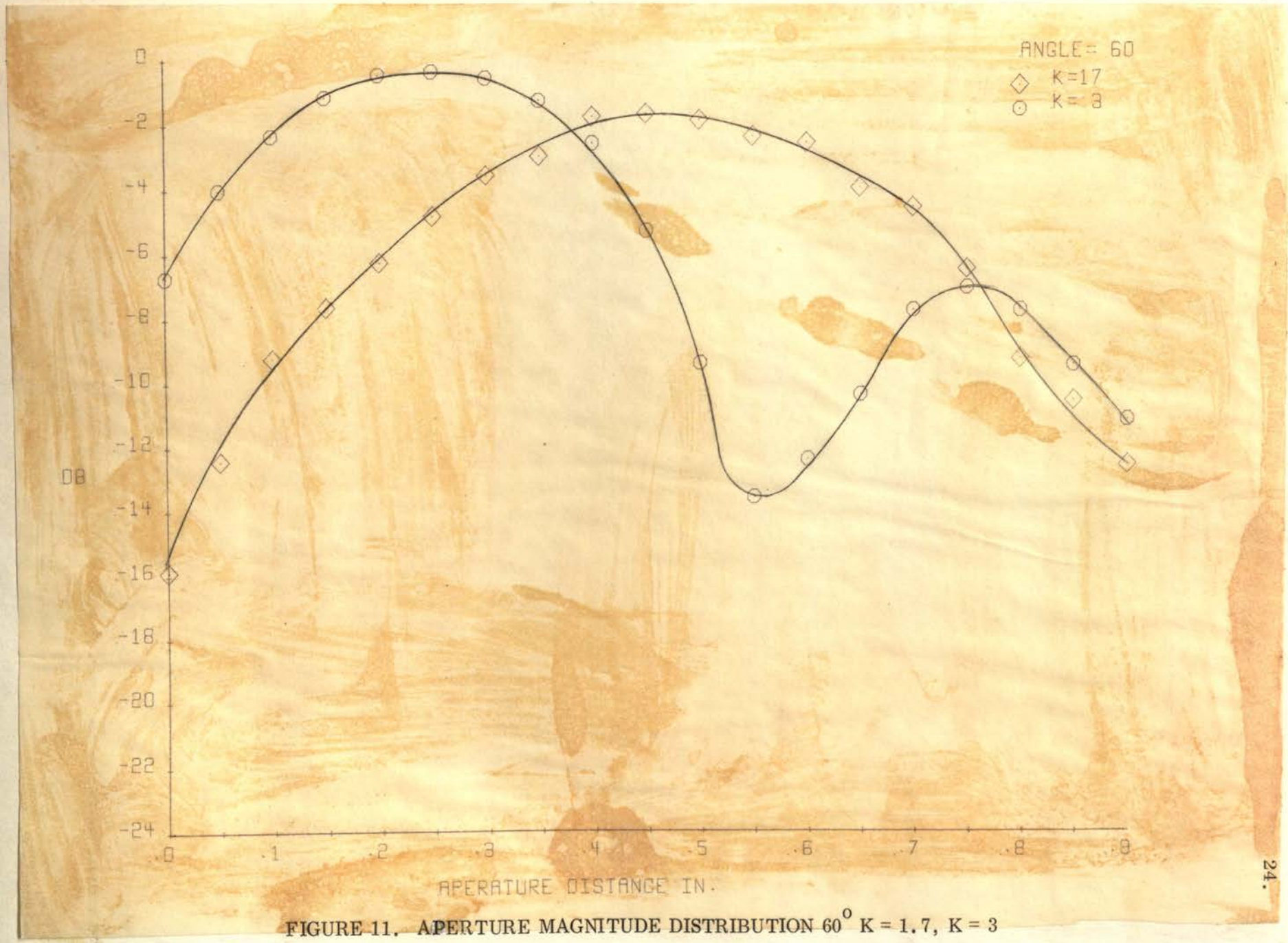

FIGURE 11. APERTURE MAGNITUDE DISTRIBUTION 60^{o} K = 1.7, K = 3

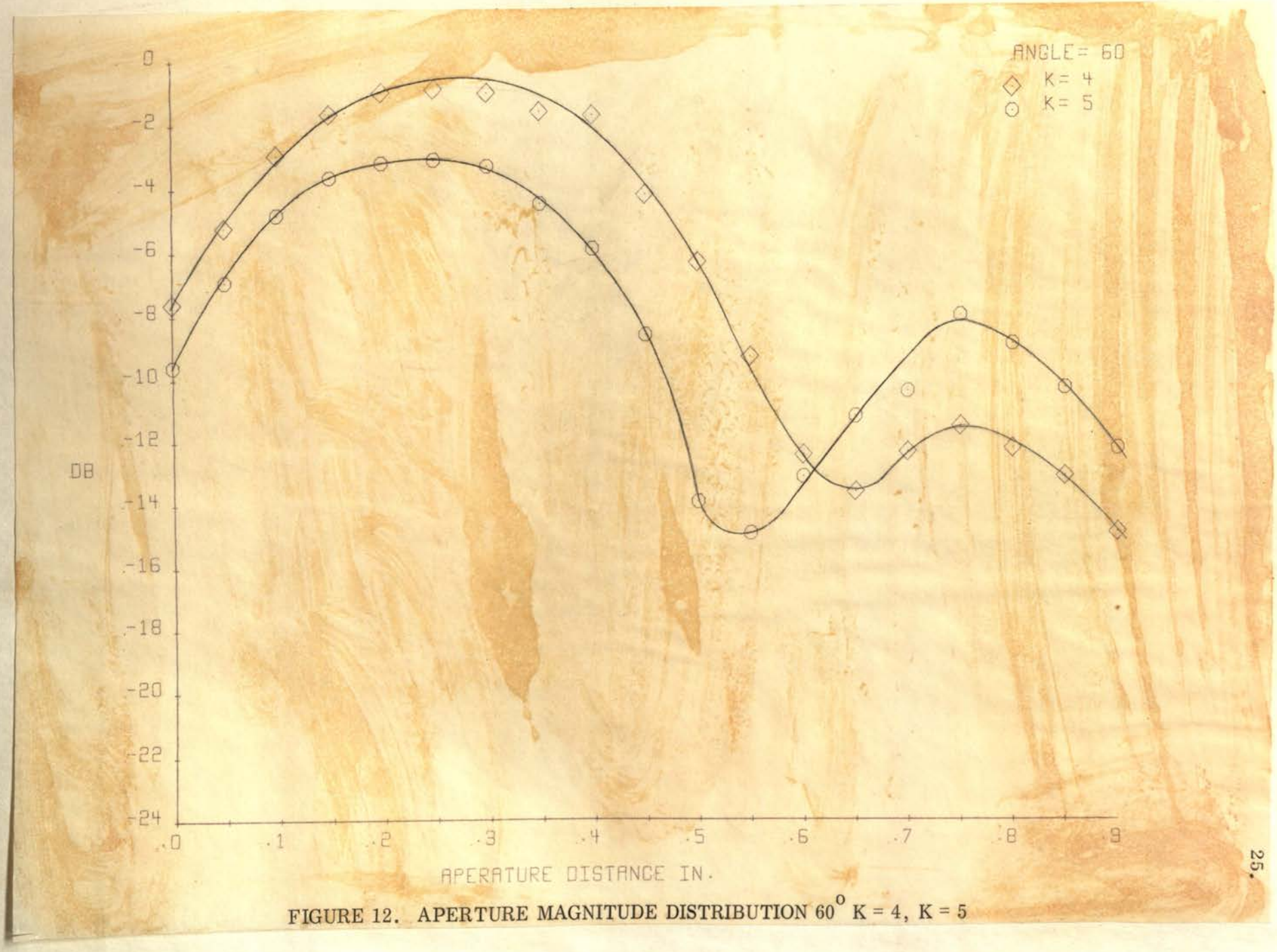

FIGURE 12. APERTURE MAGNITUDE DISTRIBUTION 60^{o} K = 4, K = 5

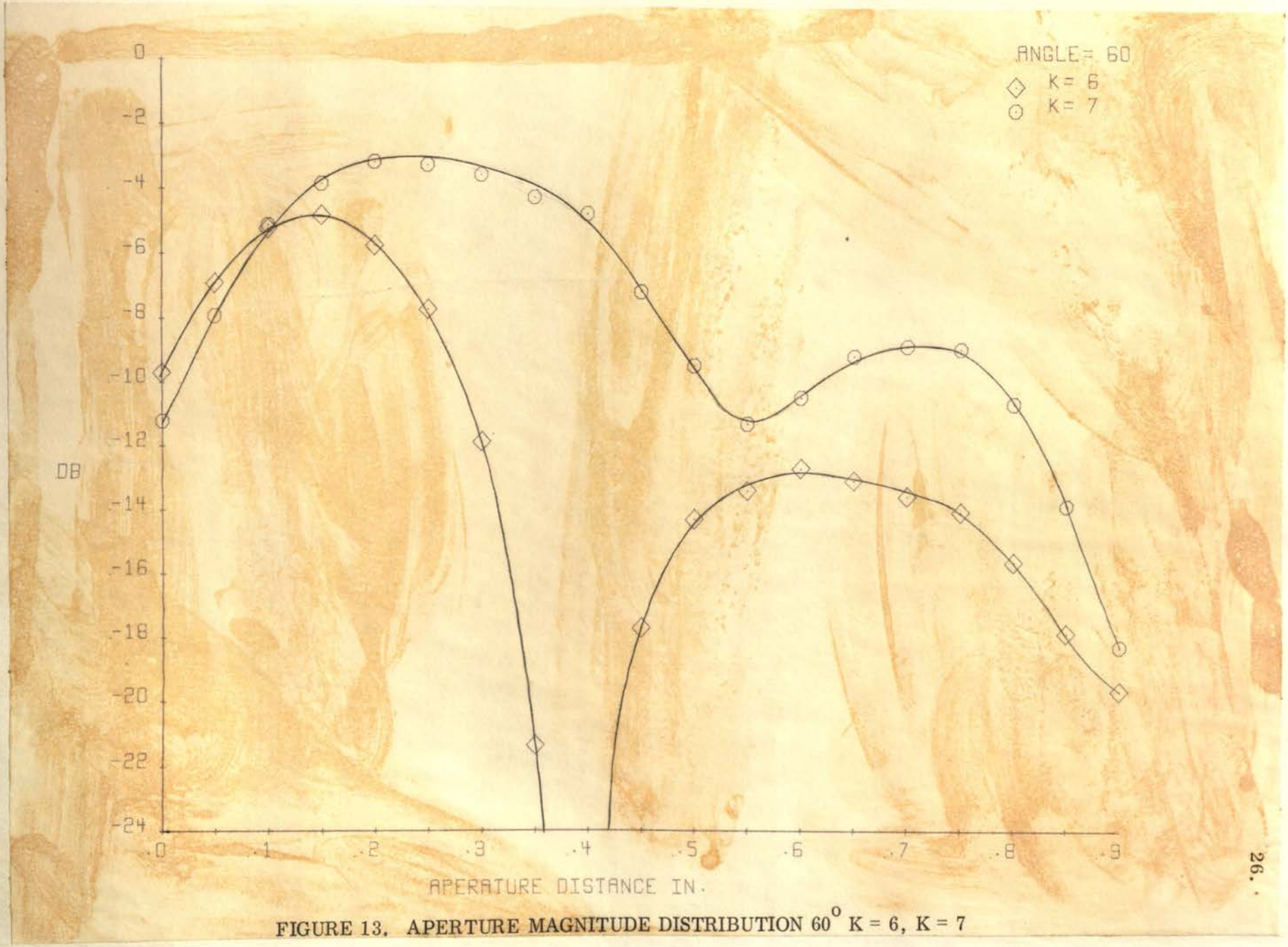

FIGURE 13. APERTURE MAGNITUDE DISTRIBUTION 60^{o} K = 6, K = 7

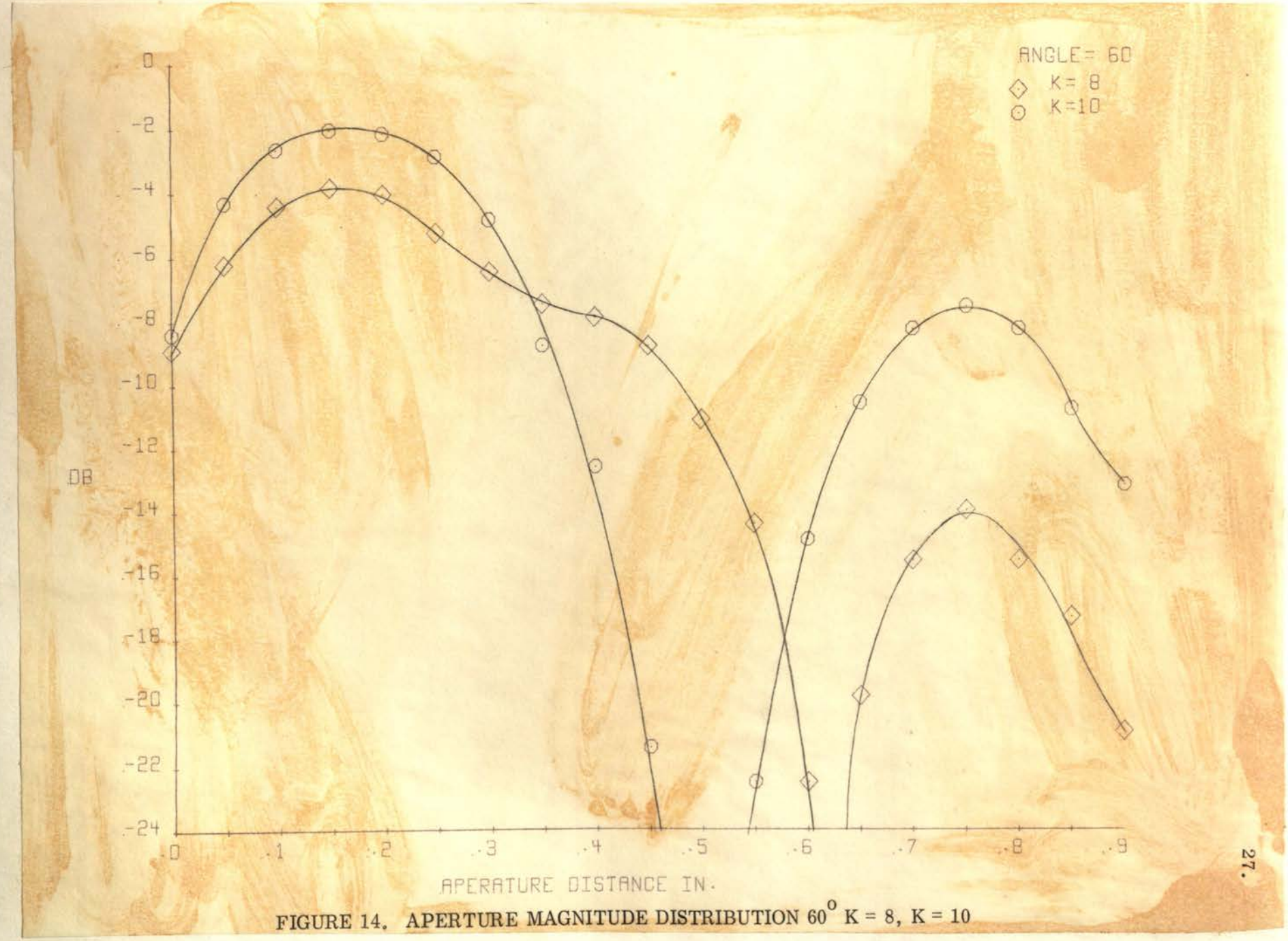

FIGURE 14. APERTURE MAGNITUDE DISTRIBUTION 60^{o} K = 8, K = 10

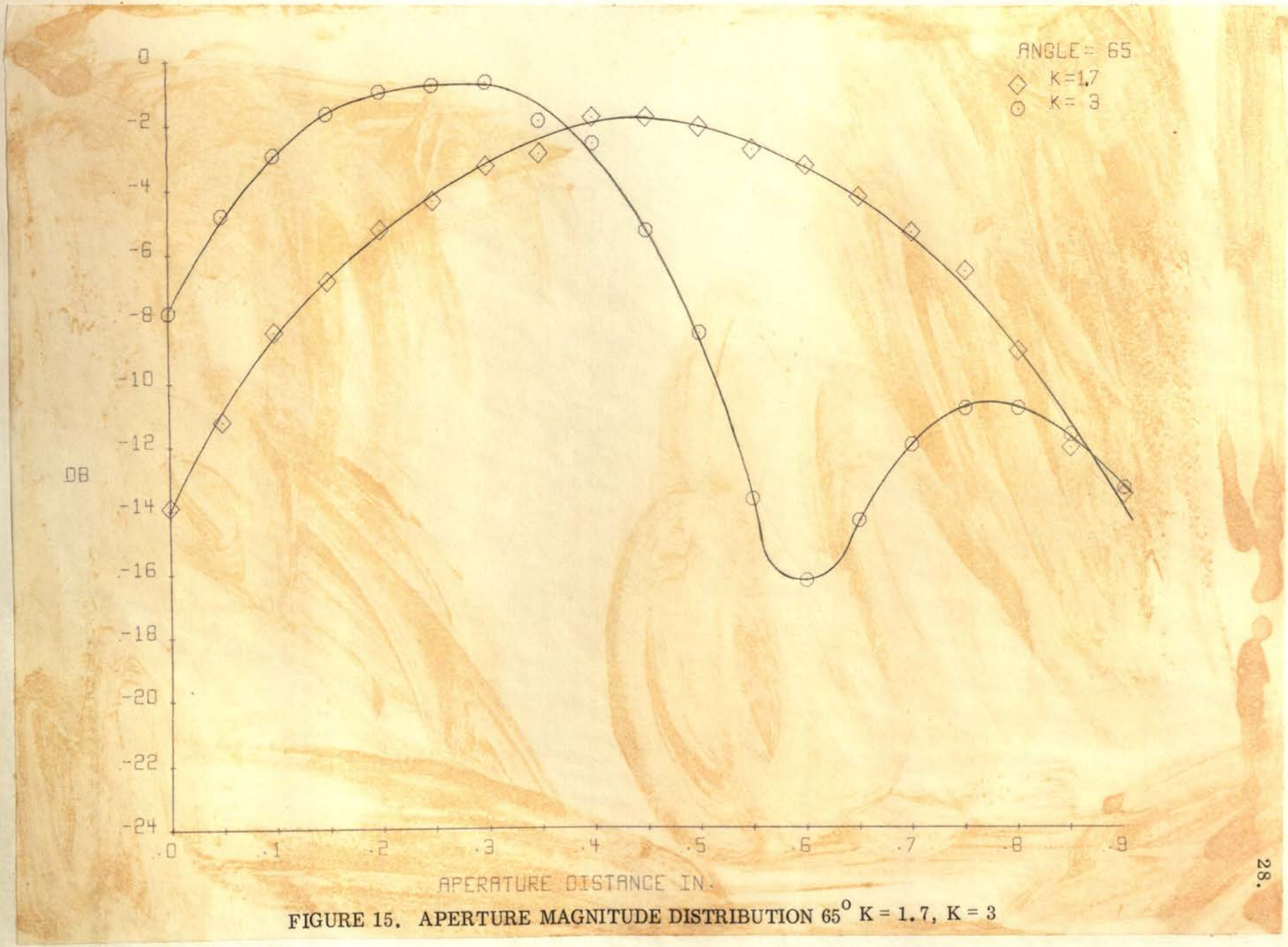

FIGURE 15. APERTURE MAGNITUDE DISTRIBUTION 65^{O} K = 1.7, K = 3

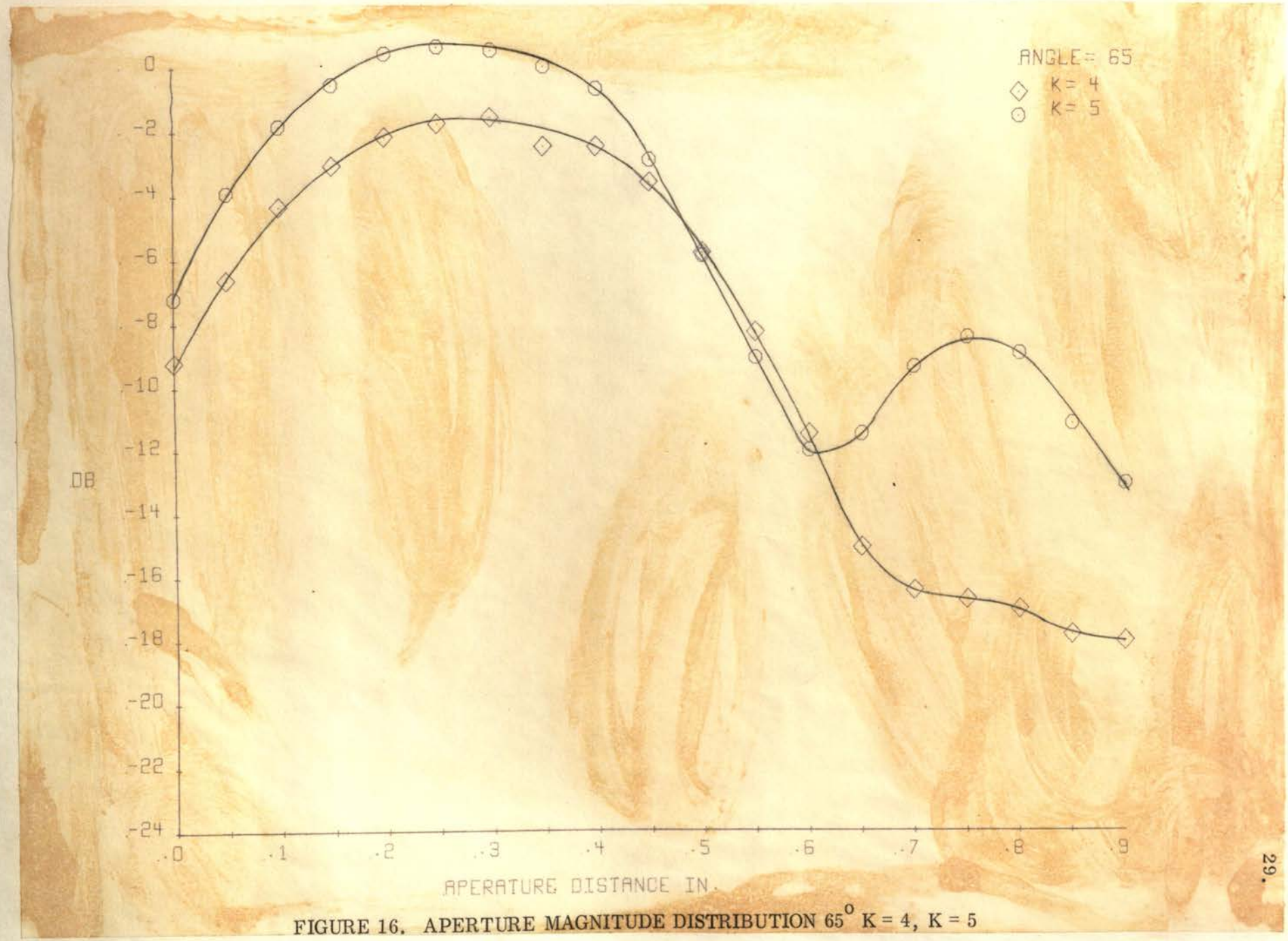

FIGURE 16. APERTURE MAGNITUDE DISTRIBUTION 65° K = 4, K = 5

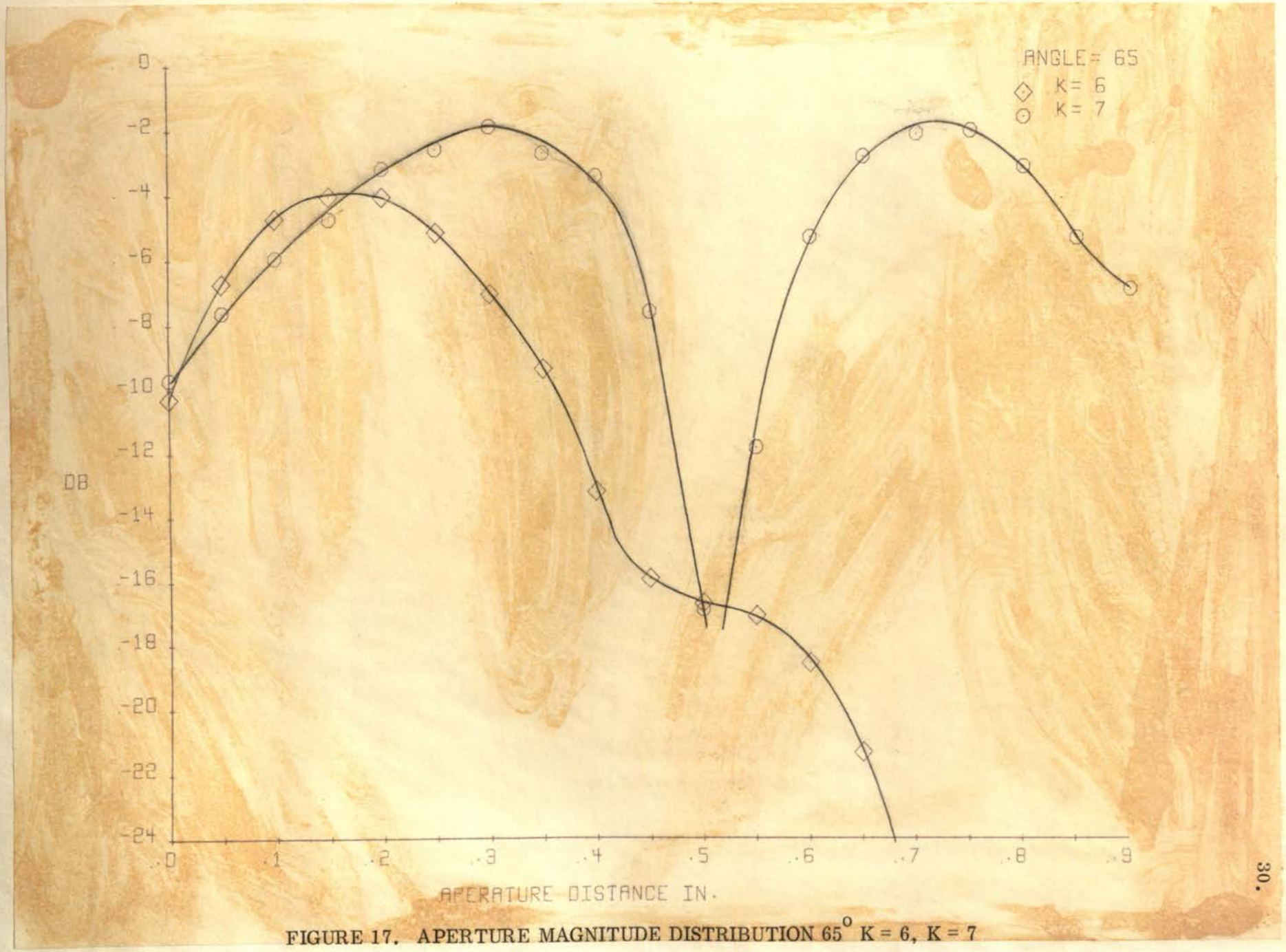

FIGURE 17. APERTURE MAGNITUDE DISTRIBUTION 65° K = 6, K = 7

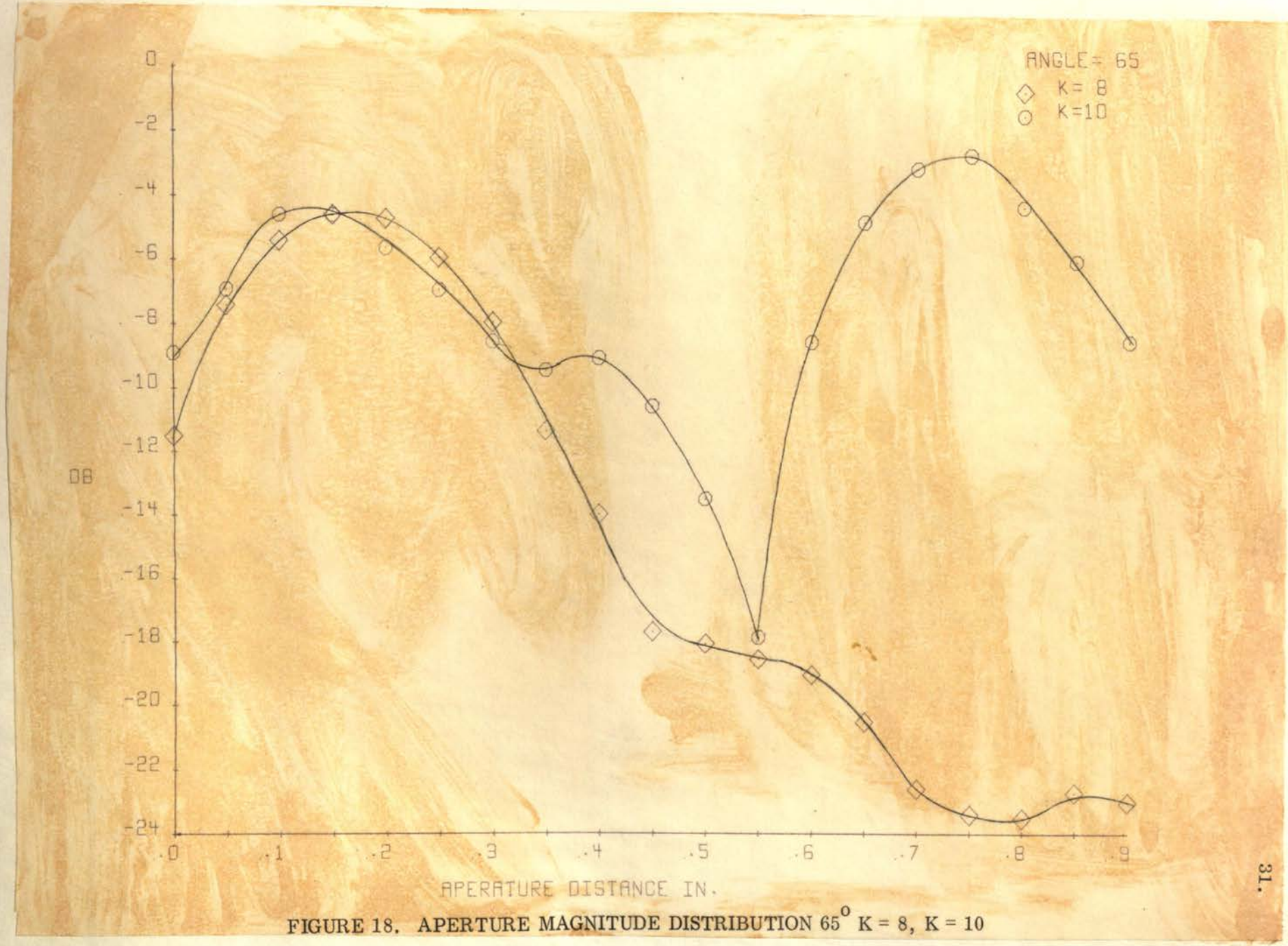

FIGURE 18. APERTURE MAGNITUDE DISTRIBUTION 65^{o} K = 8, K = 10

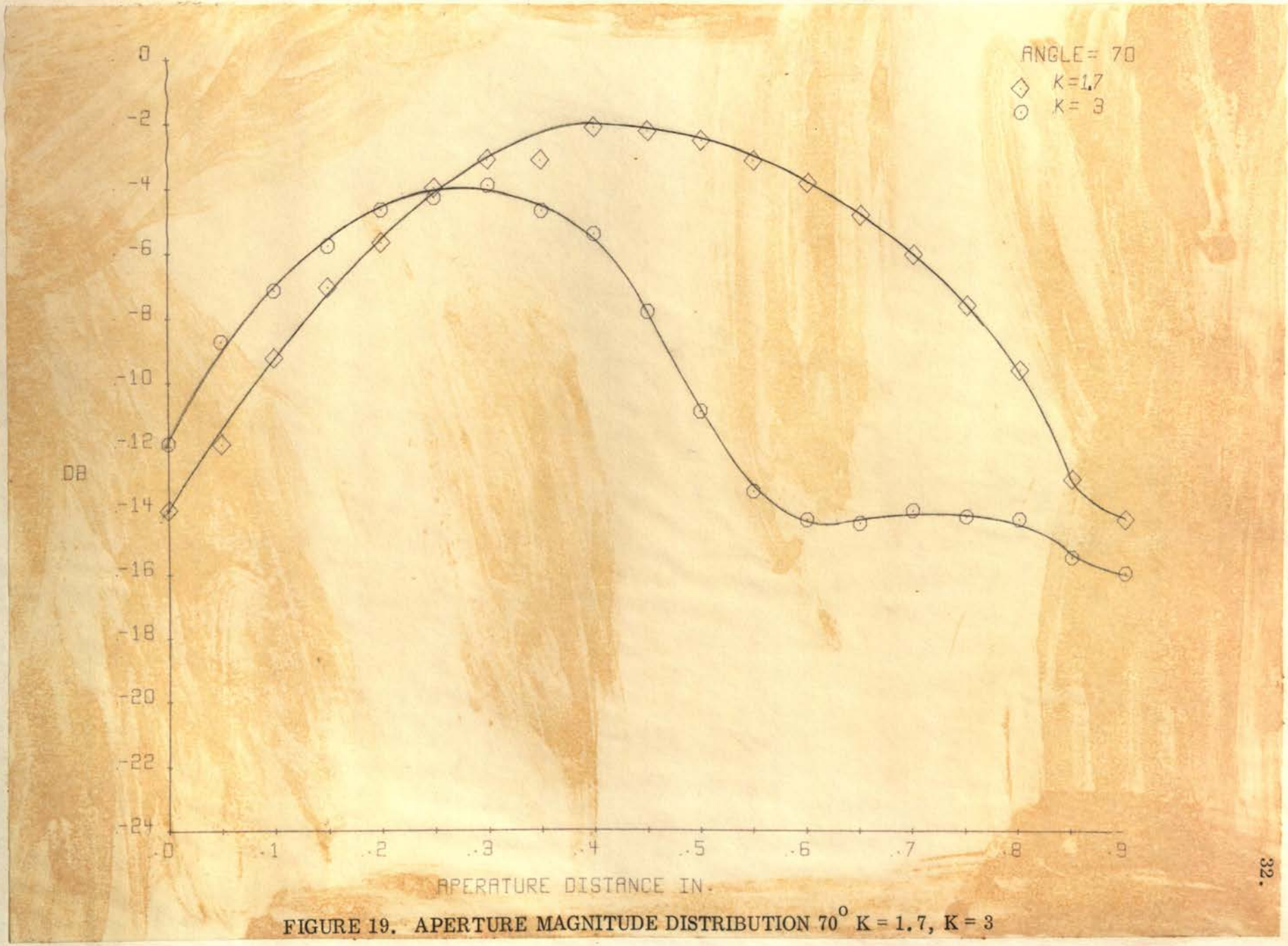

FIGURE 19. APERTURE MAGNITUDE DISTRIBUTION 70^{o} K = 1.7, K = 3

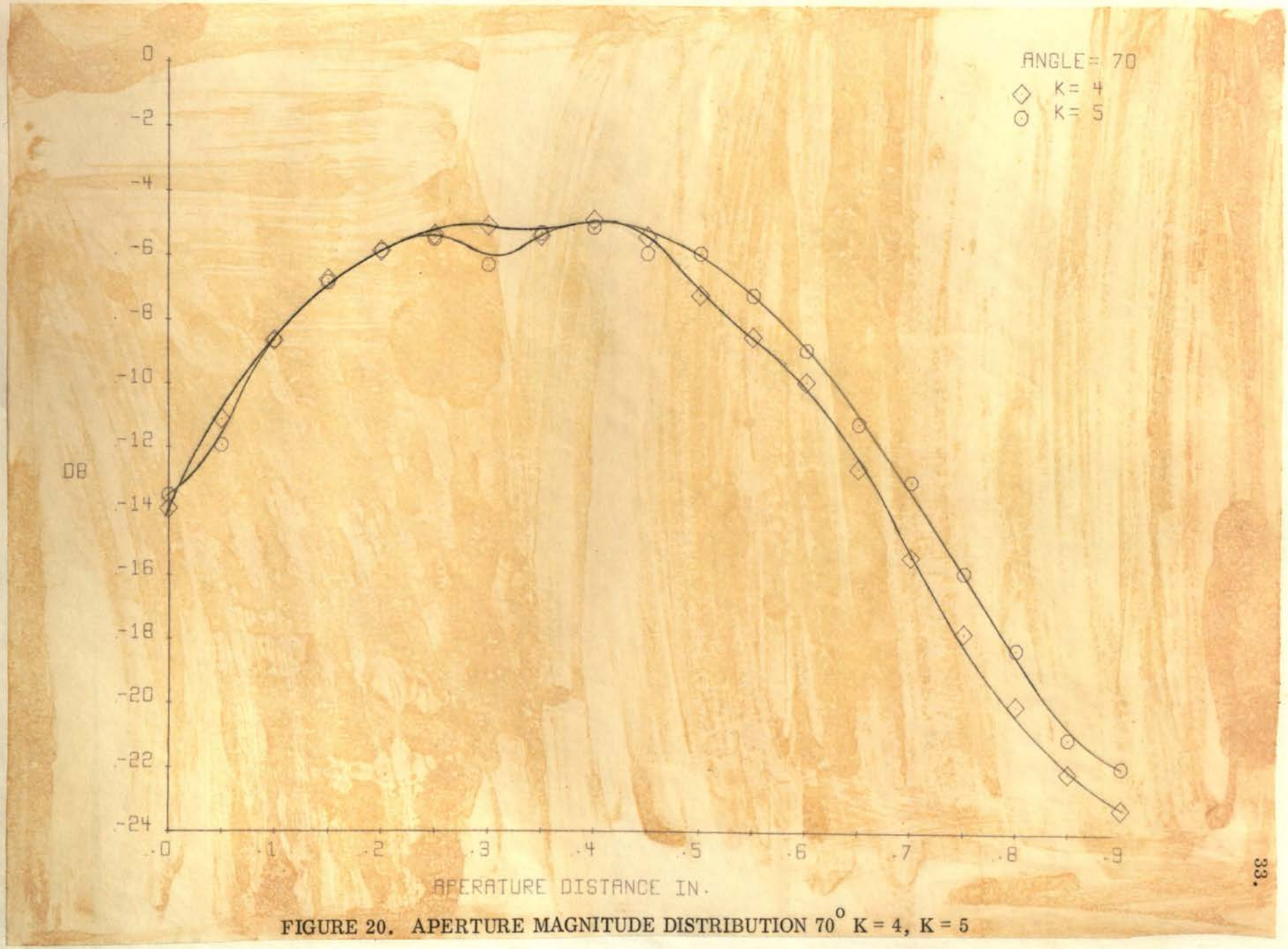

FIGURE 20. APERTURE MAGNITUDE DISTRIBUTION 70^{o} K = 4, K = 5

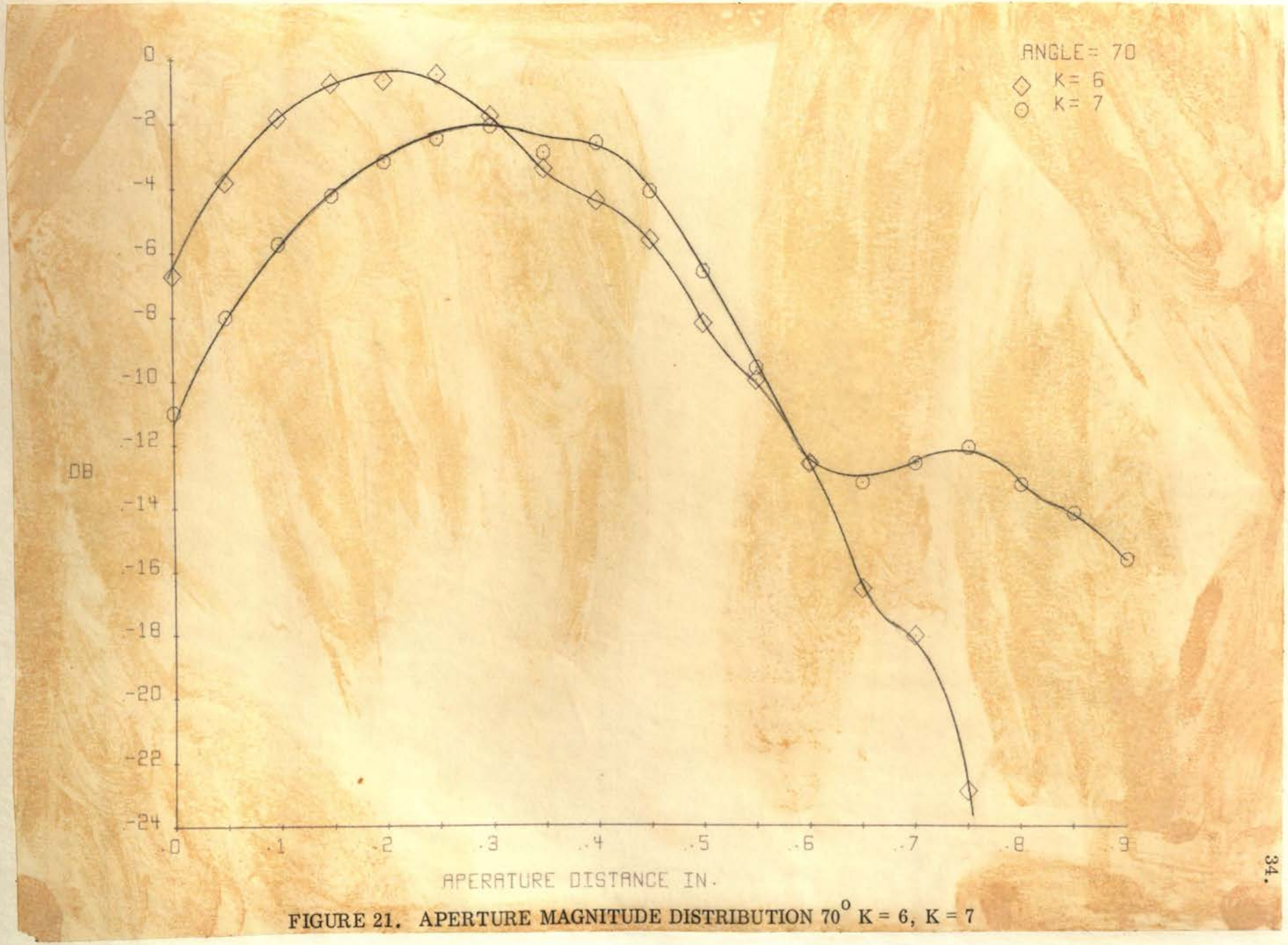

FIGURE 21. APERTURE MAGNITUDE DISTRIBUTION 70^{o} K = 6, K = 7

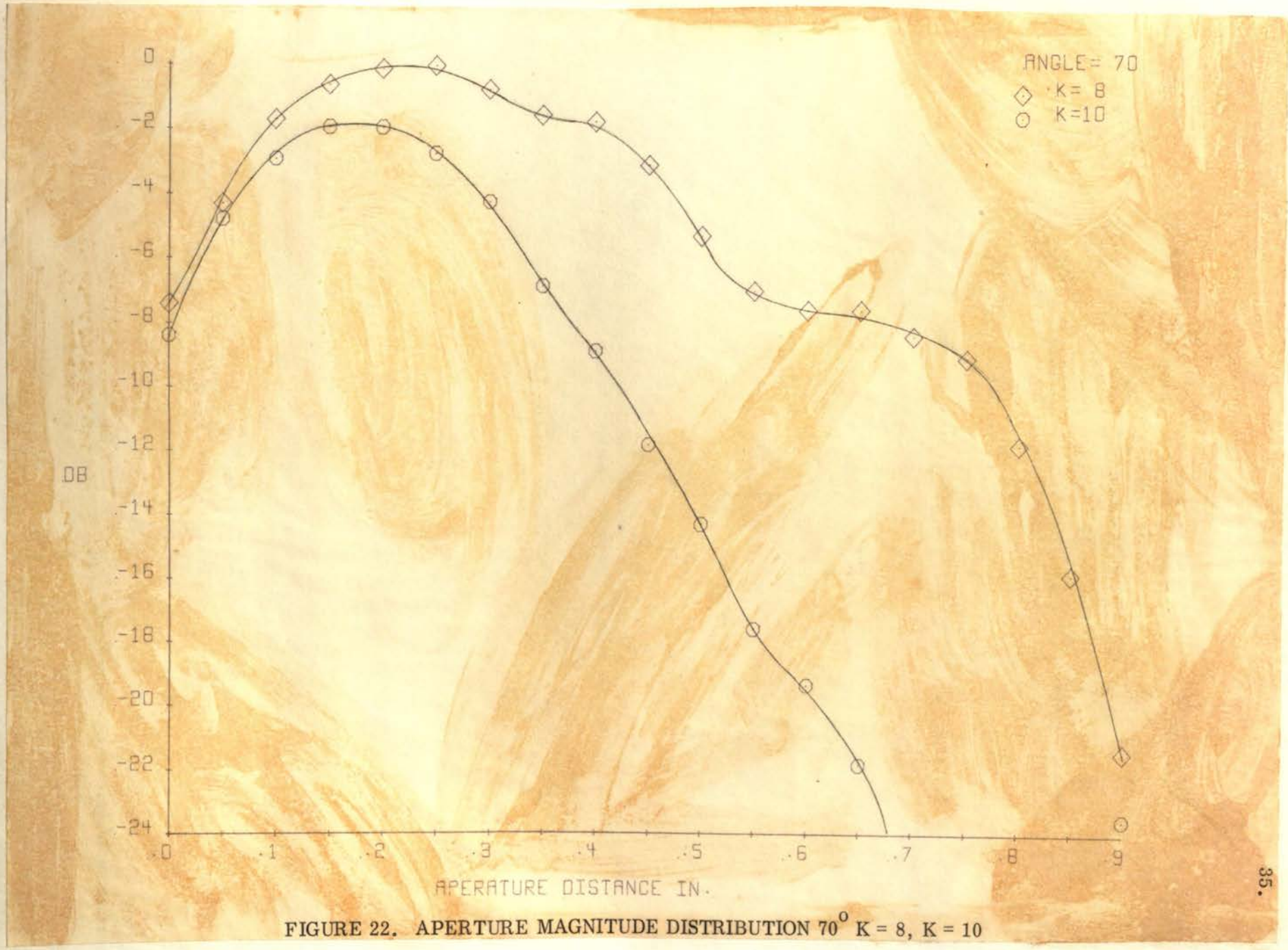

FIGURE 22. APERTURE MAGNITUDE DISTRIBUTION 70^{o} K = 8, K = 10

V. PARTIALLY FILLED WAVEGUIDE APERTURE DISTRIBUTION APPROXIMATION

A direct mathematical analysis of the wedge-loaded waveguide aperture is difficult because of the boundary region between the dielectric material and free space, which varies in the direction of propagation. It is desired to approximate this configuration with a model which is mathematically soluble. The most obvious approximation of this nature is the partially filled waveguide, illustrated below:

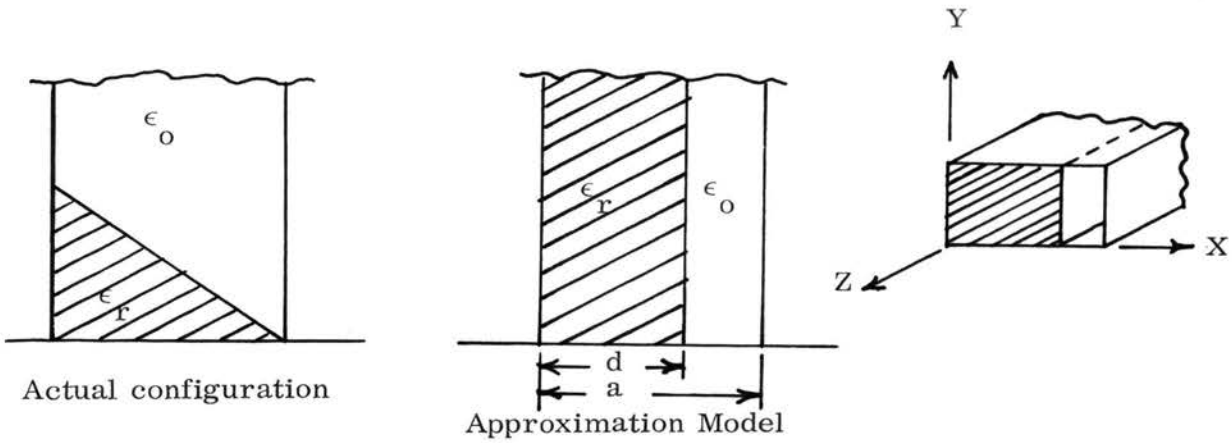

The distance d is a parameter which can be varied to produce amplitude distribution which correspond to those measured in the actual configuration. Ideally, a distance should be found which is fixed for a given wedge angle θ. That is, the geometry of the approximation model should not have to vary with changes in permittivity.

The solution of the partially filled waveguide is discussed by Pincherle[12] and Harrington[6] and is summarized in Appendix A. As there shown, modes with electric fields in both the Y and Z directions are possible. However, because the aperture was fed with the TE_{10} mode with electric field in the Y direction only, and the boundary was parallel to this direction, it was expected

that only TE_{mo} modes should be produced in the actual configuration. Correspondingly, only these modes should appear in the approximation model. With this restriction, the electric field in the dielectrically filled section of the partially filled waveguide is (see Appendix A):

$$E_1 = C_1 \sin K_{x1} X e^{jk_z Z} \tag{1}$$

and in the free-space region:

$$E_2 = C_2 \sin K_{x2} (a - x) e^{jk_z Z} \tag{2}$$

The propagation constants must satisfy the separation equations:

$$K_{x1}^2 + K_z^2 = \omega^2 \mu_1 \epsilon_1 \qquad \text{where } \epsilon_1 = \epsilon_r \epsilon_o \tag{3}$$

$$K_{x2}^2 + K_z^2 = \omega^2 \mu_2 \epsilon_2 \qquad \epsilon_2 = \epsilon_o \tag{4}$$

and also the characteristic equation determined by matching at the dielectric-free-space boundary:

$$\frac{K_{x1}}{\mu_1} \cot K_{x1} d = \frac{-K_{x2}}{\mu_2} \cot K_{x2} (a - d) \tag{5}$$

Subtracting 1) from 2) and substituting into the characteristic equation, and also noting that $u_1 = u_2 = u_o$:

$$K_{x1} \cot K_{x1} d = -\sqrt{K_{x1}^2 - \omega^2 \mu_o (\epsilon_r - 1)} \cot \sqrt{K_{x1}^2 - \omega^2 \mu_o (\epsilon_r - 1) \epsilon_o} (a - d) \tag{6}$$

This equation must be solved numerically for K_{x1}, and then K_{x2} evaluated from (1) and (2). The difficulty in solution lies in the fact that the equation has multiple roots and also that K_{x2} may be imaginary for real K_{x1}.

E_2 then has the form:

$$\mathbf{E}_2 = C_2 \sin jK_{x2}(a - x) = j\, C_2 \sinh E_{x2}(a - x) \tag{7}$$

where K_{x2} itself is a real constant.

The separation equation becomes:

$$K_{x1} = \cot K_{x1} d = \sqrt{K_{x1}^2 - \omega^2 \mu_o (\epsilon_r - 1)\epsilon_o} \coth \sqrt{K_{x1}^2 - \omega^2 \mu_o (\epsilon_r - 1)\epsilon_o}\,(a-d) \tag{8}$$

Thus the solution can be either the matching of two sine functions, or a sine function and a hyperbolic sine function.

The above analysis will be applied in an attempt to approximate the 50^o, K = 1.7, K = 5, and K = 10 amplitude distributions, for which relatively clean fundamental, second, and third order modes appear, respectively. From (1), a maximum real value of K_{x2} can be calculated:

$$(K_{x2})^2_{\text{maximum}} = \omega^2 \mu_o \epsilon_o \tag{9}$$

For a frequency of 10 GHz:

$$K_{x2\ \text{maximum}} = \frac{2\pi \times 10^{10}}{3 \times 10^8} = 209.5 \tag{10}$$

The maximum value of the argument (K_{x2}) x equals:

$$209.5 \times .0254 \cong 5.3 < 2\pi \tag{11}$$

Thus the solution in the free-space region must be a slowly varying sinusoidal function if K_{x2} is real. If K_{x2} is imaginary, the hyperbolic sine solution in the free-space region will not vary rapidly. This greatly restricts this approximation since the rapidly changing peaks or lobes in the amplitude response curves must be restricted to the dielectric region. (Figure 23)

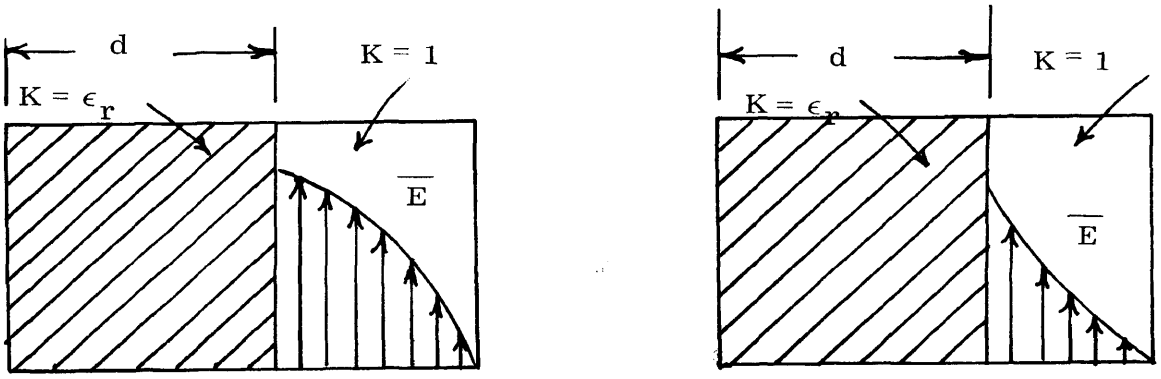

Figure 23 Possible Solutions in Free-Space Region

The resultant solutions as obtained in the numerical evaluation, obtained by digital computer interation, are as follows:

Dielectric Constant	K_{x1}	K_{x2}	
1.7	138.3	107.5	imaginary
5	282.6	309.2	"
10	431.4	456.9	"

The plots of these solutions, given in Figures 24 through 26, showing their approximations to the actual distributions. Note that the dielectric boundary was placed almost entirely across the aperture with a d equal to 0.8". This was necessary in order to match the third order mode peaks in the K = 10 dielectric. It was left fixed at this position in order to form a consistant approximation model, i.e., one in which d is fixed. The phase distribution of the approximation model is constant across the aperture for the K = 1.7 approximation and has a single 180^{o} discontinuity at 0.42" for the K = 4 approximation. For the K = 10 approximation model, there will be two 180^{o} discontinuities one at 0.28" and one at 0.56". These phase distributions

agree very well with the experimental plots. See Figures 29 and 35.

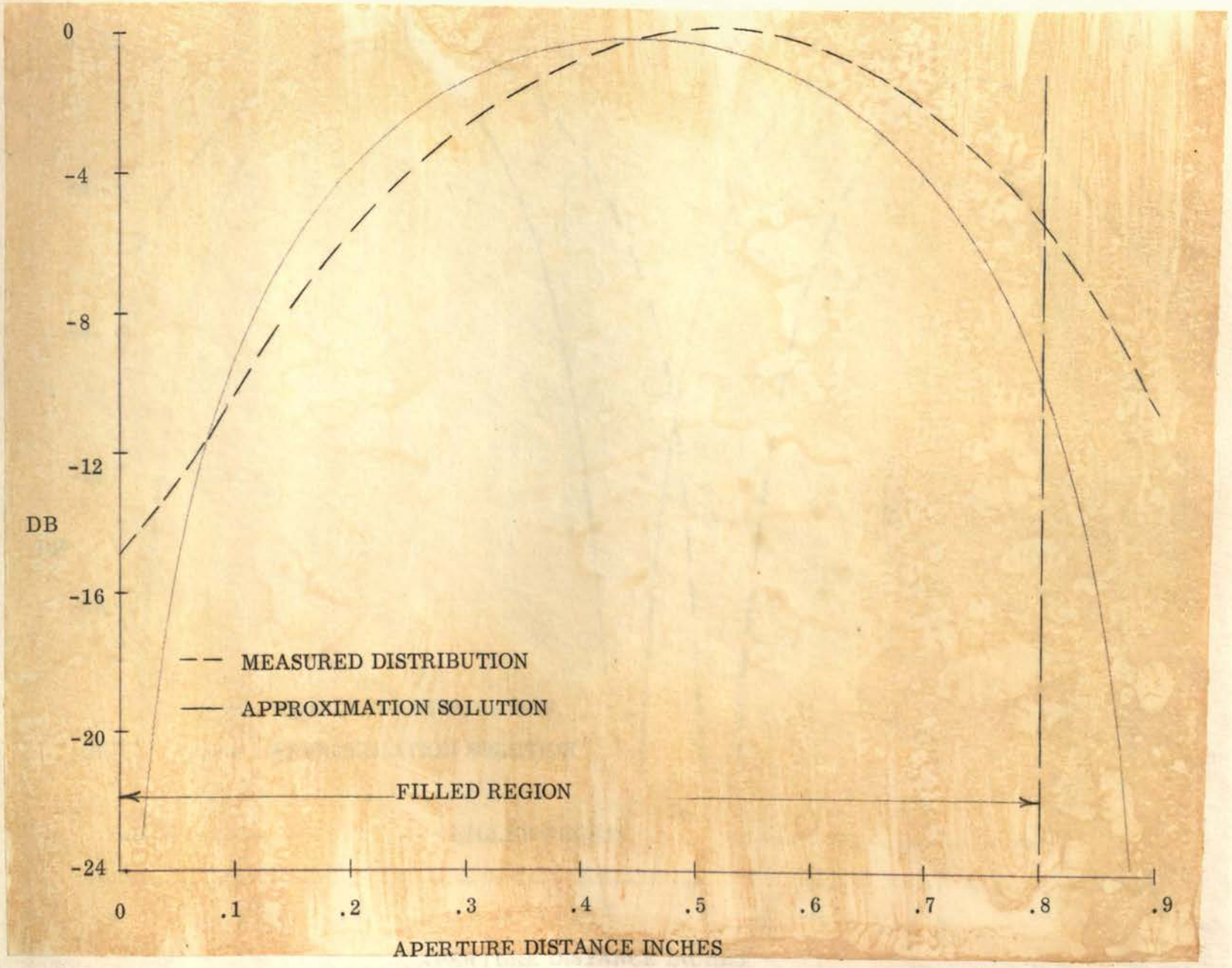

FIGURE 24. APPROXIMATION SOLUTION 50^{O} WEDGE, K = 1.7

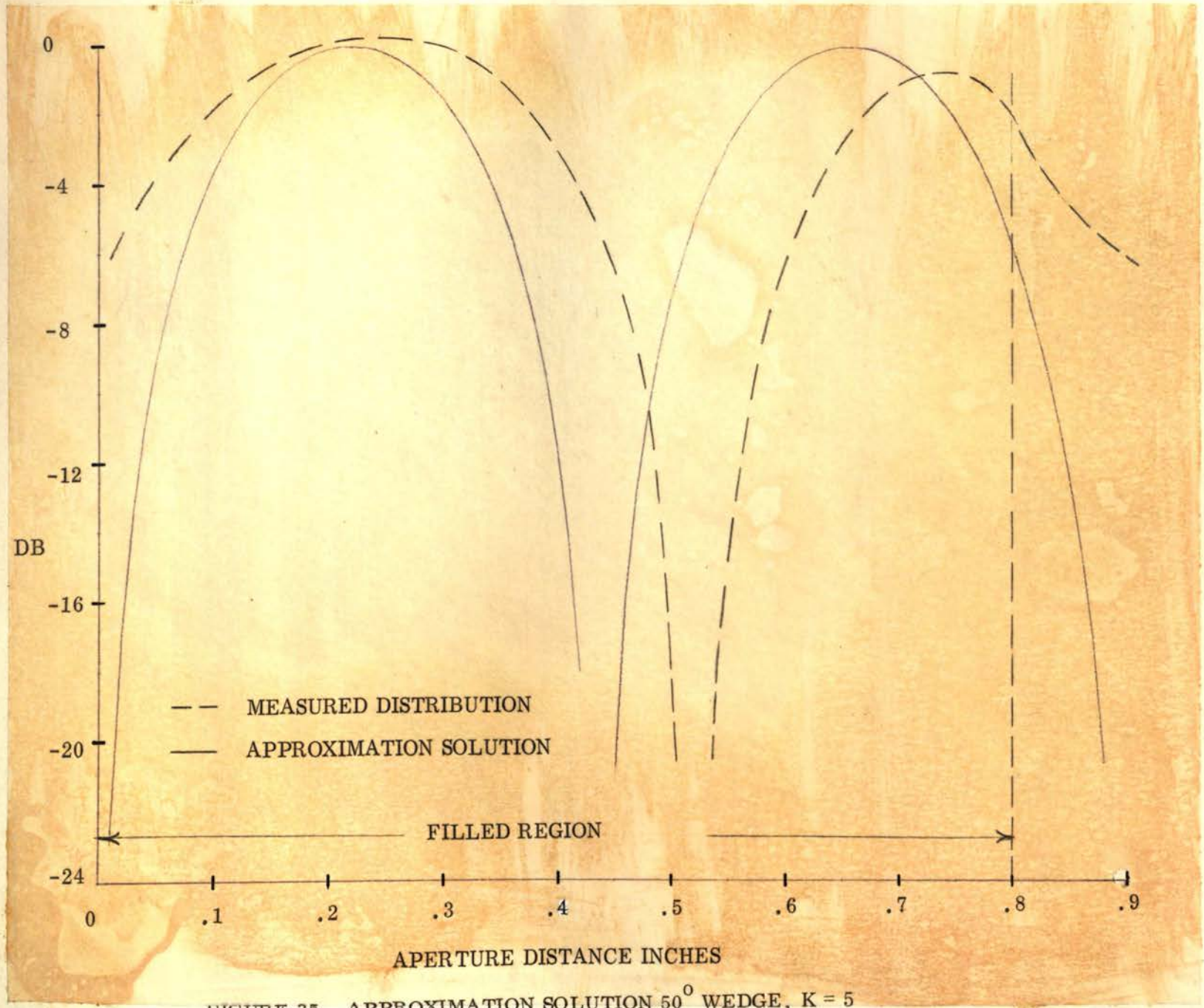

FIGURE 25. APPROXIMATION SOLUTION 50° WEDGE, K = 5

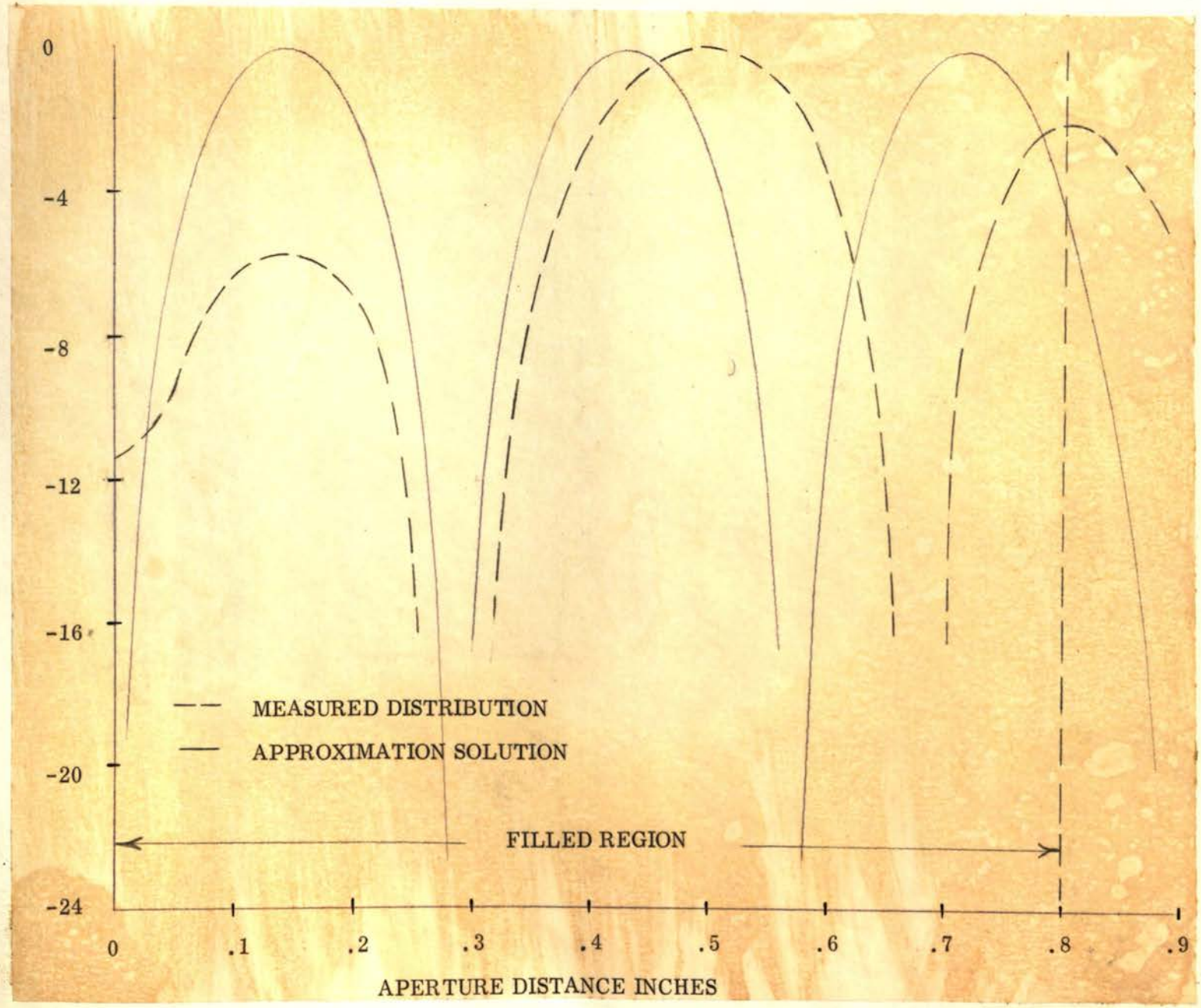

FIGURE 26. APPROXIMATION SOLUTION 50° WEDGE, K = 10

VI. CORRELATION OF APERTURE DISTRIBUTIONS AND FAR-FIELD PATTERNS

The relation between the change in permittivity and the change in far-field pattern for a fixed angle is ultimately the consideration of most importance. This relation is, lacking a definite mathematical solution, of an empirical nature. However, a correlation can be made between the appearance of higher order modes in the waveguide aperture and the far-field pattern shape. As shown by Harrington and others, the far-field pattern is directly related to the magnitude and phase of the electric field in each segment of the aperture. This relationship, outlined in Appendix B, was the basis for the numerical integration used to predict far-field patterns. Associated with the appearance of higher order modes are large phase shifts, especially at minimum amplitude points, which have significant effect on the appearance of the far-field patterns.

A. 50° WEDGE INSERTS

An excellent example of the effect of a pronounced higher order mode is shown in the far-field pattern for the 50°, K = 5 dielectric wedge. (Figure 28) The amplitude distribution is shown in Figure 4 and the phase distribution in Figure 29. Here the definite second order mode appears in the amplitude distribution, with a 180° phase shift in the phase distribution at the amplitude minimum. The resulting far-field pattern shows a definite two-lobe structure with an inflection along the central axis of the pattern (90° in azimuth). This pattern is to be expected from the symmetry of the

magnitude and phase curves and is verified by the pattern produced by numerical integration (Figure 30).

The patterns for the lower permittivity at this angle have the single-lobed distribution approximating that of the open aperture. The higher order mode appearing in the K = 3 and K = 4 amplitude distributions seems to have little effect on the far-field except perhaps to produce a slight broadening.

The unusual amplitude distribution of the K = 6 wedge produces a skewed pattern with largest far-field magnitude toward the side of the aperture with larger magnitude distribution.

The semi-third order mode of the K = 7 amplitude distribution produces a double-lobed pattern symmetric about the central axis. The phase distribution (Figure 32) also has a symmetrical shape approximating that of the third order mode phase distribution. Logically, a symmetrical magnitude and phase distribution should produce a symmetrical far-field pattern, and this pattern is verified by numerical integration. (Figure 33)

Despite the unusual shape of the K = 8 amplitude curve, the far-field pattern reverted to a single-lobe pattern. The fundamental mode was still dominant in producing the far-field pattern. The K = 10 aperture distribution again produces a double-lobe pattern, but slightly asymmetric, with the minimum shifted 20° from the center axis.

For the 50° wedge inserts, no stable points were found in the far-field pattern shape with respect to change in dielectric constant. The patterns alternated between single and symmetrical double lobes, the double-

lobe patterns corresponding to the appearance of relatively "clean" higher order modes in the waveguide aperture. In theory, an aperture distribution which is symmetric in both magnitude and phase should produce a far-field pattern which has a maximum on the central axis. This would include the K = 7 and K = 10 far-field patterns. The variations in the patterns from this theoretical distribution are indicative of the highly critical dependence of the far-field pattern on the aperture phase distribution.

B. 60^{o} WEDGE INSERTS

The patterns for the 60^{o} wedges, especially at the higher dielectric constants, form the most interesting and useful patterns. For the K = 6 dielectric wedge, a slight double lobe occurs (Figure 38) with the maximum of the larger lobe 35^{o} from the central axis. This corresponds to the appearance of the second order mode in the aperture amplitude distribution.

For the K = 7 wedge the far-field pattern collapsed back to the single-lobe pattern, but with the lobe angle tilted about 10^{o} from the central axis. The energy appeared to be concentrated in the right quadrant of the radiation area. This return to a single lobe coincides with the re-establishment of the fundamental mode in the aperture. The numerical integration (Figure 40) agrees with the measured pattern.

The K = 8 wedge produced the most drastically shifted single lobe with a very minor secondary lobe (Figure 41). The major lobe direction is shifted about 35^{o} to the right of the central axis with almost no energy appearing in the left quadrant. The beam width of this main lobe was fairly broad,

about 50^{o}. The corresponding aperture distribution has become extremely complex, with several higher modes and a deep minimum at 0.6". The phase shift (Figure 42) changed significantly near the minimum.

The K = 10 far-field pattern breaks into two lobes, the major lobe resembling that for K = 8. This was expected, as the aperture magnitude distribution approached that for the second order mode.

The numerical integrations for the K = 8 and K = 10 wedges did not agree very well with the measured patterns. Probably there were errors in the phase distribution due to the complex higher order modes. The measured phase distributions appear in Figure 42.

The range from K = 6 to K = 10 at this 60^{o} wedge angle produced large and fairly well coordinated shifts in radiation pattern. By modulating permittivity over some part of this range, a useful scanning action could be produced.

C. 70^{o} WEDGE INSERTS

The 70^{o} patterns (Figures 43-46) were realtively uninteresting because there was almost no change in far-field pattern with permittivity change. This was expected, as there had been no large changes in aperture amplitude distribution so that the fundamental mode dominated for each wedge insert.

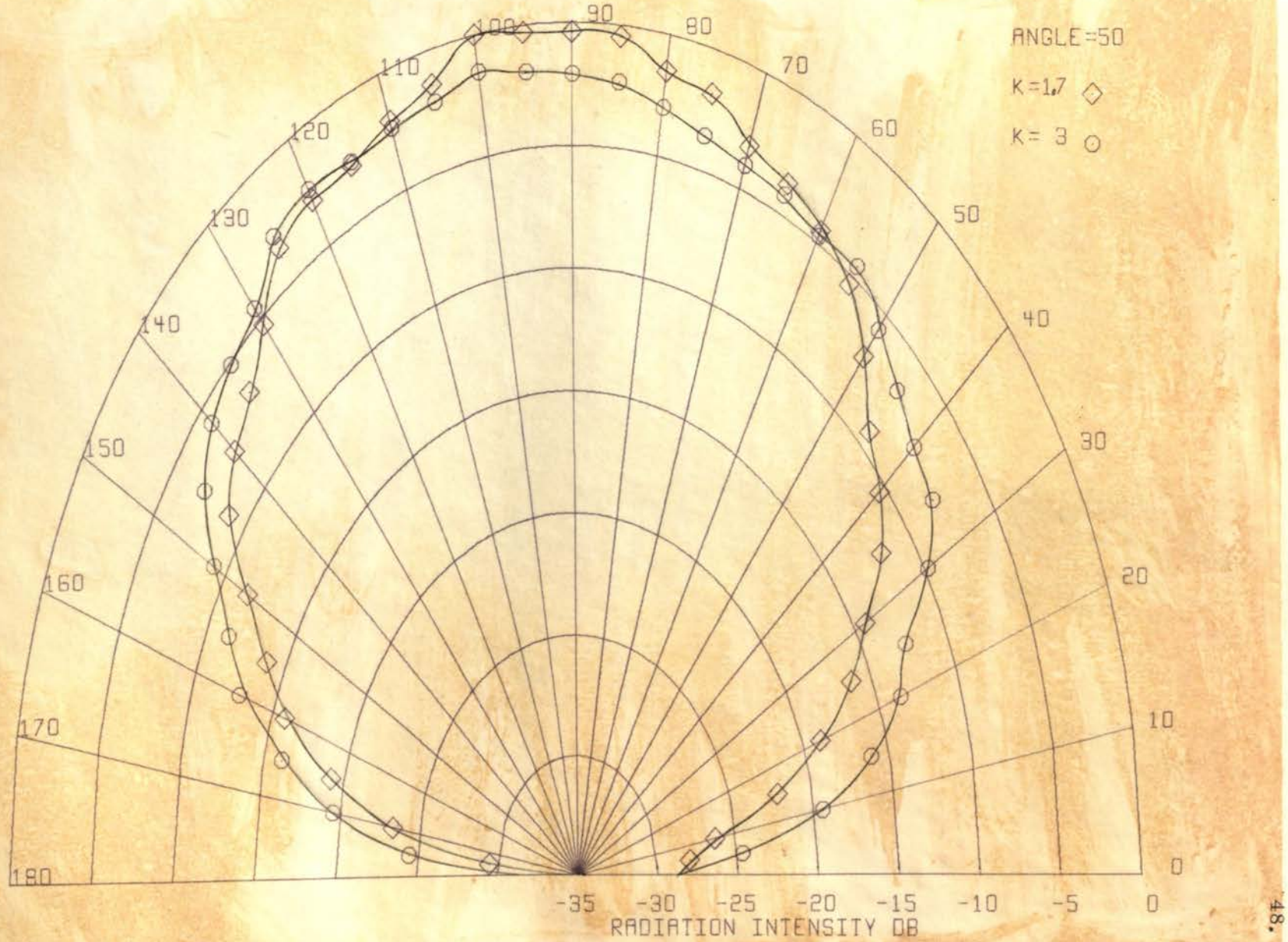

FIGURE 27. MEASURED RADIATION PATTERN 50^{O} K = 1.7, K = 3

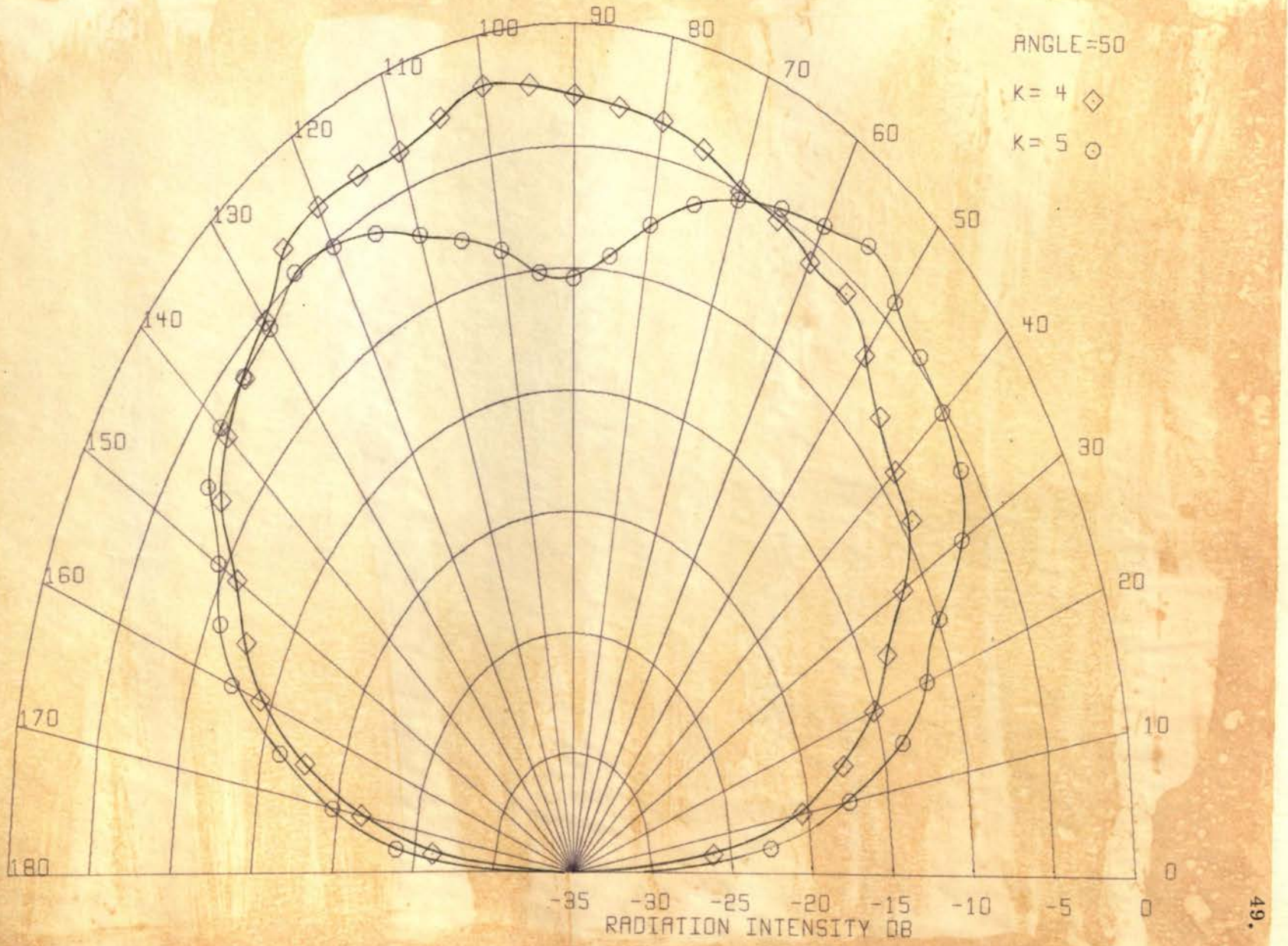

FIGURE 28. MEASURED RADIATION PATTERN 50^{o} K = 4, K = 5

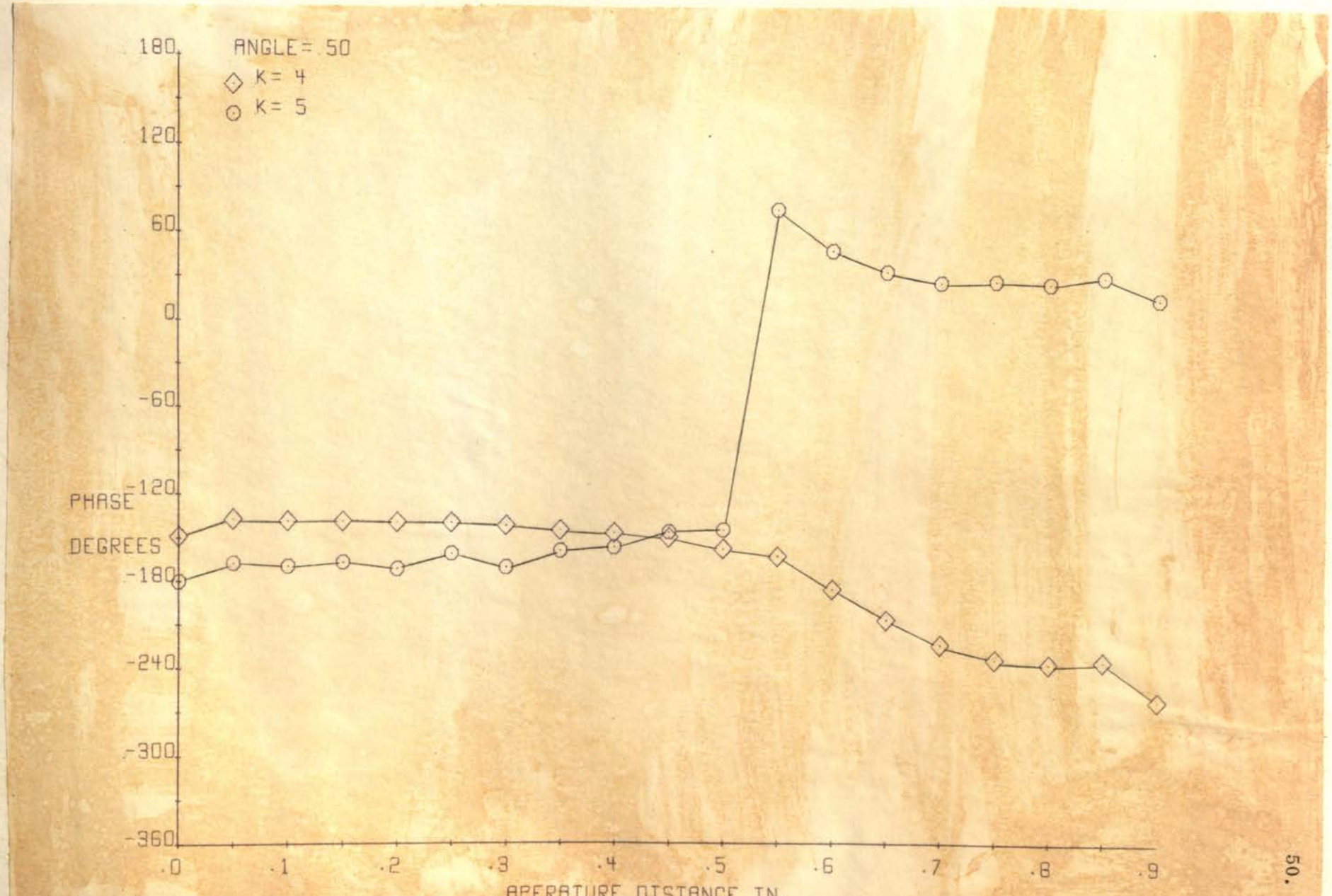

FIGURE 29. APERTURE PHASE DISTRIBUTION 50^{o} K = 4, K = 5

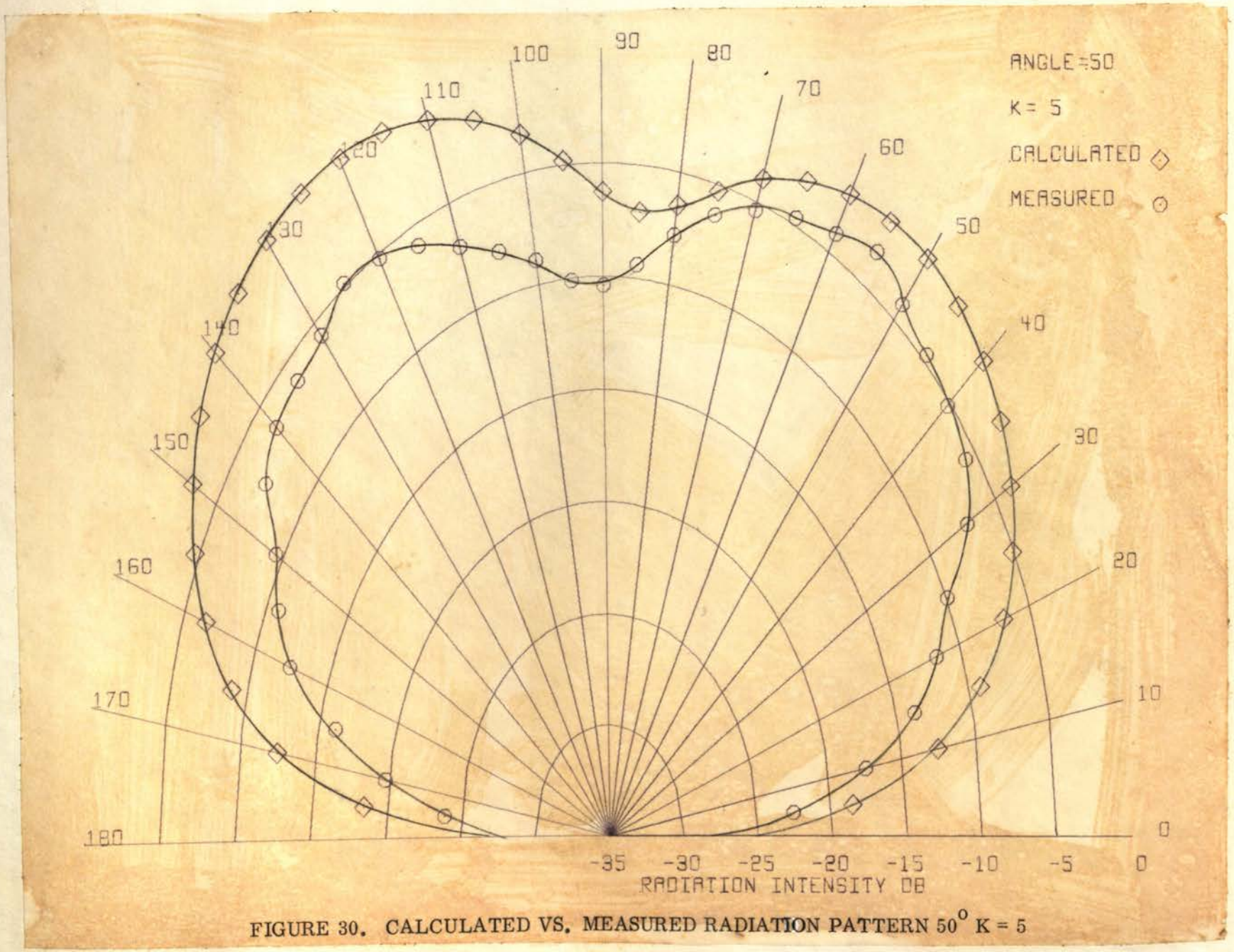

FIGURE 30. CALCULATED VS. MEASURED RADIATION PATTERN 50^{o} K = 5

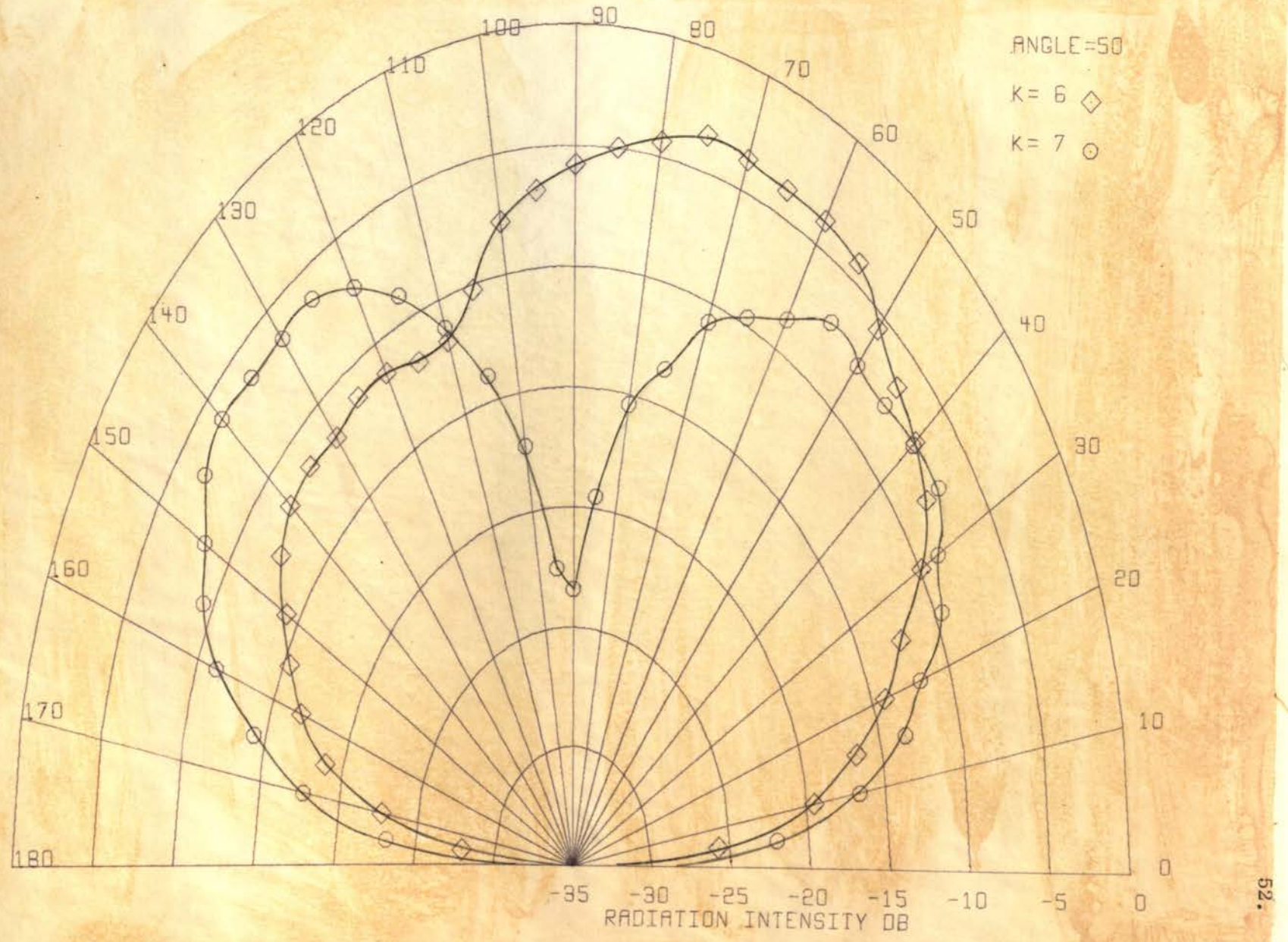

FIGURE 31. MEASURED PATTERN 50° K = 6, K = 7

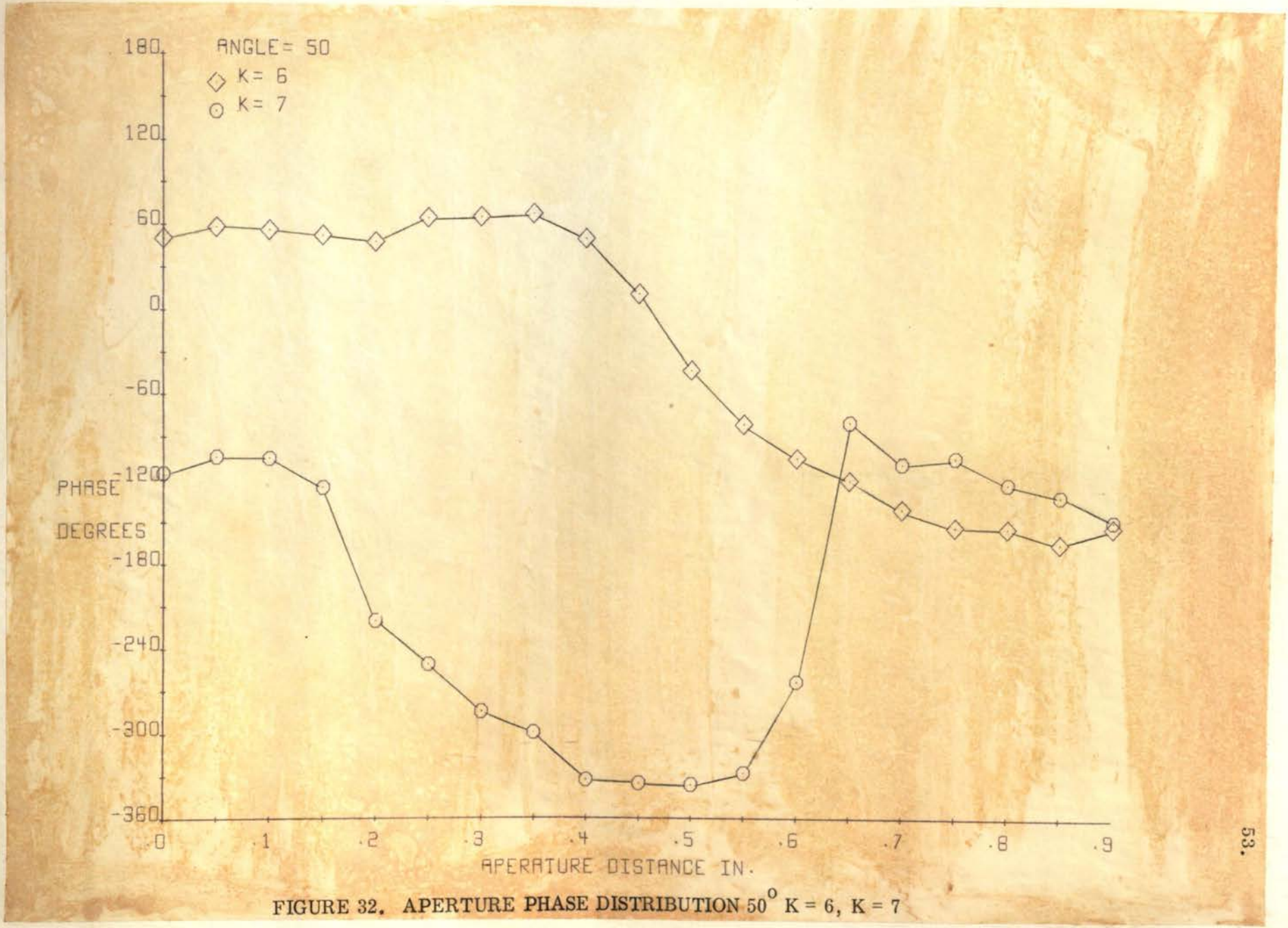

FIGURE 32. APERTURE PHASE DISTRIBUTION 50^{o} K = 6, K = 7

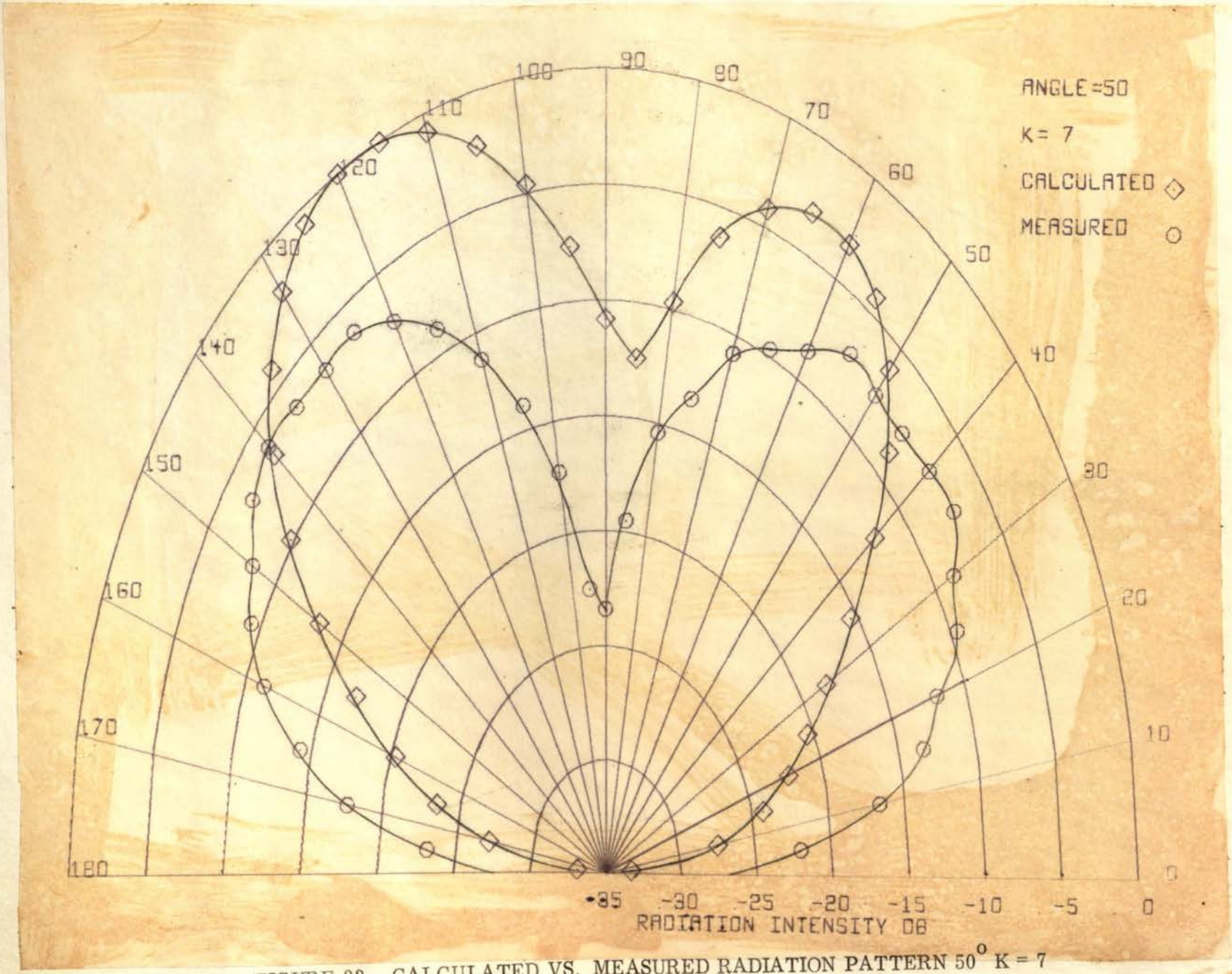

FIGURE 33. CALCULATED VS. MEASURED RADIATION PATTERN 50° K = 7

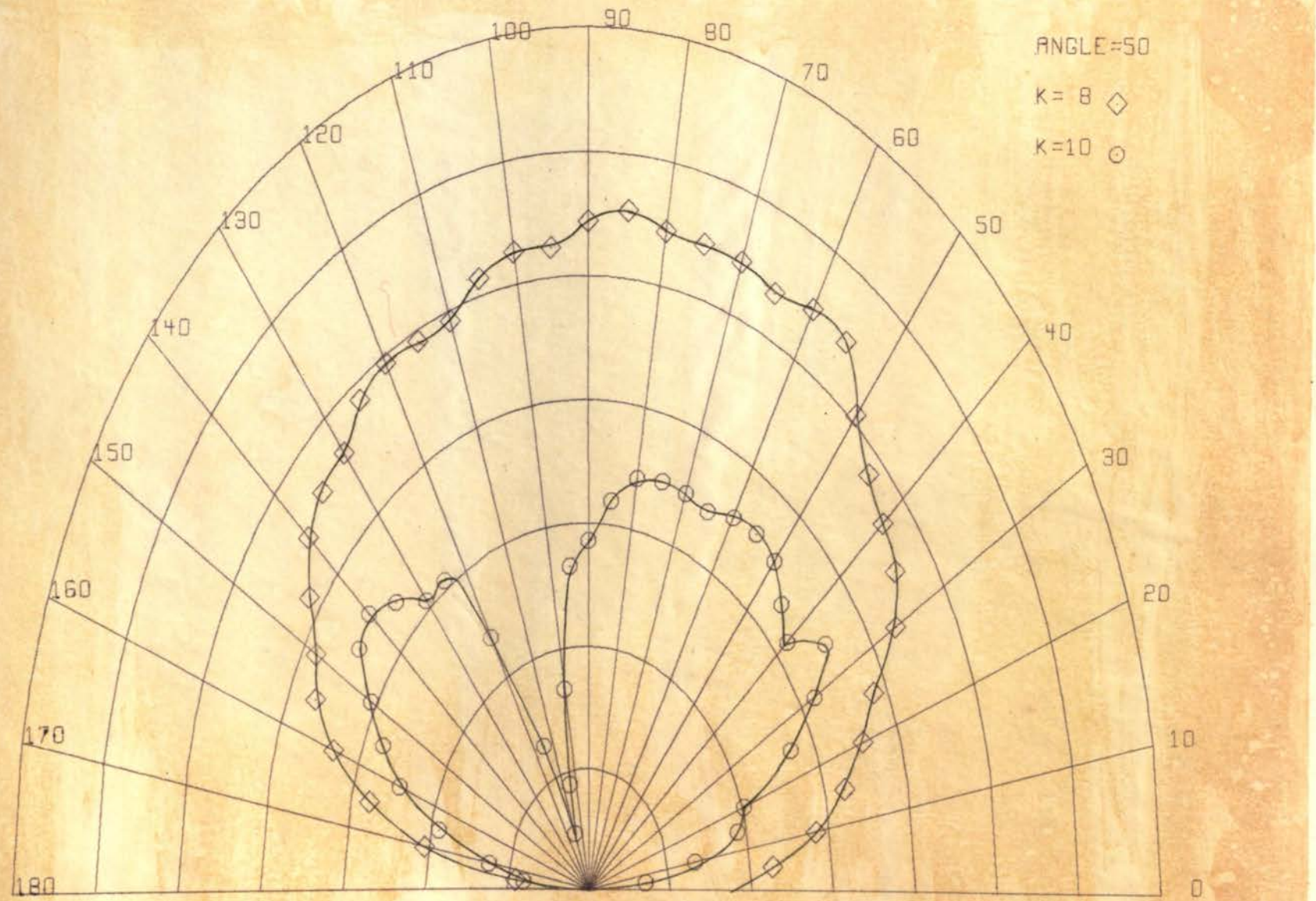

FIGURE 34. MEASURED RADIATION PATTERN 50^{o} K = 8, K = 10

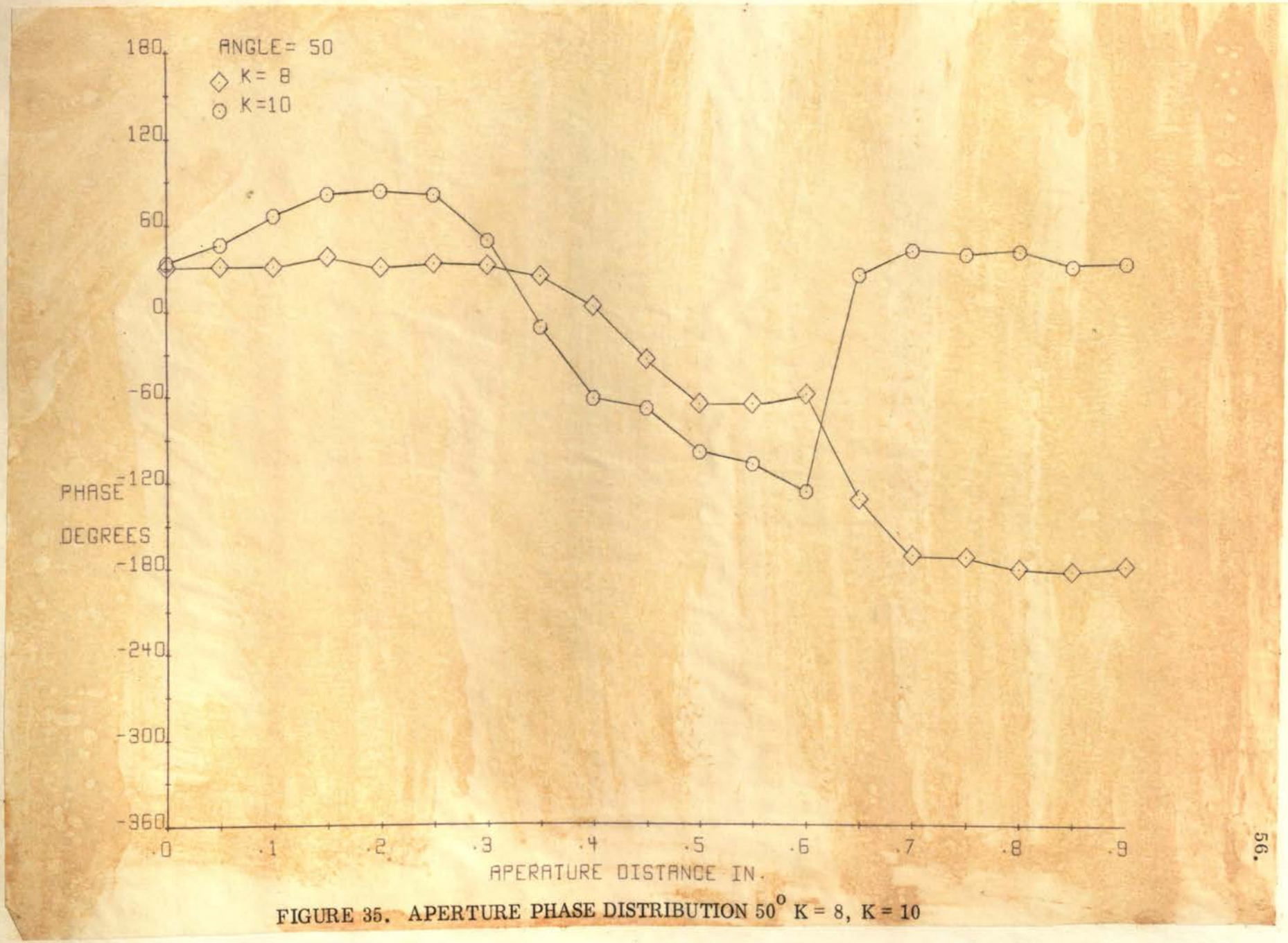

FIGURE 35. APERTURE PHASE DISTRIBUTION 50^{o} K = 8, K = 10

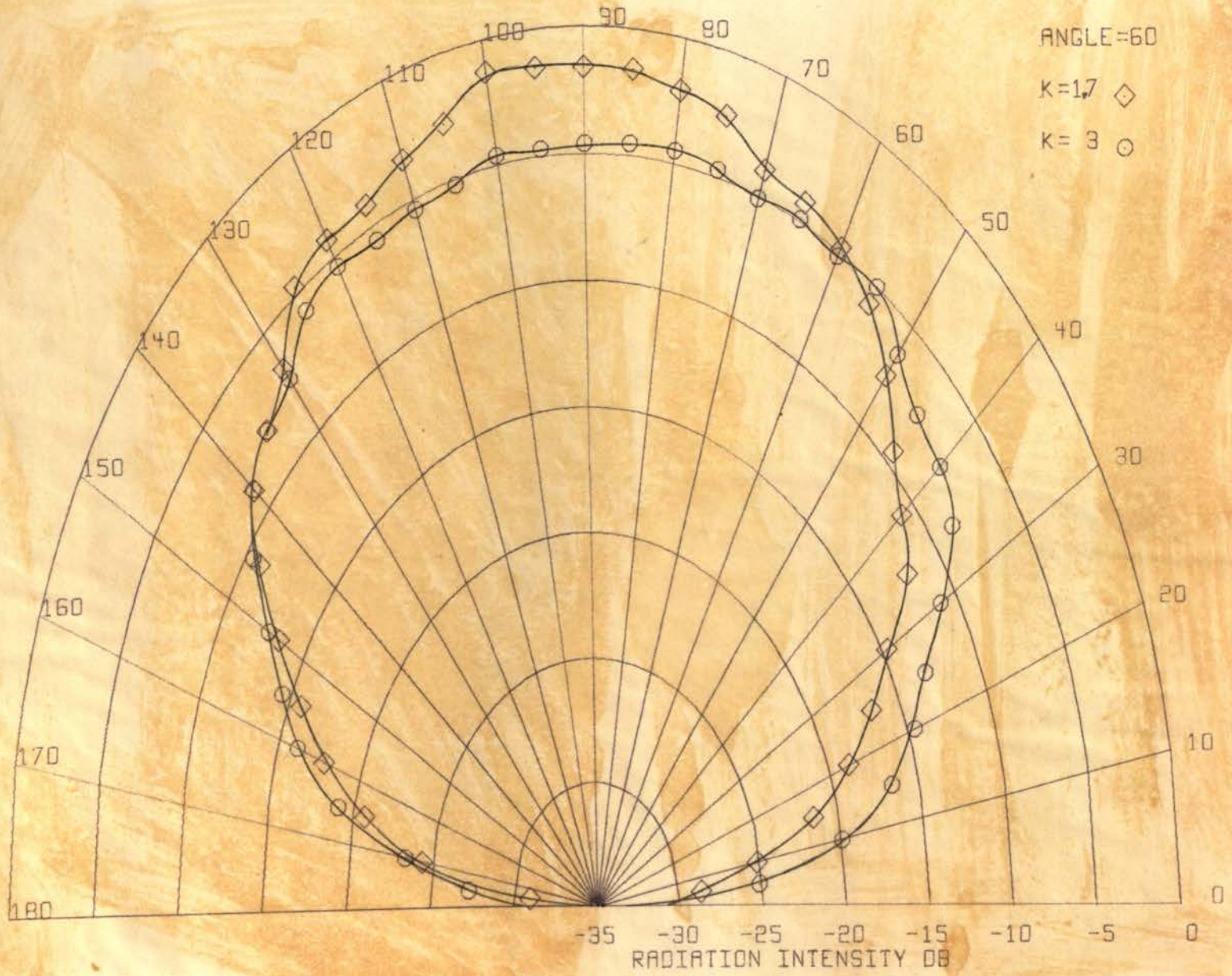

FIGURE 36. MEASURED RADIATION PATTERN 60^{o} K = 1.7, K = 3

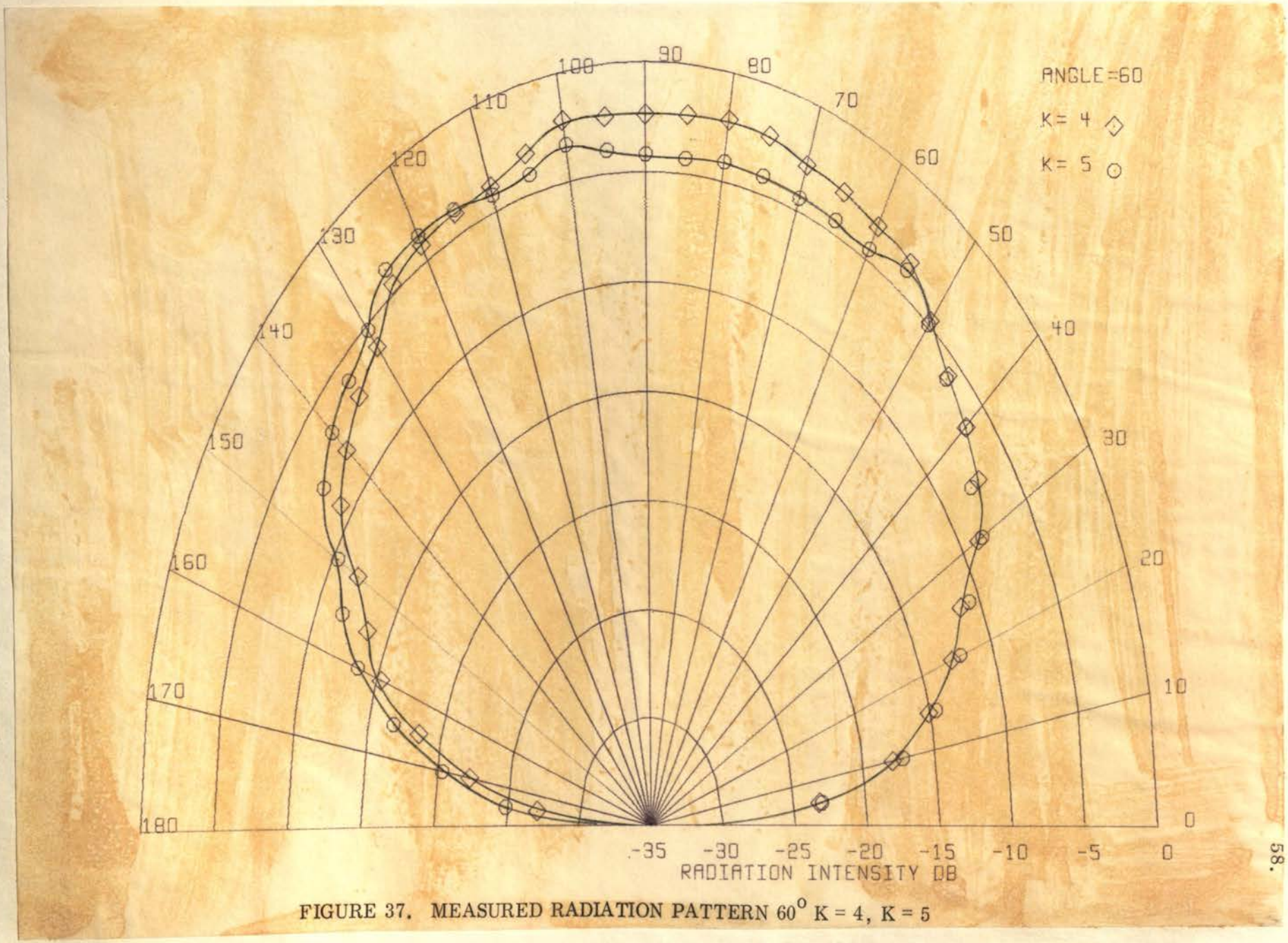

FIGURE 37. MEASURED RADIATION PATTERN 60^{o} K = 4, K = 5

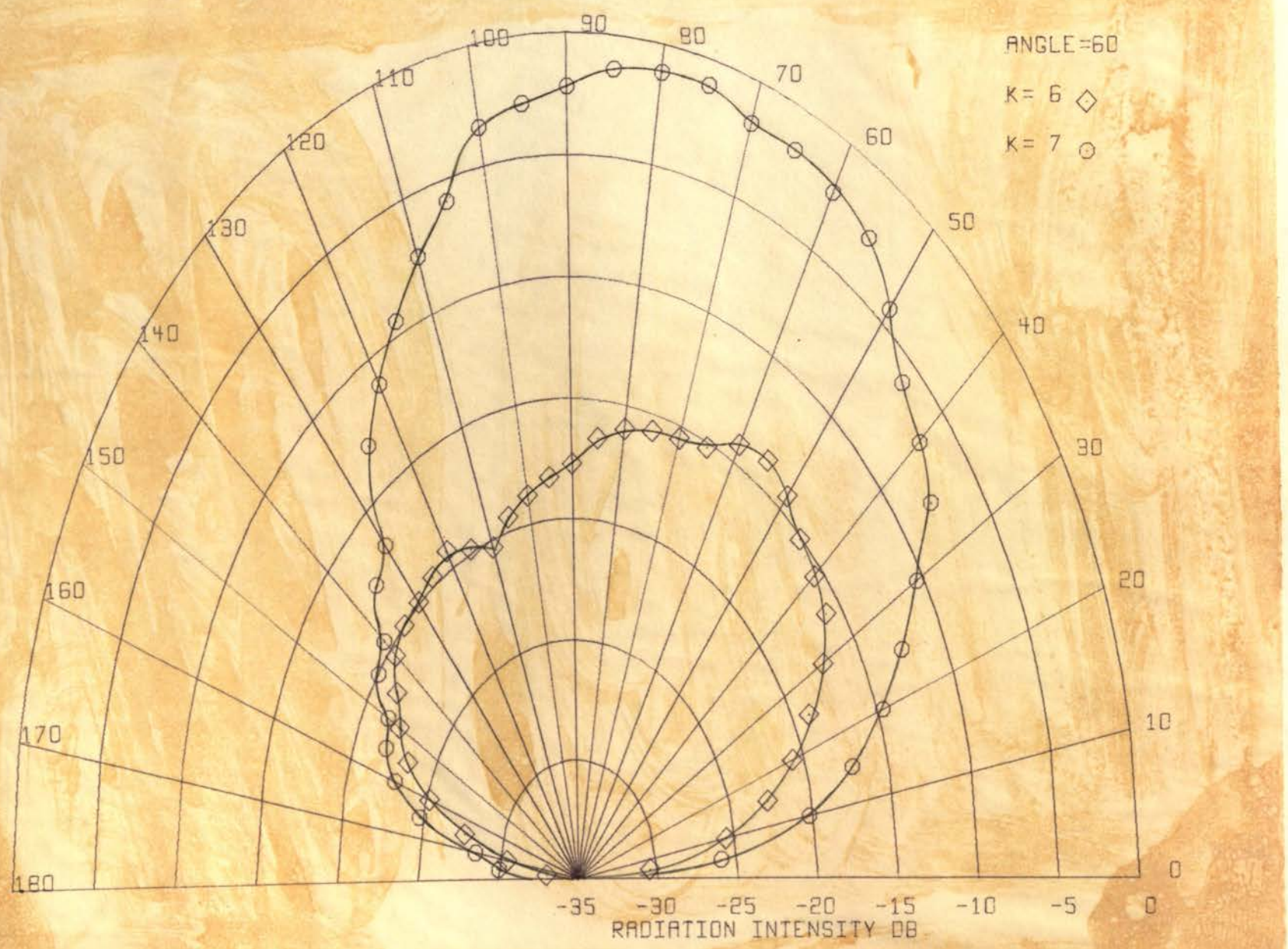

FIGURE 38. MEASURED RADIATION PATTERN 60^{o} K = 6, K = 7

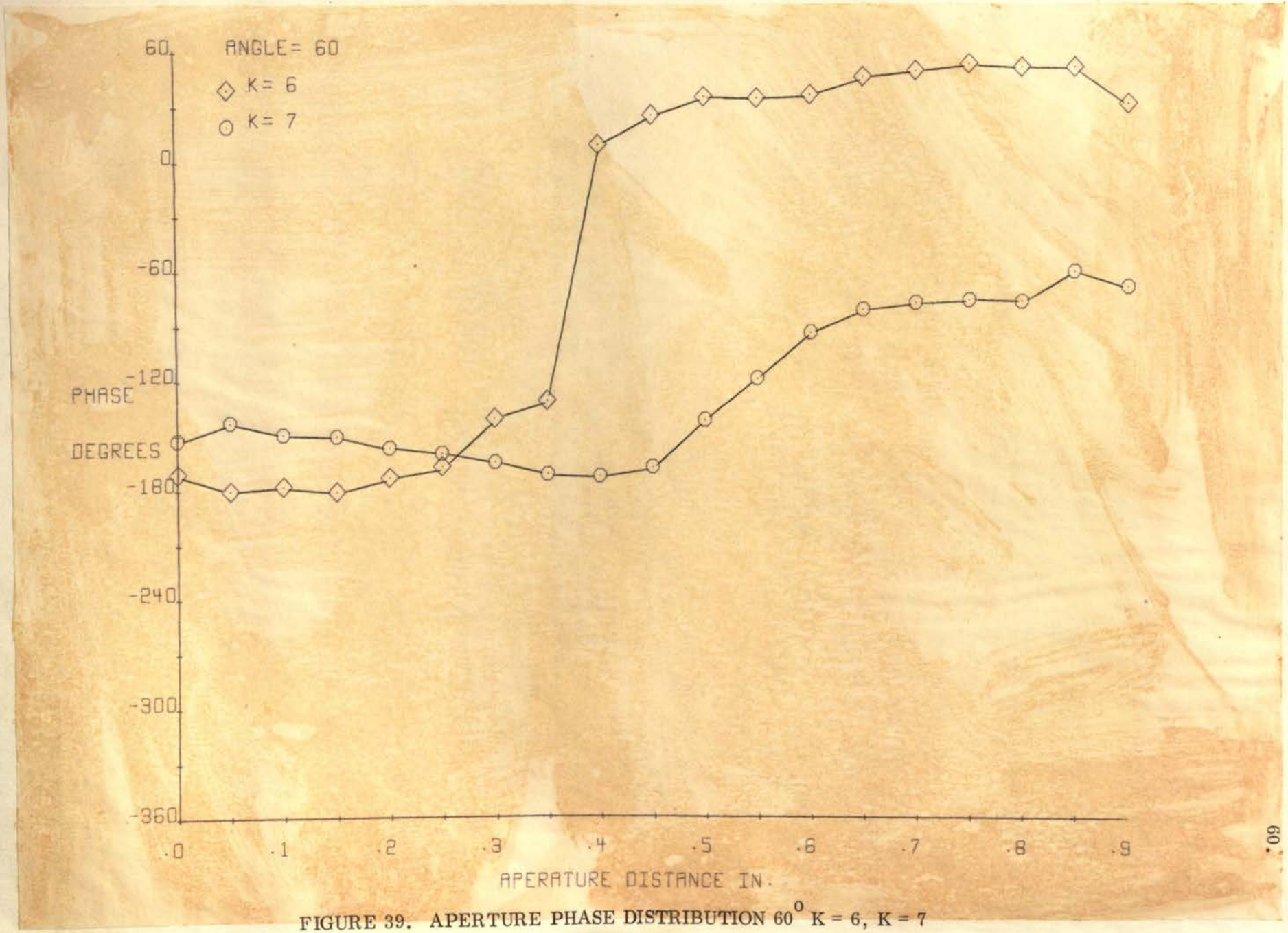

FIGURE 39. APERTURE PHASE DISTRIBUTION 60^{o} K = 6, K = 7

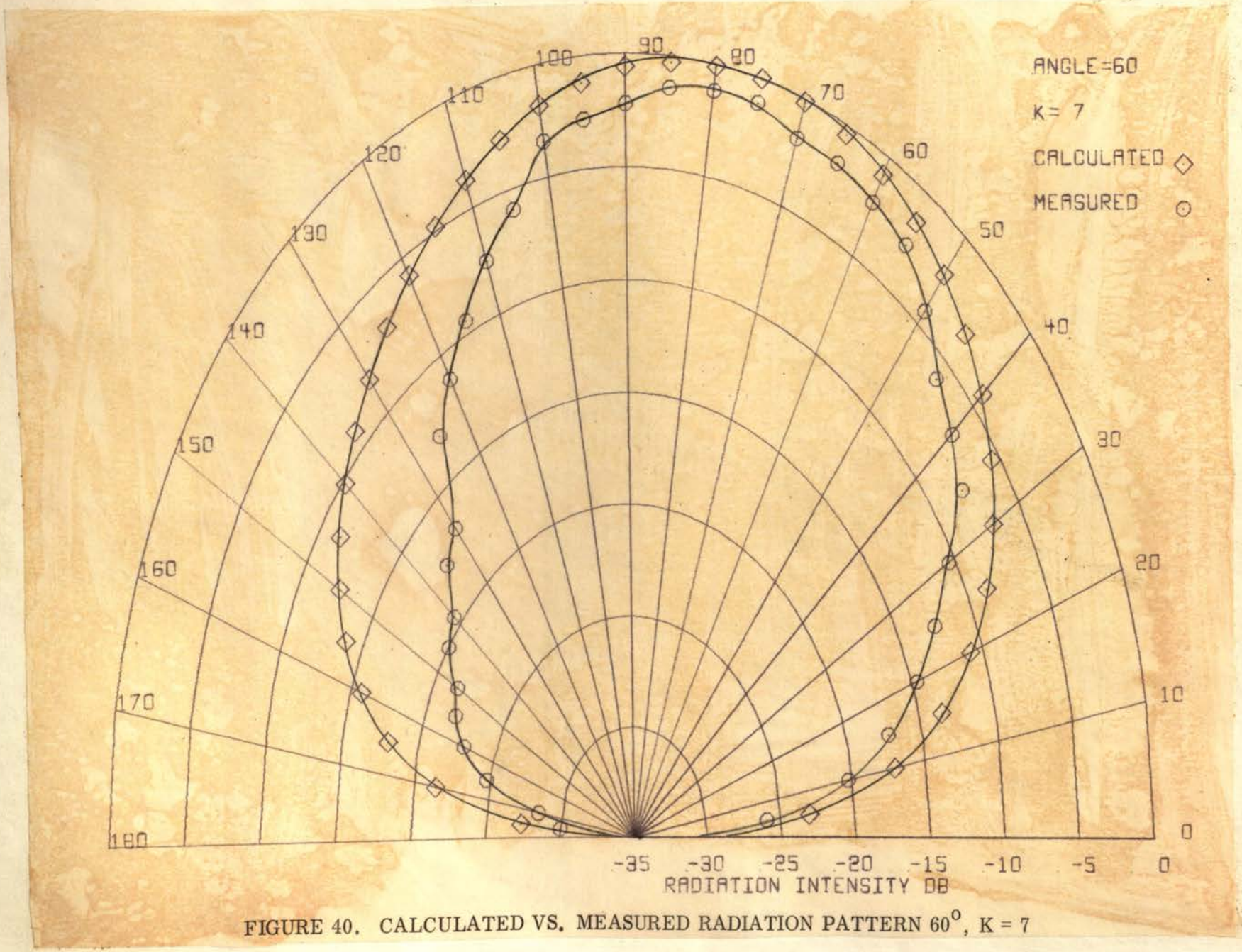

FIGURE 40. CALCULATED VS. MEASURED RADIATION PATTERN 60^{o}, K = 7

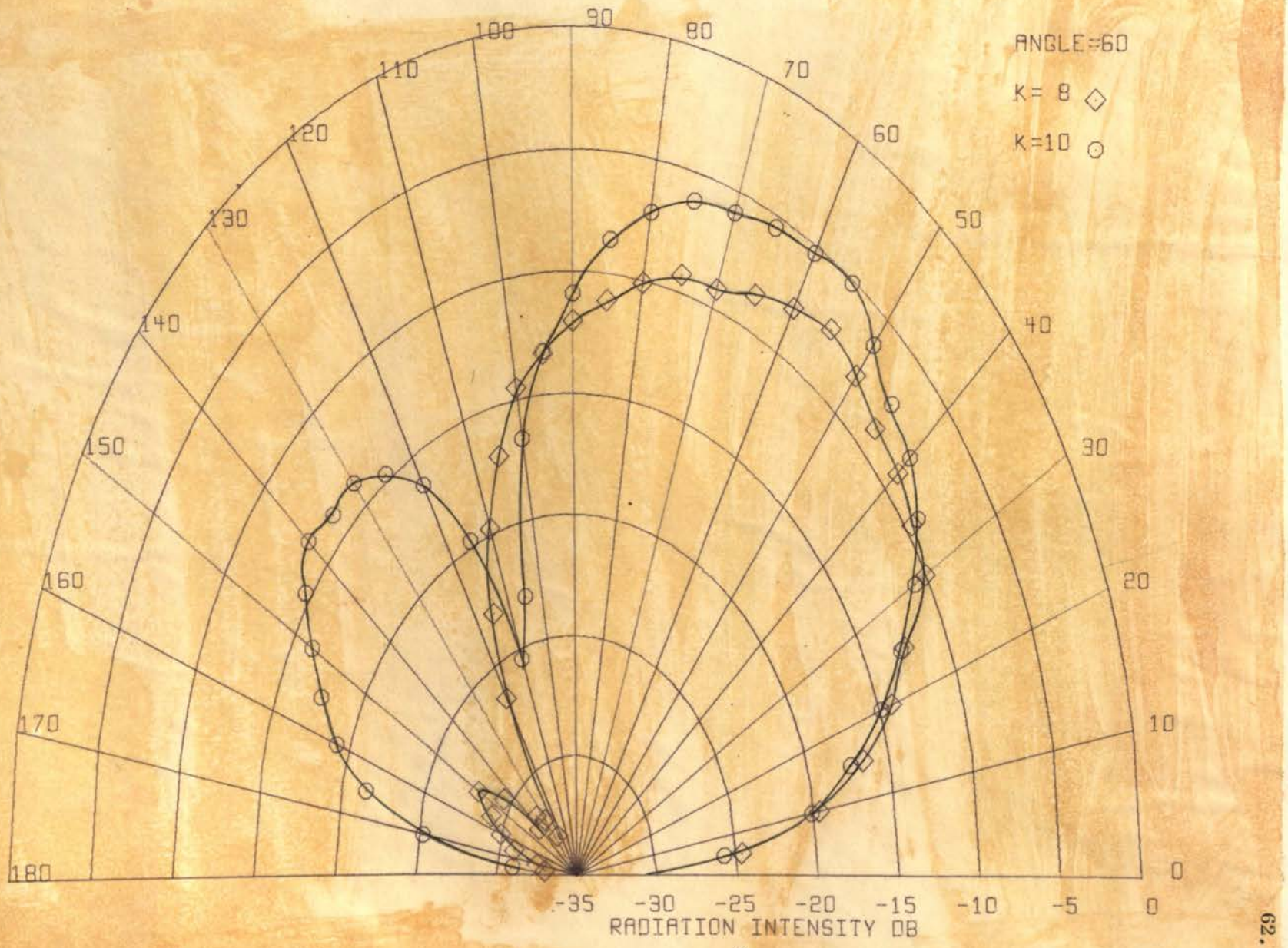

FIGURE 41. MEASURED RADIATION PATTERN 60° K = 8, K = 10

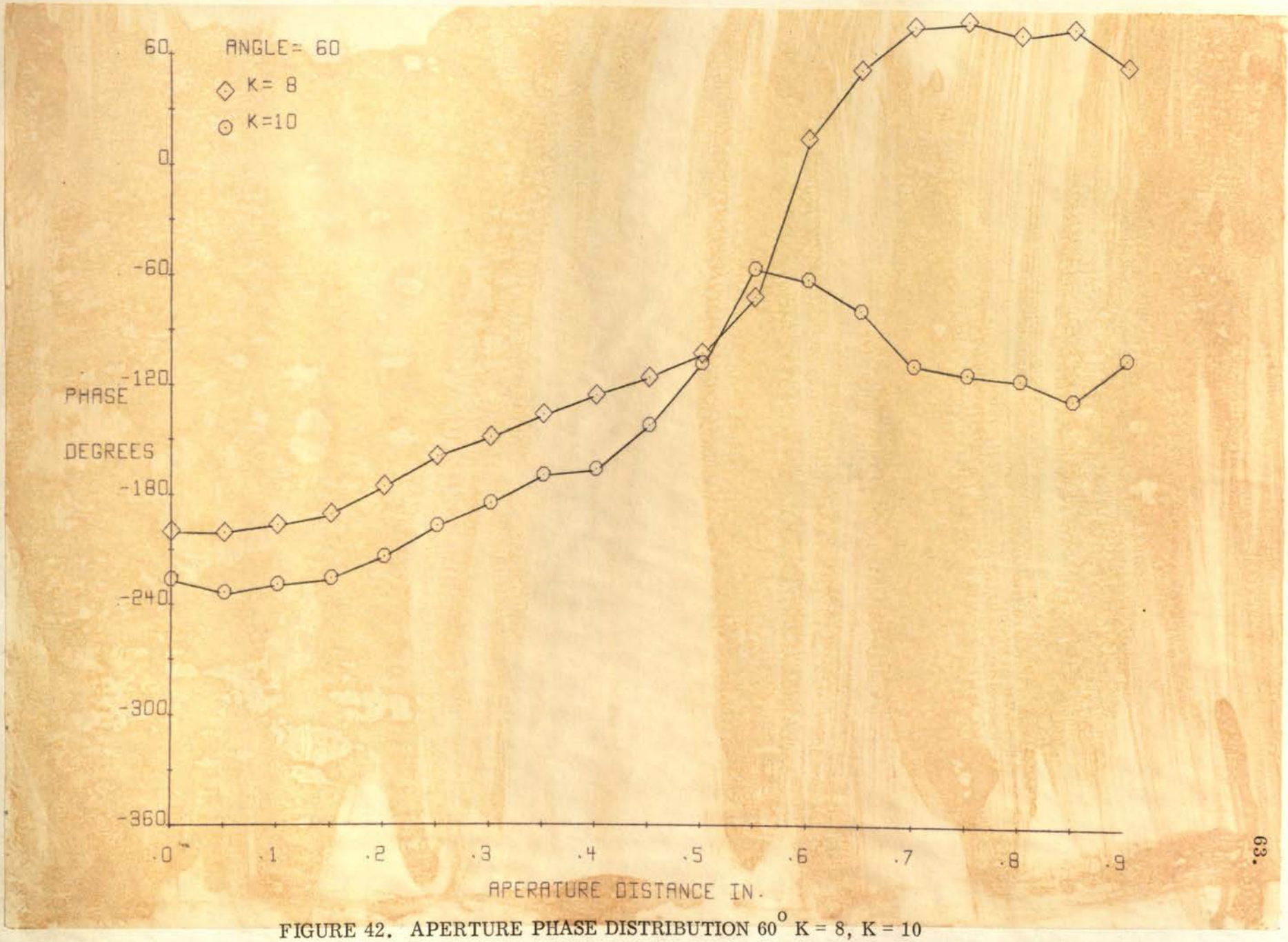

FIGURE 42. APERTURE PHASE DISTRIBUTION 60^{o} K = 8, K = 10

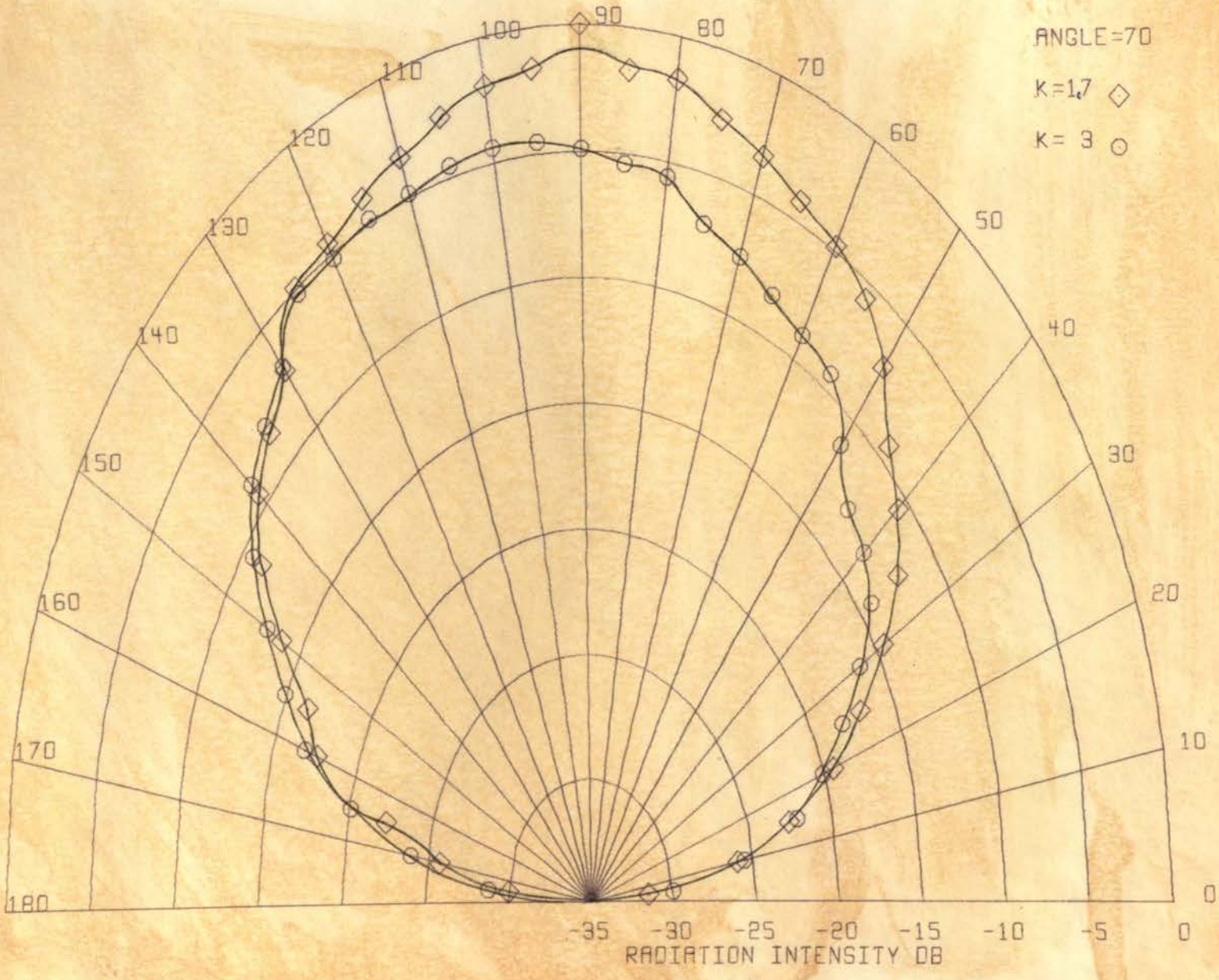

FIGURE 43. MEASURED RADIATION PATTERN 70^{o} K = 1.7, K = 3

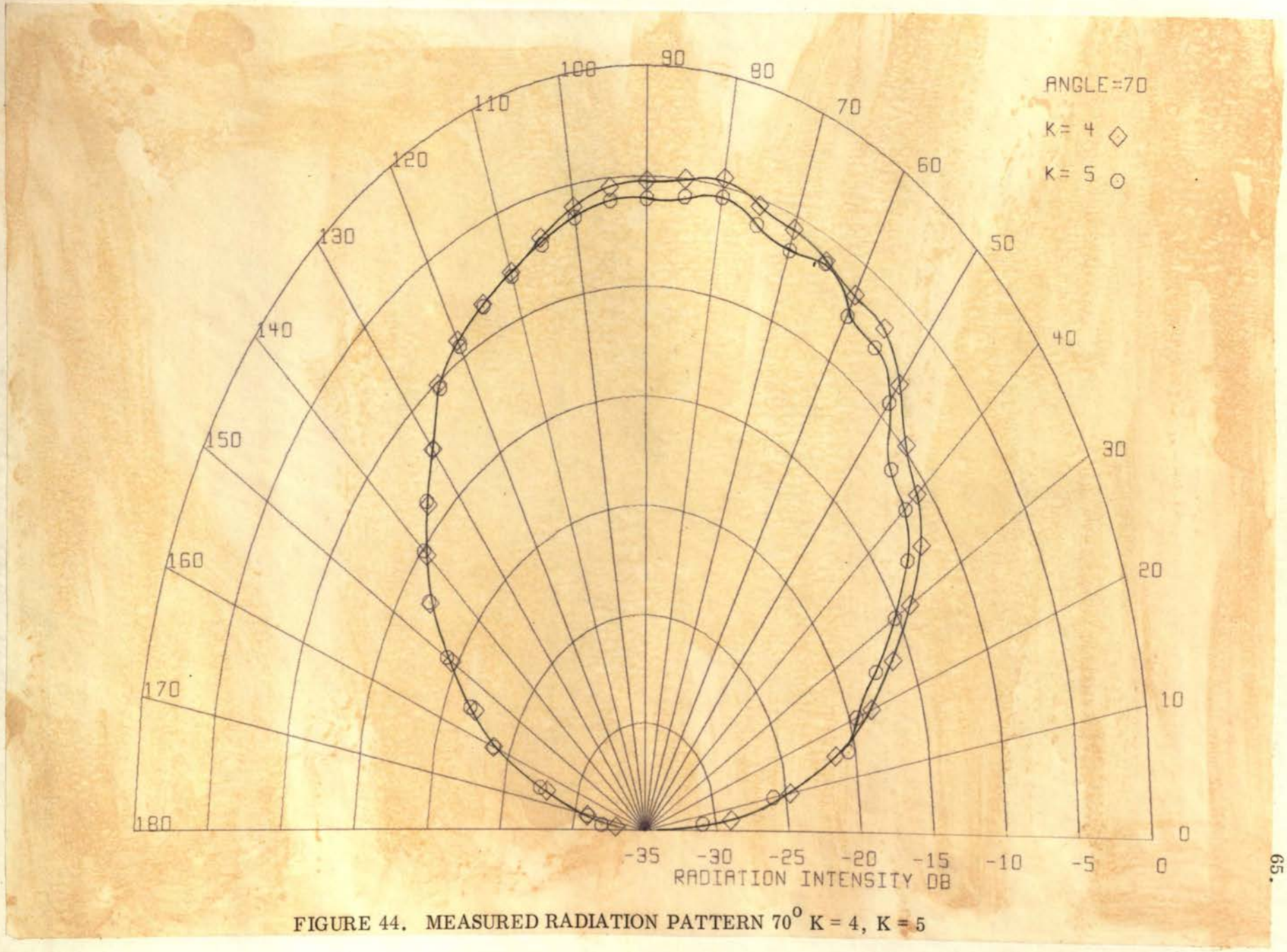

FIGURE 44. MEASURED RADIATION PATTERN 70^{O} K = 4, K = 5

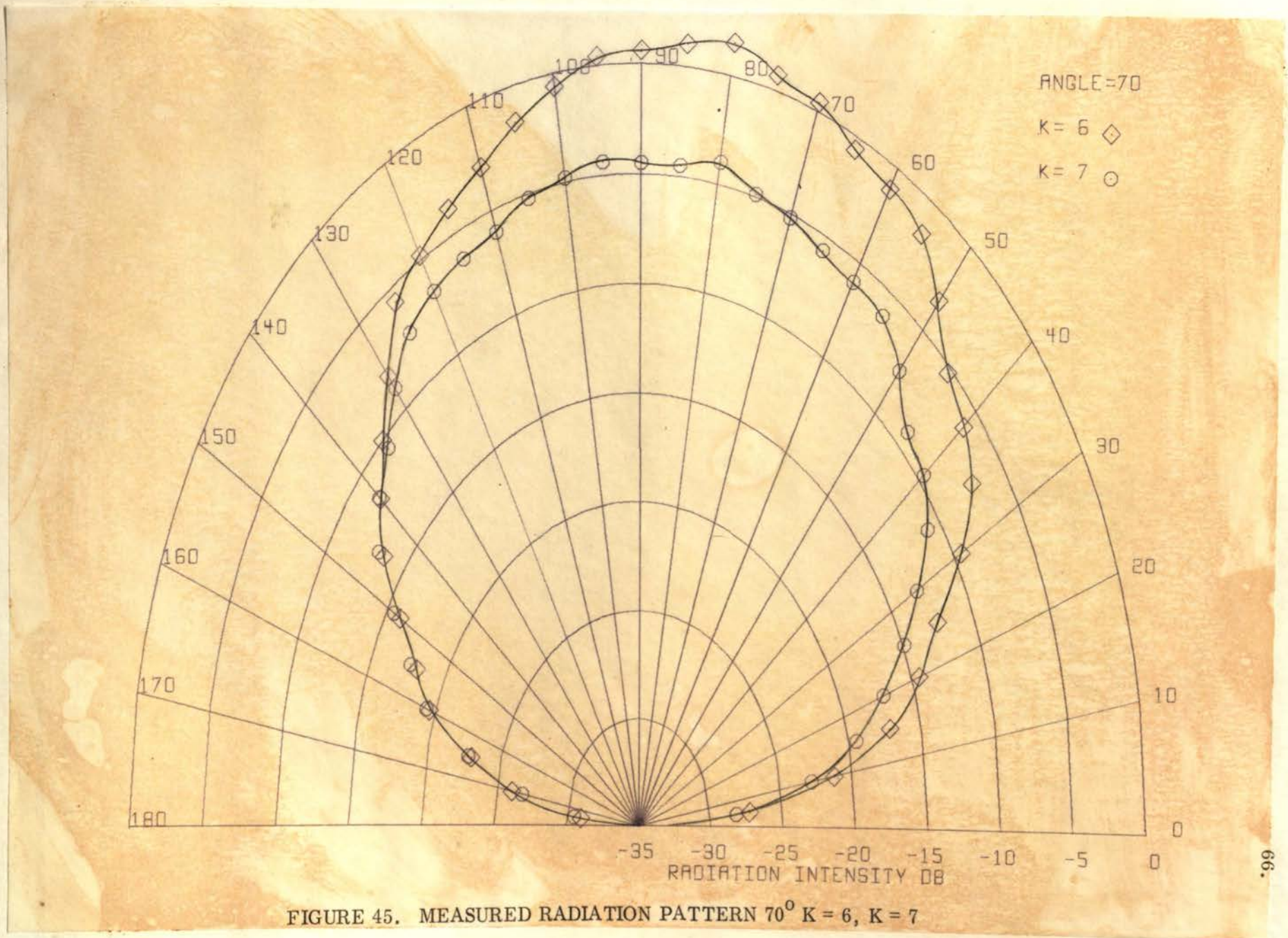

FIGURE 45. MEASURED RADIATION PATTERN 70^{O} K = 6, K = 7

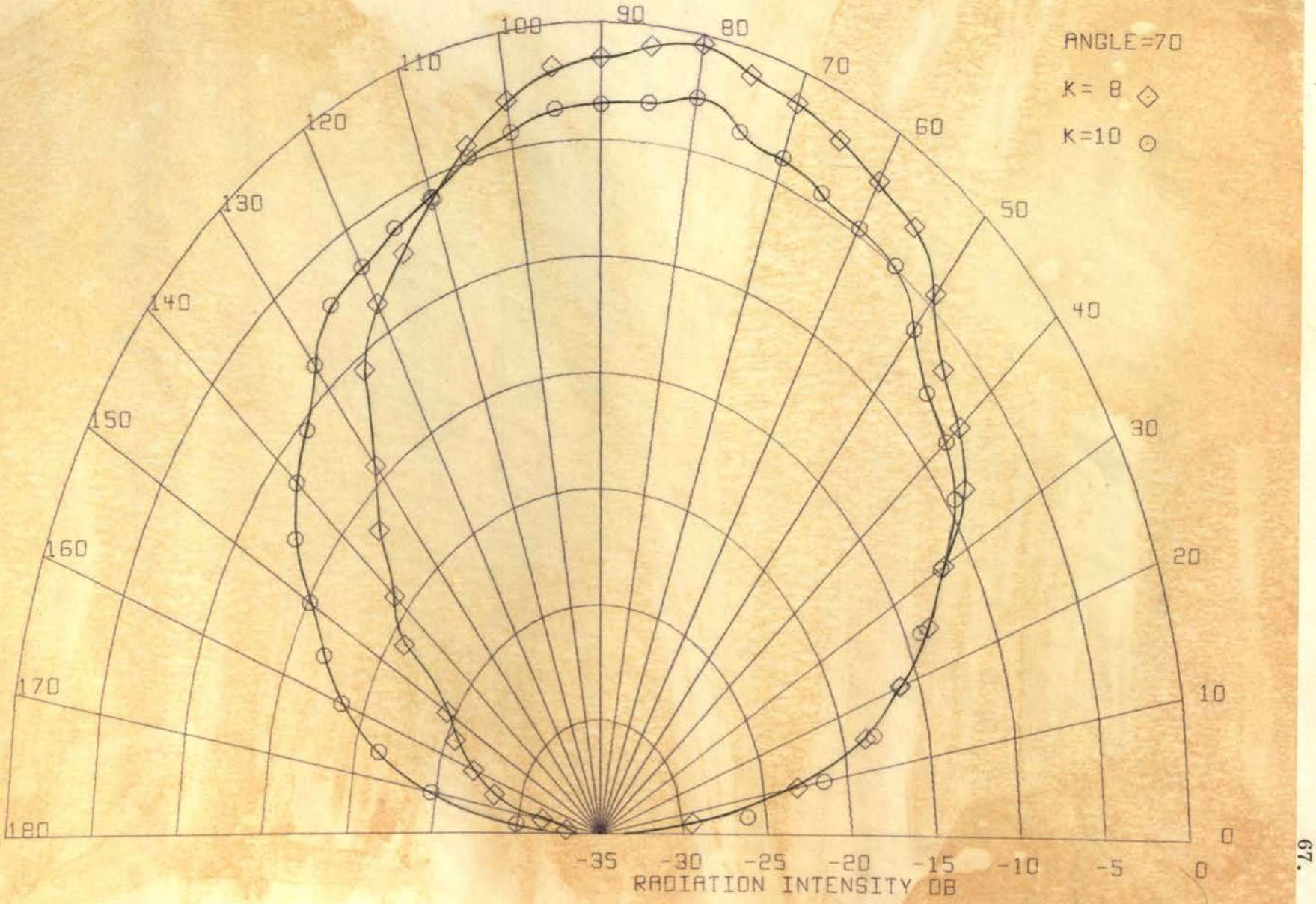

FIGURE 46. MEASURED RADIATION PATTERN 70^{O} K = 8, K = 10

VII. CONCLUSIONS

Within the range of wedge angles and permittivities tested, definite fundamental, second, and third order modes appeared in the aperture amplitude distributions, as well as other undetermined higher order modes. Associated with these modes were pronounced changes in the radiation far-field patterns, the only significant changes in these patterns occuring at the higher dielectric constants from 6 to 10 for which the third and higher order modes were present in the aperture.

The 60^{o} wedges were the only ones tested for which the changes in radiation pattern were fairly well coordinated with the increments in permittivity, and therefore useful for scanning action. The drastic changes in pattern with dielectric constant for the majority of the angles indicate that modulation over a very small range could produce useful pattern shifts at other angles.

The obvious extension of this work is to actually devise a variable permittivity wedge insert, so that a continuous range of permittivity could be investigated.

The partially filled waveguide approximation produced aperture mode distributions which approximate those of the actual configuration, but the model is limited by the choice of a free-space region for one portion of the guide. A more powerful model is needed, within the realm of mathematical solubility.

VITA

The author was born on March 23, 1942 in St. Louis, Missouri. He received his primary education in St. Louis and his secondary education in St. Clair, Missouri. He enrolled at the University of Missouri at Rolla in September, 1959, and received his Bachelor of Science Degree in Electrical Engineering in August, 1963.

From August, 1963 to September, 1964, he was employed by the Federal Aviation Agency and was engaged in the installation of aircraft navigation equipment.

He has been enrolled in the Graduate School of the University of Missouri since September, 1964, and has held a National Defense Education Act Fellowship from September, 1965 to the present.

BIBLIOGRAPHY

1. Schelkunoff, S.A, Generalized Telegraphists Equations for Waveguides, Bell System Technical Journal, Vol. 31, July, 1952, pp. 784-801.

2. Hord, W.E., 1966, Continuously Tapered Dielectric Matching Transitions for Waveguides, Thesis, University of Missouri at Rolla, 107 pages.

3. Blumberg, L., 1966, Phase and Amplitude Disbrigutions in an Unsymmetrically Fed Ground Plane Aperture, Thesis, University of Missouri at Rolla, 55 pages.

4. Angelakos, D.J., and Korman, M.M., Radiation from Ferrite Filled Apertures, Proc. IRE, Vol. 44, Oct., 1956, pp. 1463-1468.

5. Lewin, L., Theory of Waveguide Fed Slots Radiating into Parallel Plate Regions, J. Appl. Phys., Vol. 24, Feb., 1953, p. 232.

6. Harrington, R.F., 1961, Time-Harmonic Electromagnetic Fields, McGraw-Hill, New York, pp. 95-135, pp. 158-163.

7. Allen, C.C., Radiation Patterns for Aperture Antennas with Non-Linear Phase Distributions, Nat. Conv, Rec. IRE, 1953 Part 2, pp. 9-17.

8. Silver, S., 1963, Microwave Antenna Theory and Design, Boston Technical Lithographers, Boston, Mass., pp. 169-182.

9. Kraus, J.D., 1950, Antennas, McGraw-Hill, New York, pp. 353-381.

10. Harvey, A.F., 1963, Microwave Engineering, Academic Press, London, pp. 648-668, pp. 579-615.

11. Bolljahn, J.T., Some Properties of Radiation from a Rectangular Waveguide, Proc. IRE, Vol. 37, June, 1949, pp. 617.

12. Pincherle, L., Electromagnetic Waves in Metal Tubes Filled Longitudinally with Two Dielectrics, Phys. Rev., Vol. 66, No. 5, Sept., 1944, pp. 118-130.

APPENDIX A

This appendix treats the solution of the partially filled waveguide problem. Following the approach of Pincherle[12], a scalar function Ψ is chosen in each region, the function being the solution of Helmholt's scalar wave equation in that region:

$$\nabla^2 \Psi = k^2 \Psi \qquad \text{(A-A-1)}$$

where $k = j\omega\sqrt{\mu\epsilon}$

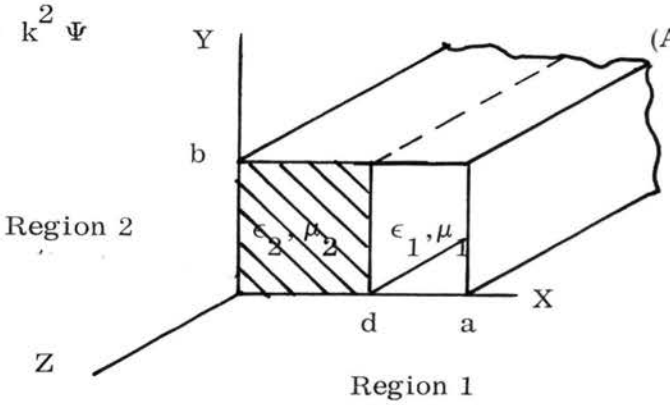

The above illustration gives the geometric configuration corresponding to the equations developed below. For modes with electric fields transverse to the X direction, the functions are related to the actual components of the electric and magnetic fields as follows:

$$E_x = 0 \qquad H_x = (j\omega\mu)^{-1}\left(\frac{\partial^2}{\partial X^2} + k^2\right)\Psi \qquad \text{(A-A-2)}$$

$$E_y = \frac{\partial \Psi}{\partial z} \qquad H_y = (j\omega\mu)^{-1}\frac{\partial^2 \Psi}{\partial X d_y}$$

$$E_z = \frac{\partial \Psi}{\partial y} \qquad H_z = (j\omega\mu)^{-1}\frac{\partial^2 \Psi}{\partial X \partial z}$$

The Ψ functions are chosen in each region to give the required vanishing components of electric field at the metal walls:

$$\Psi_1 = C_1 \sin K_{x1} X \cos\frac{n\pi}{b} y \, e^{-jkz^z} \qquad \text{(A-A-3)}$$

$$\Psi_2 = C_2 \sin k_{x2} (a - x) \cos \frac{n\pi}{b} y \, e^{-jkz^z} \qquad \text{(A-A-4)}$$

The Y and Z variations are chosen with the same variation in each region. Also, for TE_{mo} modes, which are the only ones being considered, n = 0 and therefore cos $n\pi y/b = 1$. Solving Helmholt' s equations yields two separation equations:

$$K_{x1_2}^2 + K_z^2 = \omega^2 \mu_1 \epsilon_1 \qquad \text{(A-A-5)}$$

$$K_{x2}^2 + K_z^2 = \omega^2 \mu_2 \epsilon_2 \qquad \text{(A-A-6)}$$

Continuity of the Y component of the electric field at the dielectric boundary (x = d) requires that:

$$Ey_1 \Big|_{x = d} = Ey_2 \Big|_{x = d} \qquad \text{(A-A-7)}$$

Therefore:

$$C_1 \sin k_{x1} d = C_2 \sin [k_{x2} (a - d)] \qquad \text{(A-A-8)}$$

Also, the Y component of the magnetic field must be continuous at x = d. This yields:

$$\frac{C_1}{j\omega\mu_1} k_{x1} \cos k_{x1} d = \frac{-C_2}{j\omega\mu_2} k_{x2} \cos k_{x2} (a - d) \qquad \text{(A-A-9)}$$

Combining (8) and (9) yields the characteristic equation:

$$\frac{k_{x1}}{\mu_1} \cot k_{x1} d = \frac{-k_{x2}}{\mu_2} \cot [k_{x2} (a - d)] \qquad \text{(A-A-10)}$$

This is solved with (5) and (6) to obtain the x variation of the fields and if required the propagation constant k_z.

APPENDIX B

NUMERICAL EVALUATION OF FAR-FIELD PATTERNS

This appendix describes the technique for evaluating the radiation far-field pattern of the ground-plane aperture from knowledge of the aperture magnitude and phase distributions.

By the equivalence principle (see Harrington[6]), the effects of the electric field across the aperture, considering only the half space into which the aperture is radiating, can be duplicated by an equivalent sheet of magnetic current placed in front of an infinite ground plane:

$$\overline{M}_s = \overline{E} \times \overline{n} \qquad \text{(A-B-1)}$$

where $\overline{M}_s$ is the magnetic sheet current, $\overline{E}$ the aperture electric field, and $\overline{n}$, the unit vector normal to the aperture face.

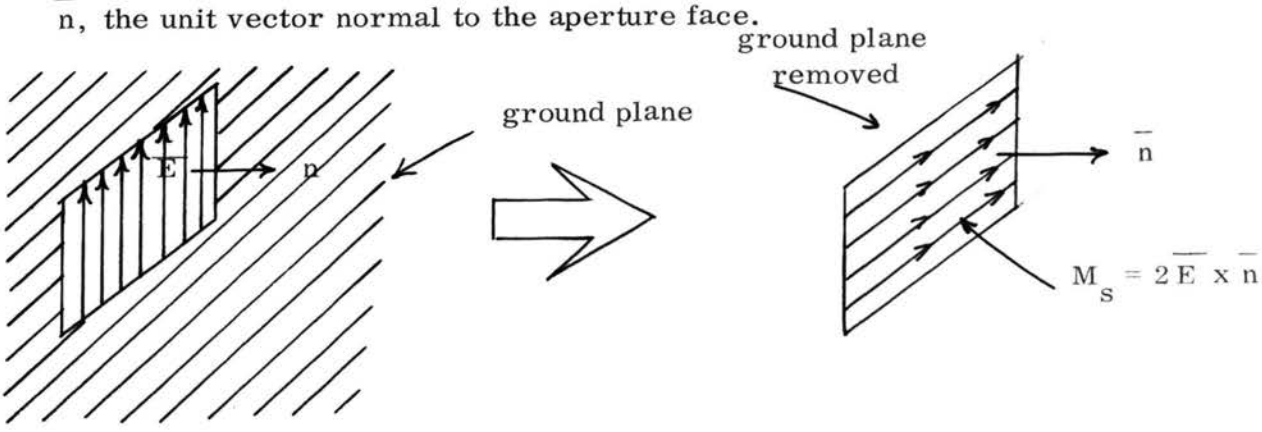

Original Problem

Equivalent Problem

By the image principle, the ground plane can be removed and $\overline{M}_s$ doubled. The problem is now one of finding the field of the magnetic sheet current. This is done by first calculating the vector electric potential:

$$F = \frac{1}{4\pi} \int_{\text{surface}} \frac{\overline{M}_s \; e^{jk\left|\bar{r} - \bar{r}'\right|} \; d\bar{r}'}{\left|\bar{r} - \bar{r}'\right|} \qquad \text{(A-B-2)}$$

Where $\bar{r}'$ represents the aperture coordinates, $\bar{r}$ the distance to the point in the radiation field and k the propagation constant, equal to $2\pi/\lambda$

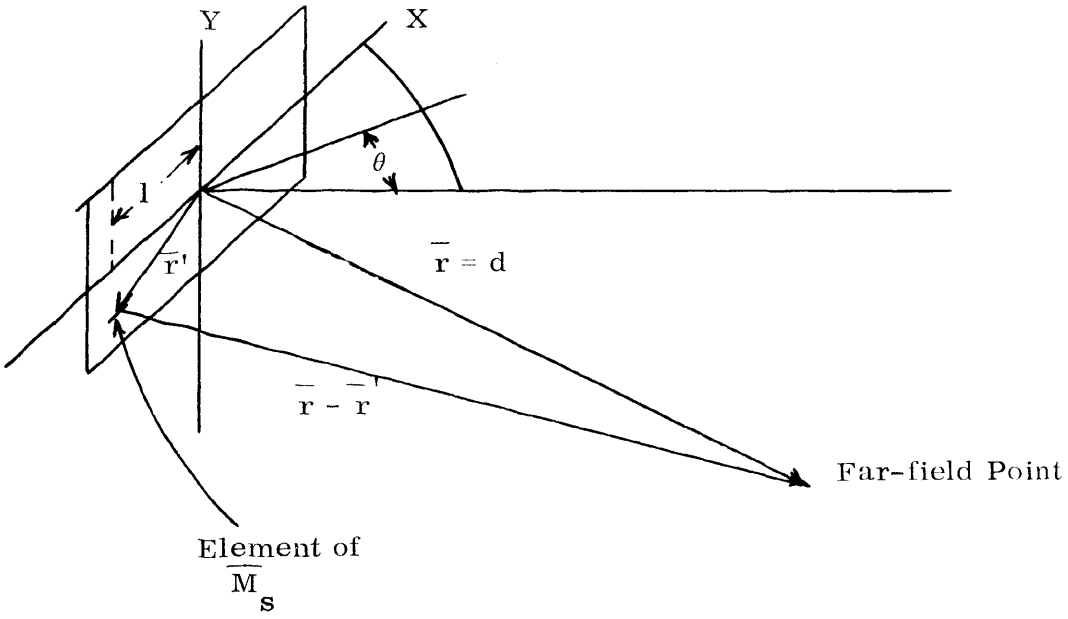

The integration is effectively adding the effects of each element of $\overline{M}_s$, taking into account their relative phase differences upon arrival at the far-field point. In determining the principal pattern (along a semi-circle in the X-Z plane) the integration can be reduced to one dimension since $\overline{M}_s$ is not a function of Y and therefore the contributions of elements not on the X-axis merely change the magnitude at each point.

The actual electric field in the far field is found by taking the curl of $\overline{F}$:

$$\overline{E}_{\text{radiation}} = -\nabla \times \overline{F} \qquad \text{(A-B-3)}$$

Along the principal plane, this is equivalent to multiplying by the cosine of

the angle θ . Since $\overline{F}$ is in the direction of $\overline{M}_s$ (the X axis), $\overline{E}_{rad}$ will be in the Y direction.

In the numerical procedure, the X axis is broken into 36 elements, the center of each representing a point source for that element. Since only 19 actual data points are available, the additional points are generated by linear interpolation. For the elements of magnetic current on the X axis, the distance to the far-field point is:

$$\overline{r} - \overline{r}' = d - l \cos \theta \qquad \text{(A-B-4)}$$

The phase term of each element is broken into a cosine and sine components:

$$e^{jk\,\overline{r} - \overline{r}'} = \cos \frac{2\pi}{\lambda} (d - l \cos \theta) + \phi + j \sin \frac{2\pi}{\lambda} (d - l \cos \theta) + \phi \qquad \text{(A-B-5)}$$

where ϕ is the relative phase as measured at each element in the aperture.

Let $\frac{2\pi}{\lambda} (d - l_k \cos \theta) + \phi_k = Pk$

Then the total $\overline{E}_{rad}$ for a point oriented at an angle θ is:

$$E(d,\theta) = \cos \theta \left[\left(\sum_k A_k \cos P_k \right)^2 + \sum_k A_k \sin P_k \right)^2 \Bigg]^{\frac{1}{2}} \qquad \text{(A-B-6)}$$